University of Pardubice

Faculty of Transport Engineering

WAYSIDE DIAGNOSIS OF RUNNING GEAR RELATED FAULTS IN RAILWAY VEHICLES

PhD Student: **Onur KILINC, M.Sc.**

2017

Programme of study:

P3710 Technique and Technology in Transport and Communications

Branch of study:

3706V005 Transport Means and Infrastructure

Supervisor: *Ing. Jakub Vágner, Ph.D.*

Specialist supervisor: doc. Ing. Michael Lata, PhD.

Dissertation came into being at department:

Department of Transport Means and Diagnostics

I hereby confirm that:

I have written this dissertation thesis independently. All the reference literature and information used in this work are quoted in the list of reference literature.

I hereby acknowledge that all the rights and duties resulting from Act No. 121/2000 Coll., the Copyright Act, apply to my written work, especially that the University of Pardubice has the right to make a license agreement of use of this written work as a school work pursuant to to § 60 section 1 of the Copyright act. On the condition that the written work shall be used by me or a license shall be provided to another subject for the use hereof, the University of Pardubice shall have the right to require from me a relevant contribution to reimburse the costs incurred for the making of such work including all relevant costs and total overal expenditure and expenses incurred.

I agree with making the work accessible in the University Library.

This work has been accomplished by using technologies of the Educational and Research Centre in Transport.

Dated in Pardubice on 7. 4. 2017

ONUR KILINC

I would like to thank my supervisors doc. Ing. Michael Lata, PhD and Ing. Jakub Vágner, PhD. for helpful approach and precious advice during the writing of my dissertation work. I am also thankful to project TAČR TE01020038 for providing data about metros and the maintenance information of metro train sets from DP Praha

ANNOTATION

The work focuses on the diagnosis of running gear faults like wheel defects, wheelset and traction motor bearings and gearbox faults using model based and wayside diagnosis techniques based on acoustic and vibration sensors. Firstly, a brief background information about railway vehicle condition monitoring systems is given. Main aim of the work was proposing the methods that are efficient in recognizing vehicle faults. In the next section, proposed methods are validated by experimental measurements, real information from maintenance and simulated faulty cases of running gear components. With the contribution of advanced pattern recognition techniques and model based filtering, an efficient diagnosis framework was proposed. It provides a cost effective maintenance for railway vehicles.

KEYWORDS

Wayside diagnosis, maintenance, fault detection, vibration based diagnosis, time-domain features, model based filtering.

TITUL

Diagnostika poruch pojezdu kolejových vozidel měřením na trati

ANOTACE

Práce se zaměřuje na diagnostiku pojezdu kolejových vozidel jako jsou vady dvojkolí, poruchy ložisek nebo mechanické části pojezdu, a to za použití wayside diagnostiky měřením hluku a vibrací na trati. V úvodu jsou popsány existující systémy monitorování stavu kolejových vozidel. Hlavním cílem práce bylo navrhnout metody pro efektivní rozpoznání poruchy vozidla. V další části jsou navržené metody validovány pomocí experimentálních měření, skutečnými informacemi z údržby a pomocí simulovaných případů poruch pojezdu vozidla. S přispěním moderních technik zpracování signálů jako: advanced pattern recognition techniques and model based filtering byl navržen účinný rámec diagnostiky. Ten umožňuje snížit náklady při údržbě kolejových vozidel.

KLÍČOVÁ SLOVA

Wayside diagnostika, údržba, detekce poruch, vibrodiagnostika, analýza signálu v časové oblasti, filtrace na základě modelu.

TABLE OF CONTENTS

LIST OF TABLES

LIST OF FIGURES

LIST OF ABBREVIATIONS

1D	One-dimensional
2D	Two-dimensional
ADASYN	Adaptive Synthetic Sampling
AR	Auto-Recursive
ASDEK	Rolling Stock Network Diagnostic
AUC	Area under (ROC) Curve
AVG	Average fixed diameter approach for determining sampling interval
BF	Ball Fault
Bw	Bandwidth
CWRU	Case Western Reserve University
CWT	Continues Wavelet Transform
Dec. Tree	Decision Tree Classifier
DWT	Discrete Wavelet Transform
E-LCP-K	Histogram Enhanced LCP-K
FK	Fast Kurtogram
FLDA	Fisher Linear Discriminant Analysis
F-TM	Traction Motor Eccentricity
FS	Feature Selection
FSS	Forward Sequential Selection
FSS-KNN-1	Forward Sequential Selection with 1-nearest Neighbor
F-z	Gear Tooth Fault
GOTCHA	Wheel Flat Detection and Axle Load Measurement System
GUI	Graphical User Interface
HC	Health Case
HE	Histogram Equalization
HH	High-high Node of the Wavelet Packet Tree
HL	High-low Node of the Wavelet Packet Tree
HPF	High-pass Filter
ID	Identification Number of Prague Metros
IRF	Inner Race Fault
K-NN	K-nearest Neighbor
KURT-ENV	Kurtogram Envelope Analysis (fifth-order)
KURT-ENV-TDFs	Kurtogram Envelope Analysis (fifth-order) and TDFs afterwards
LASCA	Laser Speckle Contrast Analysis
LASSO	Least Absolute Shrinkage and Selection Operator
LBP	Local Binary Patterns
LCP	Local Configuration Patterns
LCP-K	Local Configuration Patterns after Fast Kurtogram Method
LH	Low-high Node of the Wavelet Packet Tree

LIST OF ABBREVIATIONS (CONT.)

LPF	Low-pass Filter
MATLAB	Commercial Software for Signal Processing and Calculation
MED	Minimum Entropy Deconvolution
MODWT	Maximal Overlap Discrete Wavelet Transform
MOMEDA	Multipoint Optimal Minimum Entropy Deconvolution
MOMEDA AR	Auto Recursive Filtering after MOMEDA
MOMEDA TDFs	Time-domain features (consistent of eleven) after MOMEDA filtering
N-Bayes	Naïve Bayes Classifier
NI-CDAQ	National Instrument-Compact Data Acquisition
OMED	Minimum Entropy Deconvolution with Optimal Solution
OMEDA	OMED with AR Filter
ORF	Outer Race Fault
PERLC	Linear Perceptron Neural Network Classifier
Prod. comb	Product Combiner Classifier
REB	Rotating element bearing
RFID	Radio Frequency Identification
RMS	Root Mean Square
ROC	Receiver Operator Characteristics
SMOTE	Synthetic Minority Over-sampling Technique
STATS	Time-domain Features (consistent of five)
STFT	Short-time Fourier Transform
SVM	Support Vector Machine
SVM-I	Linear SVM Kernel
SVM-II	Second-order SVM Kernel
TDF	Time-domain Features (consistent of seven)
TDFs	Time-domain Features (consistent of eleven)
TM-IRF	Traction Motor Inner Race Fault
TM-ORF	Traction Motor Outer Race Fault
TOR	Top of rail
WF	Wheel flat
WPE	Wavelet Packet Energy
WPE_3	Third order Wavelet Packet Energy Feature Vector
WPE_5	Fifth order Wavelet Packet Energy Feature Vector
WPT	Wavelet Packet Transform
WRF	Wheel and Rail Profile Faults
W-WAV	Weighted Wavelet Energy
ZLV	Zentrum für Logistik & Verkehr (Centre for Logistic and Transport)

LIST OF SYMBOLS

g_i	i_{th} pixel intensity level in the window of LBP
A	Approximation coefficients in DWT
D	Detail coefficients in DWT
μ	Average in time-domain analysis
D_k	Average diameter of the wheels on the wheelset *[m]*
α	Ball contact angle in bearing fault investigation *[m]*
d_0	Ball diameter in bearing fault investigation *[m]*
g_c	Center pixel in the window of LBP
r	Radius of the wheel in one-period analysis *[m]*
X_n, x[n]	Discrete signal sample of length N
f_{FT}	Frequency of cage in bearing fault investigation *[Hz]*
f_{BFBI}	Frequency of inner ring in bearing fault investigation *[Hz]*
f_{BPFO}	Frequency of outer ring in bearing fault investigation *[Hz]*
f_{BSF}	Frequency of rolling elements in bearing fault investigation *[Hz]*
f_{ws}	Frequency of the wheelset in fault investigation *[Hz]*
f_{TM}	Frequency of traction motor *[Hz]*
g	Gravitational acceleration *[m/s^2]*
f_{zmws}	Modulation of tooth frequency by f_{ws} *[Hz]*
f_{zmTM}	Modulation of tooth frequency by f_{TM} *[Hz]*
n_w	Number of components in wavelet packet energy
L_w	Number of levels in wavelet packet transform
P	Number of pixels in the window of LBP
z_1	Number of teeth on the smaller wheel on gearboxes
z_2	Number of teeth on the larger wheel on gearboxes
L	Perimeter of the wheel in one-period analysis *[m]*
T	Period of the rotation of the motor in bearing fault diagnosis *[s]*
w	Radial rotation speed of the wheel in one-period analysis *[rad/s]*
v	Translational velocity of the wheelset in fault investigation *[m/s]*
$i_{\min}$	Sample difference of wheelsets; WS_1-WS_2 when passes on sensor G_A
WS_1	Sample point when first wheelset passes on sensor G_A
WS_{20}	Sample point when last wheelset passes on sensor G_A
W_S	Segmentation window in abnormal signal detection
σ	Standard deviation in time-domain analysis
d_s	The distance between the centers of opposing balls *[m]*
f_z	Tooth frequency of the gearbox *[Hz]*
f_{zh}	Tooth wear frequency of the gearbox *[Hz]*
B_0'	Two wheelsets loaded in each bogie by traction force
G_A, G_B	Optical Gates A and B
$\psi_{a,b}$	Wavelet function in DWT (dilation by a on location b)

LIST OF SYMBOLS (CONT.)

N	Signal length in DWT, TDF and MOMEDA
$\vec{t}$	Filter window in MOMEDA
n_f	Faulty impulse period by means of number of samples, in MOMEDA
X_0	Measurement signal in MOMEDA
L_m	Filter size in MOMEDA
$\vec{f}$	Filter in MOMEDA
m_o	Number of observations in adaptive synthetic sampling (ADASYN)
n_o	Length of the feature vectors in ADASYN and feature selection
N_c	Number of classes in feature selection
N_{tv}	Number of feature vectors in each training class in feature selection
$F^{training}$	Training set in feature selection
n_{fs}	Number of features in each training class in feature selection
y_{ij}	Normalized data after dimensionless analysis
x_{ij}	Normalized data before dimensionless analysis
$\bar{x}_{ij}$	Average of the observed data in dimensionless analysis
s_j	Standard deviation of the observed data in dimensionless analysis
v_f	Simulated faulty transient for running gear faults *[Hz]*
A_i	Random amplitude of the simulated frequencies
U	Number of sinusoidal in the simulated transient in each period
ω_i	Random frequency of the simulated sinusoidal in simulated faults *[Hz]*
β_i	Random initial phase of the simulated sinusoidal in simulated faults
f_c	Carrier frequency in KURT-ENV analysis *[Hz]*

INTRODUCTION

Wayside diagnostics have utmost attention of the researchers due to recent advancements in contemporary methods in railway vehicle condition monitoring. Understanding the real time or offline evaluation of sensor data tells about the health status of some specific mechanical parts of the railway vehicles is vital for low cost maintenance which superimpose periodical service of all structures on the train sets at the same time or the necessity of on-condition repairs.

Diagnostics of the running gear of a rail vehicle is the key point of ensuring a railway vehicle is running in safe mode. Ongoing stationary techniques are more focused on laboratory experiments including the experiments on a static or dynamic test stand or using on-board sensors on the specified points of the vehicle parts. Wayside diagnostics however, is more capable of determining dynamic system faults requiring less effort than stationary test environments which outperforms the condition based maintenance by means of cost efficiency. In addition to cost friendly nature of wayside diagnostics, it may serve real-time monitoring of conditions of individual vehicles and their running gear components when an efficient evaluation process is maintained. Another discriminative advantage may be counted as, when some system parameter such as dynamic response of a bogie significantly changes, which may affect the safety of the run and harm other components, these changes can only be observed and diagnosed during vehicle is in real world operation.

Strain based [1], accelerometer sensor based and gyroscope sensor based [2] methods are the fundamental way of measuring forces or detect anomalous activity in the run. Other advanced techniques are also presented for specialized diagnosis of rail vehicles like sliding wheel detectors, acoustic bearing defect detection, hot box detectors, hunting of the vehicle detectors which are only limited to a particular parts of the vehicle [3].

On-board data driven methods are also a commonly used way of monitoring safety of the run. These methods require detailed knowledge about a target vehicle and feasible set of sensors and evaluation methodology if multi-condition monitoring is to be achieved [4]. Successful application of these methods is not possible unless a very well characterized modelling besides appropriate filtering.

Noise reduction is also a vital step after acquisition process is done especially for acoustic sensors are employed. The nature of railway vehicles are significantly noisy and a proper signal modelling should be constructed to prevent adverse effects on signals.

In this thesis, in order to achieve a complete diagnosis framework for running gear, several different examples of diagnosis from model based methods to specific diagnose techniques are proposed. Proposed techniques are validated both experimental and simulated faulty data by numerous comparisons.

The organization of this thesis is as follows: The analysis of the current situation in the area of dissertation is presented in Section 1. Objectives of the area of dissertation, background information of model based faulty frequency calculations for running gear components and test environment are explained in Section 2. Proposed methodologies that are capable of detecting and simulating faults of rotating machinery on the running gear of railway vehicles are given in Section 3. Abnormal signal detection by acoustic and vibration sensors data and method validation on a ground truth database in rotating machinery related faults, detecting simulated faulty conditions of running gear components and acoustic sensor based diagnosis of traction motor bearing faults are given in Section 4 with results and discussion. Own contribution of the Ph. D. student including novel methodologies subjected to this thesis is presented in Section 5. Finally, the conclusion part that discuss the efficiency of the methods regarding to the results is given in Section 6.

1 ANALYSIS OF THE CURRENT SITUATION IN THE AREA OF DISSERTATION

Currently, all railway to road vehicles in central Europe have plenty different kinds of diagnostic systems. Road transportation diagnosis is based on electronic devices which may indicate several problems for the related vehicle. However, condition monitoring via real-time or offline diagnostic systems are not common especially in the area of railways that indicates condition of some mechanical components of the vehicle.

Ongoing techniques in the area of Czech Republic is more focused on laboratory experiments including the researches on a static or dynamic test stands. Data is collected via desired parts of the vehicles with known condition state by performing static or dynamical tests in laboratory conditions. Stationary techniques are more focused on laboratory experiments whereas wayside diagnostics are more capable in determination of dynamical system faults that requires less effort than stationary test environments. Nevertheless, acquired results and evaluation processes of signals that are recorded stationary may not help a vehicle in running conditions and lack of being real-time.

An application of wayside diagnostics in Czech railways is so called ASDEK which uses sensors mounted on a rail or close to it. The main conditions that can be monitored by the techniques of ASDEK include measurement of physical quantities like temperature of bearings, vertical force between wheel and rail. Measurements can be done at approximately while the velocity of the train is 80 km/h. Moreover, the diagnose of wheelset eccentricity and detection of wheel defects like bumping of the wheel are also available and real-time data may be provided for warnings or even for decision of stopping the run of the train [5].

The measurements of ASDEK belongs to instantaneous load and temperature and the application in metros in the area of Czech Republic is not available.

In the environment of wayside diagnosis, observing the actual response of the running gear of the railway vehicles is troublesome due to far from being ideal in comparison to modelling. Real world idealization of engineering models have always been a problem for mechanical parts and their interaction with each other [6]. Understanding the precise response of a particular mechanical system under uncertain conditions needs an exhaustive computation and lack of being ideal under circumstances of the stochastic nature of loading on different components and vagueness of material structure geometry, besides variations in the operating environment and modelling limitations [7]. To deal with uncertainties, each computational

component should be well characterized to get rid of the effects of randomness and imprecision as well as inability in modelling while maintaining the feasibility and computational efficiency.

In the passing decades, uncertainty analysis have long been used increasingly due to the presence of more powerful computers [8]. Several methods, which can be categorized into four main approaches: worst case analysis, interval analysis, probabilistic methods and fuzzy set theory, have already been proposed to overcome the unwanted effects of uncertain system parameters; means of interval analysis, which is based on the interval mathematic, is used for tolerance handling and numerical rounding errors [9] as a simple approach.

Determining structural system parameters via Kalman filter is also introduced to understand the precise solution when the system is linear, [10] otherwise, linearization process is required. Kalman filter is developed to compensate the error in the acquisition of sensor data and model parameters even if the utilized model is imperfect or noise is present in the observation environment. Although, there are some limitations in this filtering process due the lack of knowledge in covariance of the observed data [11], Kalman filter is a perfect observer and can be applied to both linear and non-linear processes in determination of running parameters like suspension or dampers [12] when the vehicle is in operation by creating a dynamical model of the vehicle and appropriate placement of the sensors. As a commonly used filter, Kalman needs to satisfy two main definitions; the dynamic model which describes the propagation of the system in long term run and the stochastic process which describes system process noise and errors in the observations. Latter has an urgent outcome by means of performance due to uncertainty in covariance parameters of process noise and observation errors which affects the weighting of measurement against dynamic model.

For mechanical vehicle vibrations, ideal theoretical model generation is a tough job since the physical character is unpredictable due to imperfections between bodies and the environment. Optimization of system parameters like damping factor and stiffness constants need further investigation under random theory [13].

In vibration diagnostics, it is urgent to use the methods that are suitable for vehicle environment. It is known that vehicle vibration signals, in many conditions, behave non-stationary random characteristics [14]. One fast and suitable technique is short-time Fourier transform (STFT), which uses overlapping windows in time, accommodating non-stationary signals. However, this method requires several experiments of the same conditions to achieve reasonable performance. In comparison with this technique, Continues Wavelet Transform (CWT) is also employed [15].

In contrast to general approaches of vibration signal processing, some methods prove their efficiency in specific jobs. Gearbox related fault detection using time domain statistics like crest factor, kurtosis, the application of discrete wavelet transform and time-synchronous averaging, which provides removal of the noise, are reported to be efficient [16]. Diagnosis of gear defects is performed via wavelets and Kurtograms [17] or other multi-scale wavelet methods [18]. To retrieve periodic faulty gear tooth signals under heavy noise, maximum correlated kurtosis deconvolution is also employed [19].

First wayside approaches [20] for wheel defect detection was placed in New York which is based on impact load measurement in 1983. Afterwards, in 1996, Swedish has used strain gages in detection of wheel defects and now they have 190 wayside systems in service. In the literature, several different sensors are used to detect wheel defects like out-of-roundness, shelling and flats which lead to excessive impact on the rail and can increase the wear and tear of the track. In strain gage measurement related to wheel defect diagnosis, the most common features of the measured vertical force are average and maximum values [20]. To deal with wheel defects by trackside level, total of 128 strain gages are placed on the rails which cover 90% circumference of the wheels in different sizes [21] and both vertical and lateral forces are measured in 16 points of the rail. According to [22], investigation of wheel position effect is performed by using strain gages in a curvature of 484 m radius, while the operation speed is up to 100 km/h in a specific research station. Afterwards, lasers and high speed cameras are located so that they can retrieve the image of the wheel profiles [23]. This combined method is used for decision making for maintenance.

Fibre-optic sensor technology which is based on the change of the refractive index of ultra-violet ray on the targeted small area, is used as an extension of strain-gage measurement. The main advantages are electromagnetic immunity, ability of fabrication numerous sensors inside a fibre, resolving the recalibration problem and cost-effectiveness, easy installation, immunity to environmental temperature change, faster response and reliability referring to the study [24]. By using Fibre-optic sensors shear strain of the rail can be determined which is proportional to vertical impact force. Moreover, it is also possible to use these sensors to count the number of axels for train identification, speed detection, [25] monitoring weight of the train and wheel imperfections [26]. However, this methods comes with speed limitations of 15 km/h.

Ultrasonic sensors are also presented for wheel defect detection in the literature which are based on pulse-echo and pulse transmission. An application of ultrasonic sensor employment in wayside for wheel crack detection is based on special sensors which do not

require liquid couplings [27]. Other implementations require complex infrastructures and limited to constant and slow speed of the run [28], [29] and [30].

Acoustic sensors are also an appropriate way of detection wheel defects but again with speed limitations. Wheel defects emit a periodic acoustic impulse respect to the speed of speed of the run. For detection of the repetitive patterns related to wheel defects, low pass filtering and root mean square of the signal is used on 40 ms time windows and Fourier transform is followed [31].

Vibration sensors (accelerometers) also provides an efficient diagnosis of the wheel defects like; wheel flat, corrugation upon making comparison of energy levels and investigating power cepstrum which is very convenient to show the repetitive patterns of the wheel flat in the noisy signal [32]. However, using these technique comes with constant speed limitations. Determination of the degree of the failure of the wheel is also possible with fuzzy-logic method [33]. To do so, vibration sensors are allocated on the foot of the rail and three urgent parameters; center frequency, velocity of the train and vibration amplitude are considered. As a result, it is shown that train speed and center frequency have utmost effect in the vibration outputs. According to a recent research [34], piezoelectric and accelerometer sensors are mounted on the rail and using wavelet based methods and direct thresholding to distinguish the severity levels of the wheel flat, is reported to be efficient.

Using shear bridges, which are consistent of multiple strain gage elements, is reported to be more convenient than accelerometer sensors because the measurements are independent from train speed and load conditions, according to the study [35]. Nevertheless, using such systems require cumbersome calibration complexity and thus additional costs.

More advanced techniques like utilization of lasers and high speed camera is also presented in the literature. In the study [36], it is reviewed that high speed cameras and lasers are used in order to analyze the wheel profiles when the operational speed is less than 15 km/h. Retrieved profiles are then saved and wear amount of each wheel is monitored. Another methodology uses lasers to emit the wheels and cameras which are mounted nearby rails shoot the photo of the wheel wheel profile of freight trains while trains are in their operating speed up to 160 km/h [37]. These images are then compared to normal wheel profiles of other trains to make the decision.

Wayside diagnosis of the bearings is performed by microphone sensors and Doppler effect eliminator method [38]. Vibration based diagnosis of the inner, outer and rolling element faults of bearings of varying speeds, which may be suitable to wayside diagnosis, is performed by envelope analysis [39]. According to [40], worn bearing detection and crack detection may

be performed by utilizing wavelet features and least square support vector machines. In addition, harmonic wavelets are used with ideal band-pass filtration on the vibration signals in order to identify bearing defects [41]. Minimum entropy deconvolution is also applied on the faulty signals that behaves impulsive characteristics for bearings [42] and then envelope analysis is performed.

A few number of patented condition monitoring systems are existed across Europe for railway vehicles which is reviewed in a recent literature [43].

GOTCHA is an open wayside monitoring platform which is capable of wheel defect detection and load determination for wheels which is founded in Netherlands. The operational speed is 15-350 km/h while accuracy of 3% load measurement between 30-70 km/h operational speed is reported. Vehicle identification is maintained by Automatic Vehicle Identification (AVI) tags.

In Germany, LASCA makes the detection regarding to the deflection of a laser beam of deformation of the loaded rail and determine directional deformation of the rail which is proportional to Q-forces. The accuracy of 2-3% is reported in load measurements with operational speeds up to 350 km/h. Identification of railway vehicles is provided by ZLV bus. MULTIRAIL makes it able to monitor rail safety factors like vertical wheel forces and wheel set loads, as well as optimum load distribution. In MULTIRAIL, Radio-Frequency Identification (RFID) is present in order to recognize vehicles.

ARGOS, which is founded in Austria, presents step by step solutions by using strain-gage sensor based approaches to identify axle loads with a tolerance of 0.5% and measures dynamical response which may provide information about wheel irregularities and wheel-rail contact forces while the operational speed is 10-40 km/h. In addition to this, it enables determination of roundness of the wheel with a precision of 0.01 mm. Identification of the vehicles is performed by RFID. Many other techniques in company level are reviewed in the literature [44].

All in all, most of the trackside diagnosis systems are based on deformations which makes it harder to calibrate but easier to evaluate. Among all proposed methods in this section, neither an adaptation of a trackside measurement system inside metro tunnels is existed nor the proposed approaches belong to vibration based accelerometers or acoustic sensors.

1.1 Critical assessment and analysis of the current situation

Mechanical faults have similar behavior which leads to the possibility of same diagnosis framework implementation in multi-fault detection. Other systems such as strain gage arrays in

diagnosis of running gear provides monitoring however their principle of working is mostly based on force measurement which is easier to handle than evaluation of vibration based signals since the interaction of different structures and multiple presence of the same components affect output badly. However, these systems require dynamic modelling and additional calibration which is hard to maintain.

As well as vibration sensors, in the proposed diagnosis framework, acoustic sensors are also introduced. Using such sensors requires advanced filtering before further implementations of fault diagnosis may be applied due to heavy noise presence in tunnels. Moreover, other diagnostic systems deal with different vehicles that run on the same track passage whereas in the experiments related to this thesis all train sets are identical and no significant load change is present even if it is fully loaded.

Fortunately, while retrieving the experimental data obtained from the passages of wayside diagnostic environment, it is possible to make measurement of the same train set a few times per day, thus abnormal sensor outputs may be ignored in the process and multiple chances to diagnose same running gear of the train sets are present. Furthermore, thanks to the number of vibration and acoustic sensors in wayside environment provides twice measurements when each train passes for a double check.

Proposed algorithms may help designing a smart diagnosis system of running gear related faults like wheel defects, wheelset eccentricity, bearing faults and gearbox faults in combination with data driven and model based approaches. The research activity belongs to thesis may have attention of the maintenance specialists and engineers that work in condition monitoring systems in railway vehicles.

2 DEFINITION OF DISSERTATION OBJECTIVES

Wayside diagnostics have utmost interest of the researchers due to availability of more computational power that makes able to use of complex methods in designing vehicle condition monitoring systems. Real time or offline evaluation of sensor data may indicate possible problems related to some specific mechanical parts of a vehicle which is vital for low cost maintenance and superior to periodical service. In addition to cost friendly nature of wayside diagnostics, it may serve real-time monitoring of individual train sets and structures when an efficient evaluation process is maintained.

One promising application may be considered as the main subject of this thesis; condition monitoring of feasible number of mechanical structures of running gears of the train sets of Prague Metro in close complex traffic using several cutting edge techniques. Upon using of retrieved acoustic and mounted mono-axial accelerometer sensors that are employed in the environment of the passages which provides data for several runs of the same train sets, a cost friendly wayside diagnosis of Prague metro type 81-71M is aimed to be achieved. Proposed methodologies; Histogram Enhanced LCP Kurtograms (E-LCP-K), different types of wavelet energy methods (WPE, W-WAV), time domain statistics, Multipoint Optimal Minimum Entropy Deconvolution (MOMEDA) and wavelet denoising, may effectively be used on the signals that are segmented from chosen healthy and faulty wheelsets and classification of health status of the vehicle or abnormal cases are then determined via state-of-art classifiers and combined classifier approaches.

Another urgent objective is to validate the proposed methods and their efficiency in structural health monitoring with measured and simulated faulty data. Since in wayside diagnostic systems, retrieval of data of the same train set multiple times is possible, it is vital to not to use all sensor data unless it is in expected range. These cases may cause false positive errors and ought to be discarded in an appropriate way.

Main objectives of the thesis are:

1) Designing an appropriate framework for fault diagnosis of running gear components like wheel, wheelset/ traction motor bearings and gearboxes in railway vehicles
2) Using cutting-edge feature extraction and classification techniques in diagnosis
3) Application of contemporary digital filtering techniques in signal processing
4) Validation of the methods both with measurement and simulated faulty data
5) Maintain a real-time monitoring by accelerometer and acoustic sensors data

2.1 Test environment and signal acquisition

In this research, two different wayside diagnostic measurements are investigated in order to build an efficient framework for metro train sets travelling inside the tunnel of Prague Metro-A line. Measurements were carrying out in the project Competence Centre of Railway Vehicles, No. TAČR TE01020038.

Firstly, in Malostranská, the passage had been selected just before the transition curve approximately 100 m from Malostranská metro station which is directed to Nemocnice Motol. The measurement system of the wayside diagnostics system has total of eight sensors; six one-axial accelerometers (Z1-Z6) of type Kistler 8702B100 which allows measurement up to 100g, on the top of feet of the rail, two prepolarized free-field microphones (M1, M2), which allows sound recording in 6.3 - 20 000 Hz range of type Brüel & Kjær 4188 are between the rails (same horizontal alignment with sensors Z1 and Z2. Two additional optical gates of type Balluff BOS016U with 500 Hz sampling rate (G_A, G_B) that accompany the accelerometer sensors to ensure wheel positions, targeting directly to the wheelset centers (Figure 1) [45] had been placed approximately 100 m from Malostranská in the direction to Nemocnice Motol metro station. Data was recorded by NI-cDAQ-9234 instrument, which provides 51.2 kHz sampling rate on all ten channels, during whole day while metros have been passing by. Malostranská database includes all passes of metro train sets in one day and always in the same direction just before the transition curve which makes it possible to retrieve the data of the same train sets more than ones. After having discarded the unusual signals due to environment or sensor overloading, total of 160 train passes are available for process.

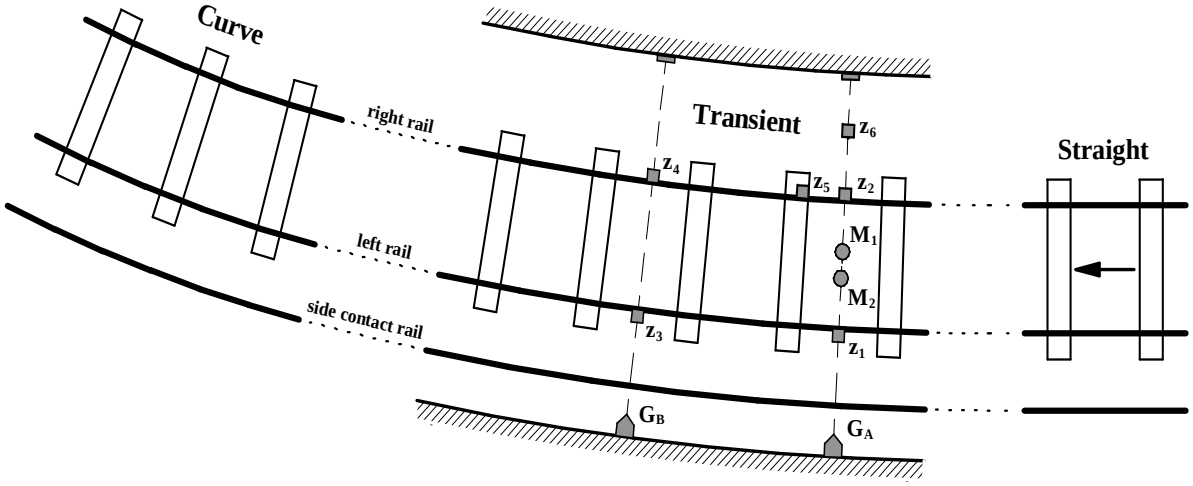

Figure 1: Sensors localization in wayside diagnostic system Malostranská towards Nemocnice Motol passage

Second experimental environment was located between Dejvická and Bořislavka metro stations. The passage was selected in the straight track with positive slope of 40‰ from

Dejvická. Five accelerometer sensors, four of which (Z1-Z2-Z3-Z4) were placed on the foot of left and right rails to observe vertical vibrations on rails while train sets are passing by. The remaining sensor (Z5) was placed on the concrete sideway of the passage. Three microphones (M1-M2-M3), one of which (M3) was placed on the tunnel wall, were also allocated in the wayside diagnostic system to obtain noise related features of different fault modes. All sensor types were identical as it had been in Malostranská wayside measurement system and all data recordings were done via NI-cDAQ-9234 instrument as in the same way in Malostranská passage with 51.2 kHz for accelerometer sensors and microphones while 500 Hz for optical gates (G_A, G_B) that targets the wheels. One day of recordings show that 226 train passes have successfully been retrieved in all channels and prepared for evaluation. Figure 2 shows the sensors on the test environment while they are in operation between Dejvická and Bořislavka.

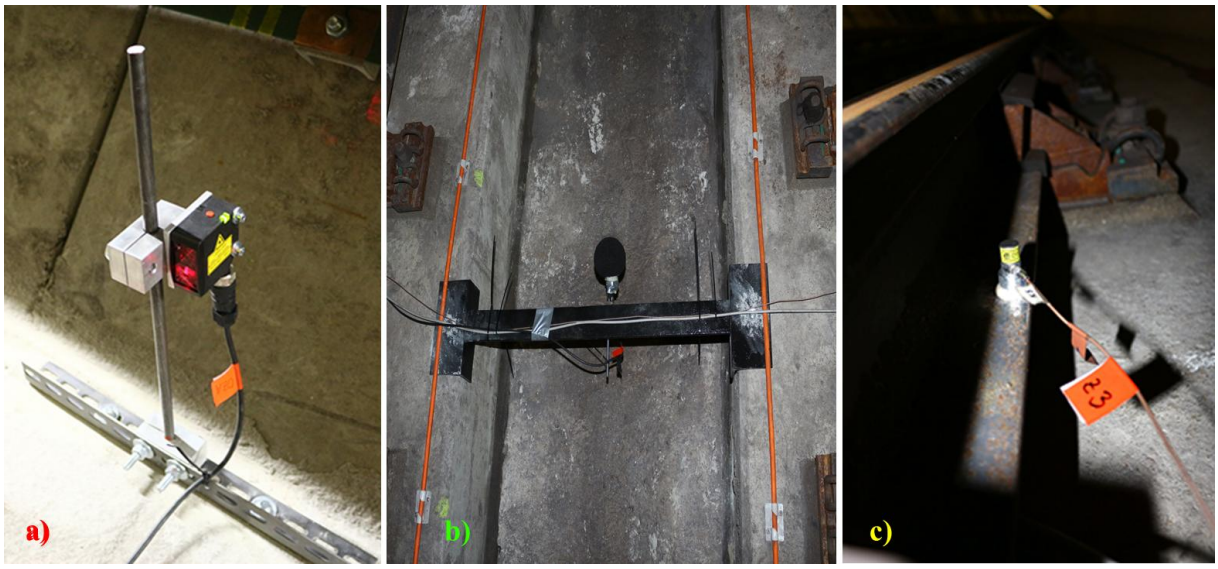

Figure 2: Balluff BOS016U optical gate (a), Kistler 8702B100 acoustic sensor (b), Brüel & Kjær 4188 vibration sensor (c) (author: Vágner J.)

Sensor localization and related dimensions on the second wayside diagnostic system are shown in Figure 3.

In the wayside experiments, all train sets have five passenger cars which are almost identical by means of dynamic behavior. The main difference that influences output signals is that they have different wheel diameters and maintenance schedule.

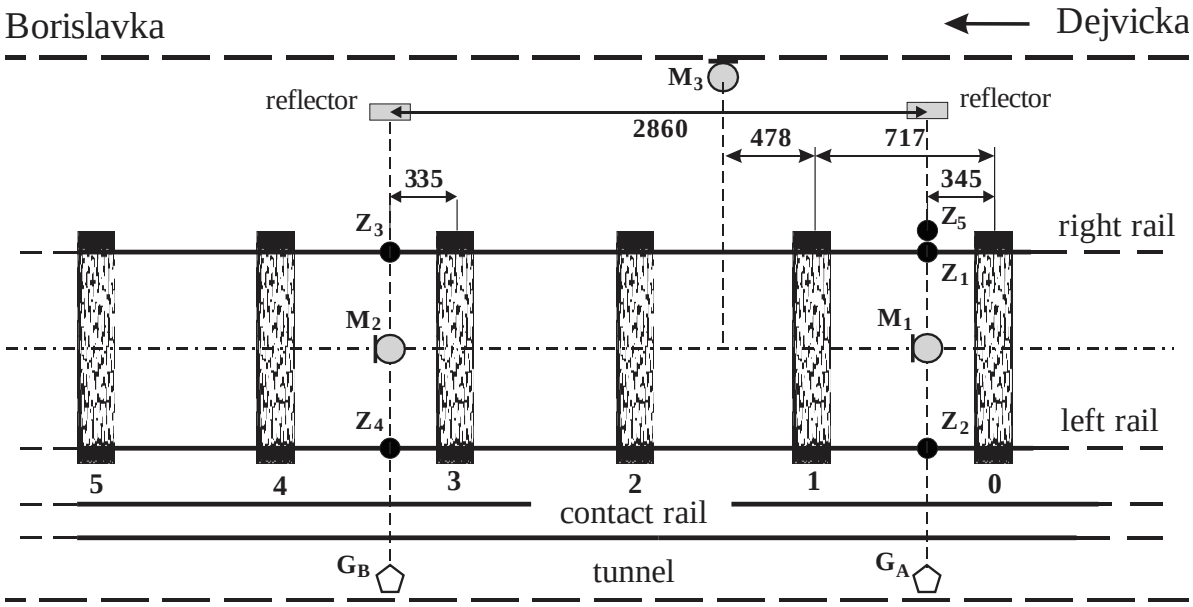

Figure 3: Sensor localization in wayside diagnostic system between Dejvická and Bořislavka metro stations

Simplified model with dimensions of metro type 81-71M, which is being used in Metro-A line in Prague, may be seen in Figure 4 and 3D model of the vehicle and track is given in Figure 5.

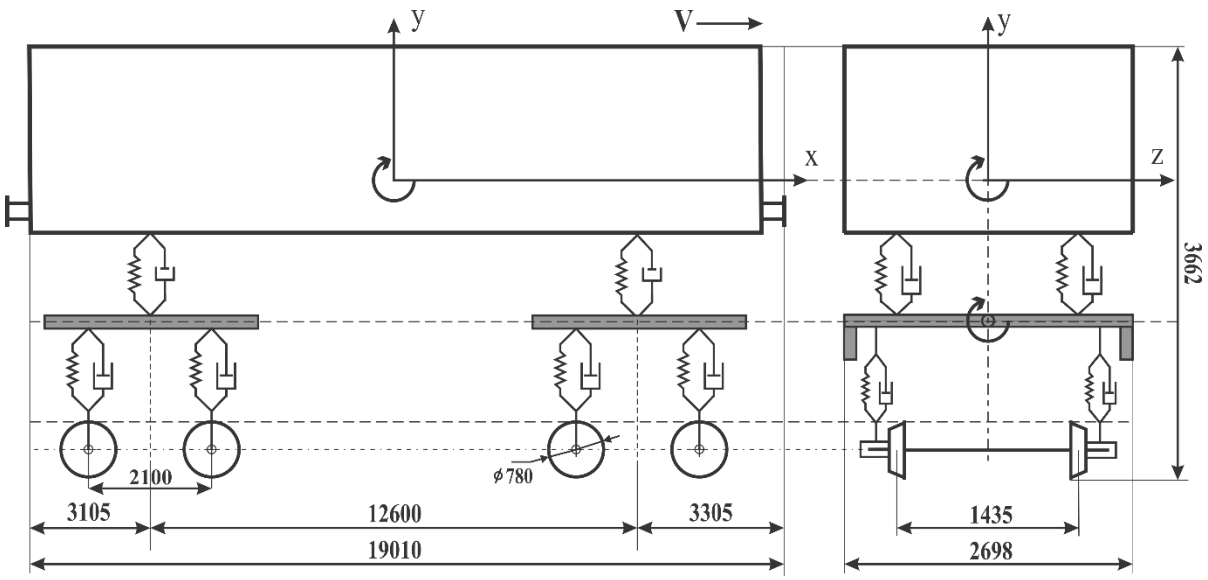

Figure 4: Model and dimensions of metro type 81-71M; side view (left), front view (right)

All train sets running in Prague Metro-A are identical type 81-71M and have five passenger cars. Wheelset arrangement of each train set is: $(B_0'B_0')+(B_0'B_0')+(B_0'B_0')+(B_0'B_0')+(B_0'B_0')$.

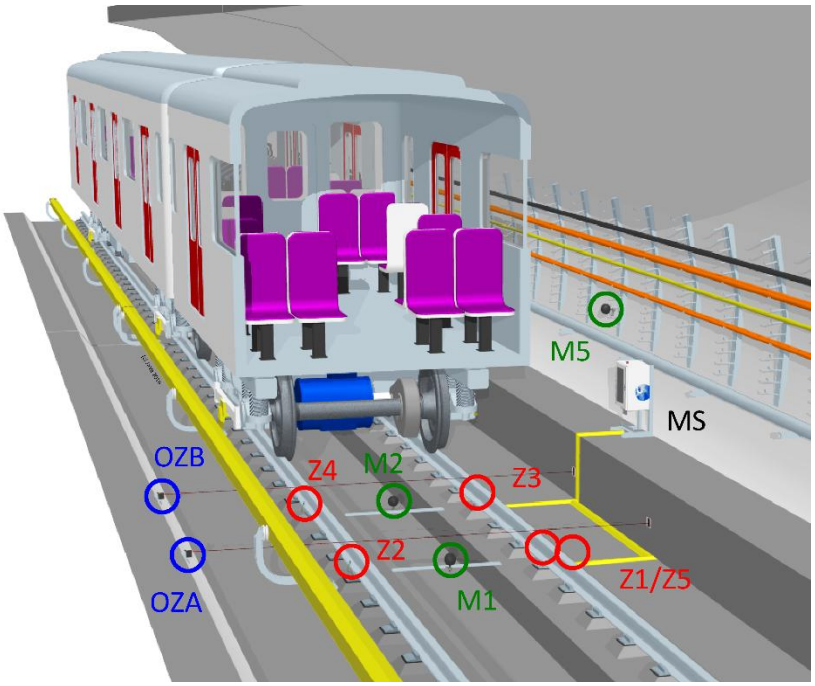

Figure 5: 3D-model of test environment between Dejvická and Bořislavka metro stations; MS: the measurement system [46]

2.2 Diagnosis of multiple faulty modes of running gear

In this section, possible faulty modes that may be identified by wayside measurements are characterized and model based approaches to calculate faulty frequencies of different structures which are existed in Prague Metros that travel between Depo Hostivař and Nemocnice Motol metro stations. These frequencies are vital to investigate in order to design a filtering scheme before further implementations are performed since they are distracted by heavy noise which is present in the environment of the measurement.

2.2.1 Wheelset related faults and characteristic frequnecies

The interaction of railway vehicle and track is mostly affected by the wheel defects and consideration of propagation of this frequency is urgent to examine the relationship between wheels and nearby structures like gearboxes and bearings. Two main fault types are assumed to be most common and significantly diminishes the quality of the run; wheelset eccentricity and wheel defects.

In the construction or mounting phase, the balance between axes of the wheelsets and wheels may be interrupted. This is due to the shift of the center of the wheelset and fails staying in the same axis of rotation. These failure is so called unbalanced eccentricity (Figure 6) and may also be observed overtime due to wear and fatigue.

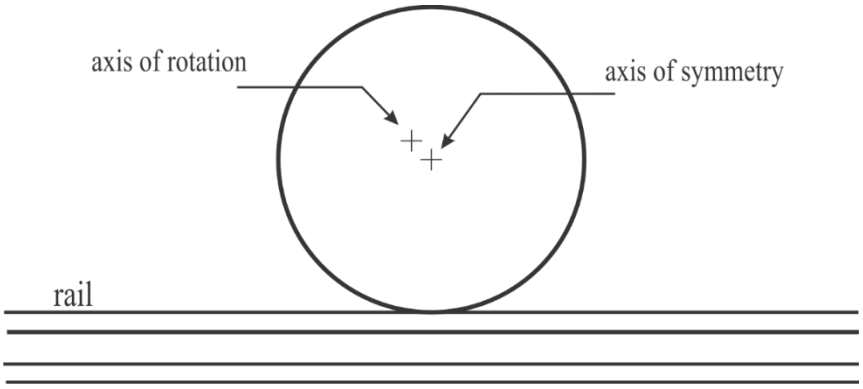

Figure 6: Wheelset eccentricity related failures

Wheelset eccentricity related faults have the same frequency as the rotation of the wheel itself. The formulation of this fail mode frequency is shown in Eq. (1) where v is the translational velocity of the train and D_k is wheel diameter which may be assumed as the average value of right and left wheels.

$$f_{ws} = \frac{v}{\pi D_k} \tag{1}$$

Since the minimum and maximum speed of the run in Malostranská passage is known, an interval of expected frequencies may be calculated which may be seen in Table 1.

Table 1: Wheelset eccentricity faulty frequency range for train set 81-71M

Location	Wheel diameter [mm]		Frequency [Hz]		
	D_{min}	D_{max}	v [m/s]	$f_{ws\ max}$	$f_{ws\ min}$
Malostranská	730	785	15	6.5	6.1
			20	8.7	8.1
Dejvická			15	6.5	6.1
			22.2	9.7	9.0

Wheelset eccentricity related faults have the same frequency as the wheel itself. The formulation of this fail mode is shown in Eq. (1).

Another fail type on the wheelset is known as wheel defects which means the degradation of the wheel material along the surface of the wheel. These defects are harmful to both running performance of the train set and the rail itself. It is possible to identify those faults by utilizing a wayside diagnostic system with accelerometers on a passage of the passing of the

train set [47]. This fault type characteristic frequency is also harmonic with the rotation of the wheel f_{ws} and the same procedure in Eq. (1) may be applied for speed-specific frequency identification. An example figure showing the profile related defects may be seen in Figure 7.

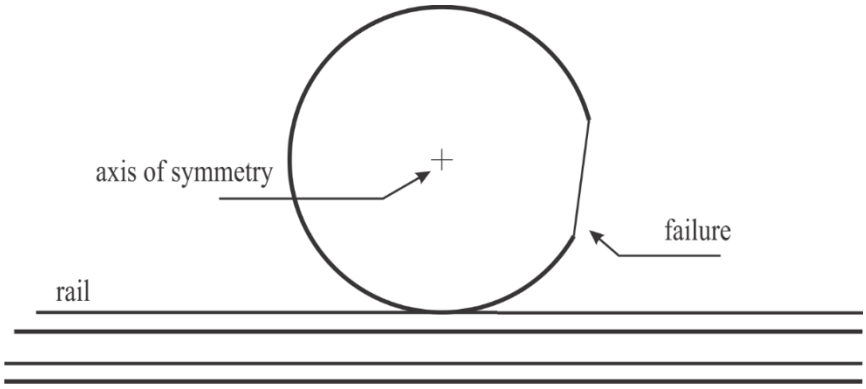

Figure 7: Wheelset defects due to degradation

2.2.2 Condition of normal and faulty gearboxes

Numerous number of fault types in connection to gearboxes, which are located to the nearby locations of the wheelsets, are existed. Gear related mechanical faults include tooth meshing faults, misalignment, cracked or worn teeth, eccentric gears while rotor and shaft related faults may also be observed; unbalance, bent shaft, misalignment, loose components and cracked shaft [16]. All given possible fault types have different symptoms by means of vibration analysis. It is known that the most important vibration signal frequency is gear meshing frequency and its harmonics. When this harmonic components increase one can imply that gearbox condition is not healthy. Heathy gearbox tooth frequency can be calculated via Eq. (2), where z_1 is number of teeth of smaller gear, z_2 is number of teeth of larger gear, f_{TM} is the frequency of traction motor and f_{ws} is the frequency of rotational frequency of the wheelset.

$$f_z = z_1 . f_{TM} = z_2 . f_{ws} \tag{2}$$

Calculation of different failure mode frequencies are demonstrated in Table 2 for Prague Metro type 81-71M in Malostranská location where k is the number of harmonics that related failure produces in frequency domain.

Table 2: Model based characteristic frequencies of gearboxes for metro type 81-71M

Parameters		**81-71M**		**Explanation**
Dk	[m]	Worn wheel	New wheel	Diameter of the wheel
		0.730	0.780	
v	[m/s]	v_{max}	v_{min}	Wheelset rotation speed
		20	15	
z2	-	80		Number of teeth on bigger wheel
z1	-	15		Number of teeth on smaller wheel
Fault Mode		**Frequency**		**Explanation**
f_{ws}	[Hz]	8.7	6.1	Wheelset defects
f_{TM}	[Hz]	46.5	32.6	Traction motor eccentricity
f_z	[Hz]	698	490	Tooth frequency
f_{zh}	[Hz]	k·698	k·490	Tooth wear
f_{zmws}	[Hz]	698 ± k·8.7	490 ± k·6.1	Modulation of tooth frequency by f_{ws}
f_{zmTM}	[Hz]	698 ± k·46.5	490 ± k·32.6	Modulation of tooth frequency by f_{TM}

Gearboxes that transmit mechanical force to the wheelsets of metro 81-71M are also identical in each bogie. The gearboxes are suspended by a rubber spring which is illustrated in Figure 8.

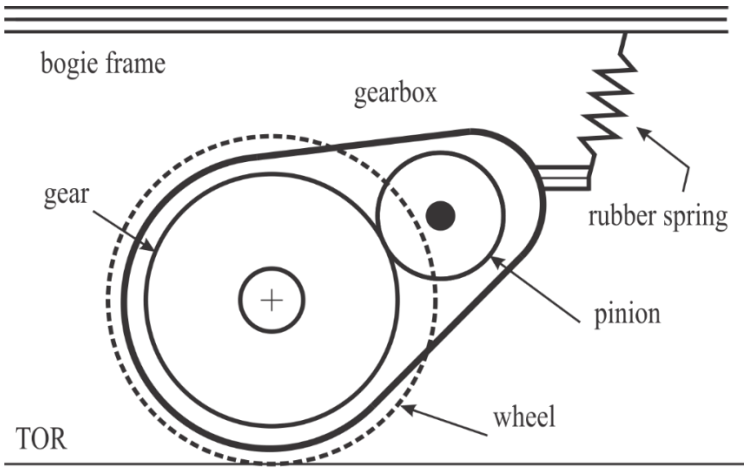

Figure 8: Gearbox drawing of metro type 81-71M bogie

Since gearbox and traction motor is always in interaction, it is urgent to consider the connection between traction motor and the gearbox which is shown in Figure 9.

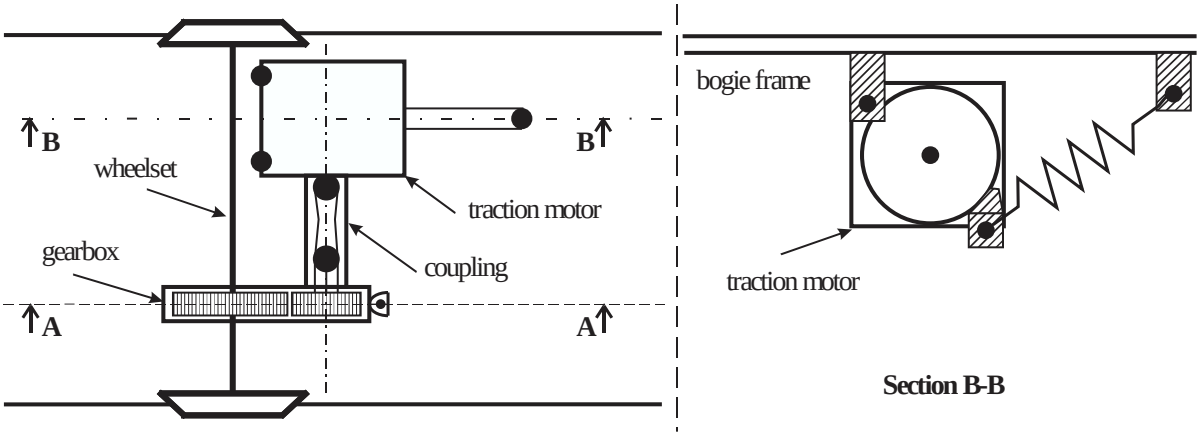

Figure 9: Gearbox interaction with traction motor of metro type 81-71M bogie; top view (Section A-A), side view (Section B-B)

The connections between bogie and traction motor and as well as gearbox are shown in Figure 10 and Figure 11 for metro type 81-71M.

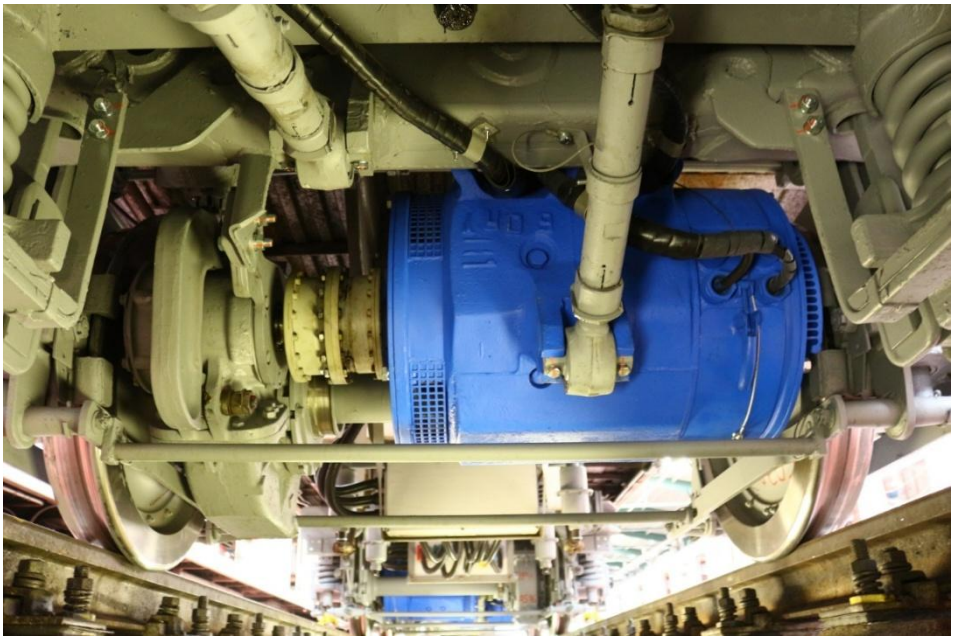

Figure 10: Traction motor localization on the bogie for metro type 81-71M (author: Vágner J.)

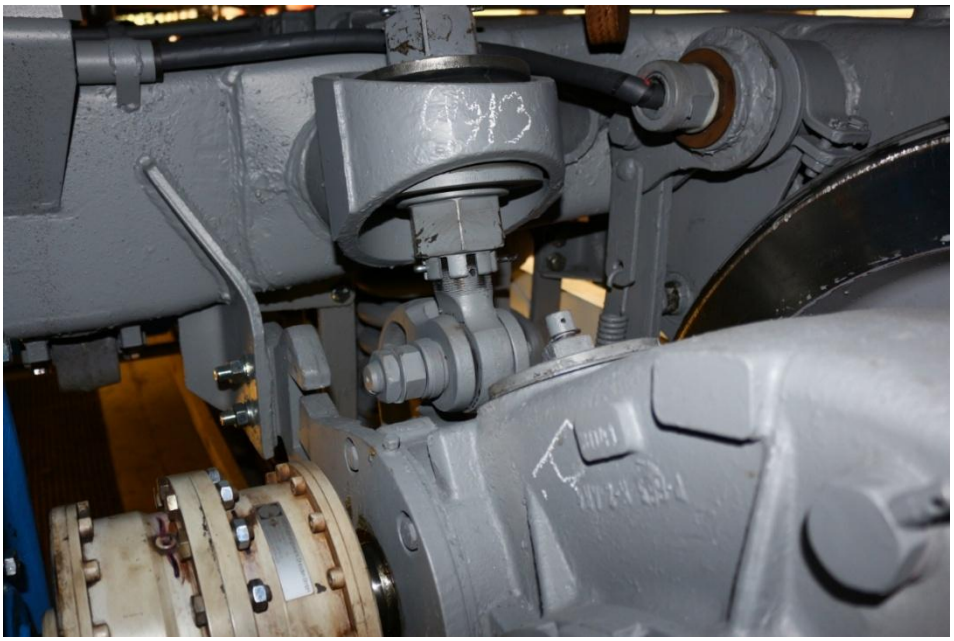

Figure 11: Traction motor connection on the bogie for metro type 81-71M (author: Vágner J.)

2.2.3 Condition of healthy and faulty bearings

Determining faulty states of rotating element bearings may be maintained via model based approaches. In rotating machinery, rolling element bearings generally has two rings; interior and exterior. Between the rings, rolling elements, which enables uniform spacing and prevents direct touch of the roller, within a cage are existed. Typical failures occur in those structures due to defects in one or more of the elements. These defects may be generated by material imperfections of the material, lubricant failure, misaligned load or excessive stress in the contacts and can be formulated using the geometry of the bearing which is formulated in Eqs. (3)-(6), [48]

$$f_{BFBI} = \frac{n}{2} f_{ws} \left(1 + \frac{d_0}{d_s} \cos \alpha \right) \qquad (frequency\ of\ inner\ ring) \tag{3}$$

$$f_{FT} = \frac{1}{2} f_{ws} \left(1 - \frac{d_0}{d_s} \cos \alpha \right) \qquad (frequency\ of\ cage) \tag{4}$$

$$f_{BPFO} = \frac{n}{2} f_{ws} \left(1 - \frac{d_0}{d_s} \cos \alpha \right) \qquad (frequency\ of\ outer\ ring) \tag{5}$$

$$f_{BSF} = f_{ws} \frac{d_s}{2d_0} \left(1 - (\frac{d_0}{d_s} \cos \alpha)^2 \right) \qquad (frequency\ of\ rolling\ element) \tag{6}$$

where d_0 is the ball diameter and d_s is the distance between the center of opposing balls and α is the ball contact angle.

In the experimental environment of Prague Metro-A line, wheelset bearings of train sets have double cylindrical bearings of type FAG 566612 and FAG 566613 which are shown in Figure 12 while traction motor bearings of train sets are type NH 310 MC3 and NH 313 MC3 which are shown in Figure 13.

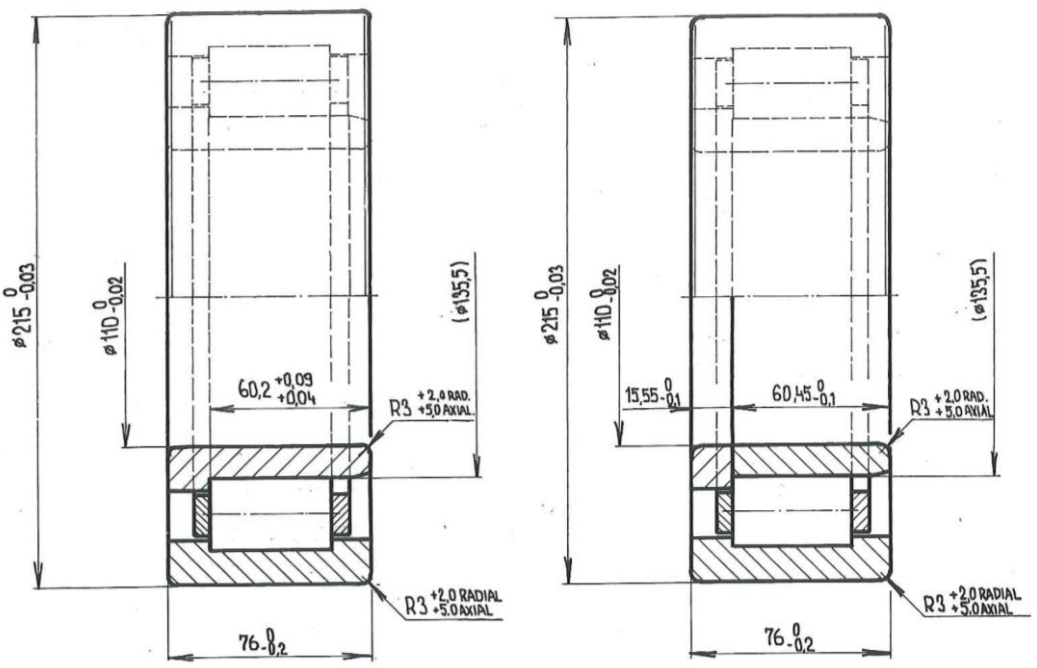

Figure 12: Schematics of bearings type FAG 566612, FAG 566613 [49]

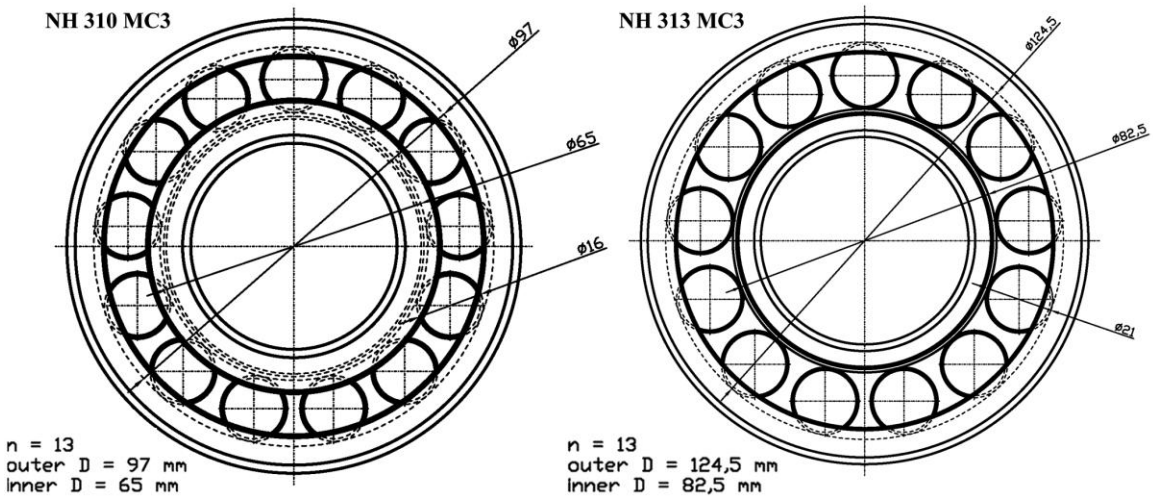

Figure 13: Schematics of bearings type NH 310 MC3, NH 313 MC3 [50]

Calculation of characteristic frequencies according to given speed interval of possible fault types of bearings that are used in Prague Metro-A are shown in Table 3.

Table 3: Model based characteristic frequencies of wheelset and traction motor bearings for metro 81-71M

Parameters			FAG 566612		NH 310 MC3	
D_k	wheel diameter	mm	785	730	785	730
v	speed	m/s	15	20	15	20
f_{ws}	wheelset frequency	Hz	6.1	8.7	6.1	8.7
d_0	rolling element diameter	mm	26		16	
d_s	pitch diameter	mm	161		97	
n	number of elements	-	15		13	
f_{BPFO}	outer race fault freq.	Hz	38.3	54.8	33.1	47.2
f_{BPFI}	inner race fault freq.	Hz	53.0	76.0	46.2	65.9
f_{BSF}	rotating element fault freq.	Hz	18.3	26.3	17.9	25.6
f_{FT}	cage fault freq.	Hz	2.6	3.7	2.5	3.6

3 OVERVIEW OF SUPPOSEDLY SELECTED METHODS

The optimal implementation of mechanical models and diagnosis of mechanical problems have always idealization problems due to the error in observed data, which could be realized in a better way, utilizing the following methodologies.

3.1 Wavelet denoising

Vibration and acoustic signals are badly affected by the noise, which can be modelled as Gaussian white noise, impulsive noise or normal distributed Gaussian noise. One common way of denoising such signals is using wavelet techniques, which is based on discrete wavelet transform, which divides the signal into desired number of scales and makes single or multi-level noise estimation and carry out the thresholding process with the specified thresholding algorithm to adjust coefficients of the decomposed signal.

3.1.1 Discrete wavelet transform

In most of the signal processing applications, Discrete Wavelet Transform (DWT), which is a time-scale representation of the discrete data with multiple scales, is used for non-stationary signals [51]. Numerous wavelet functions are introduced in the process of wavelet transform Haar, Daubechies, Symlets etc. [52] which are the modified versions of the mother wavelet function (Figure 14).

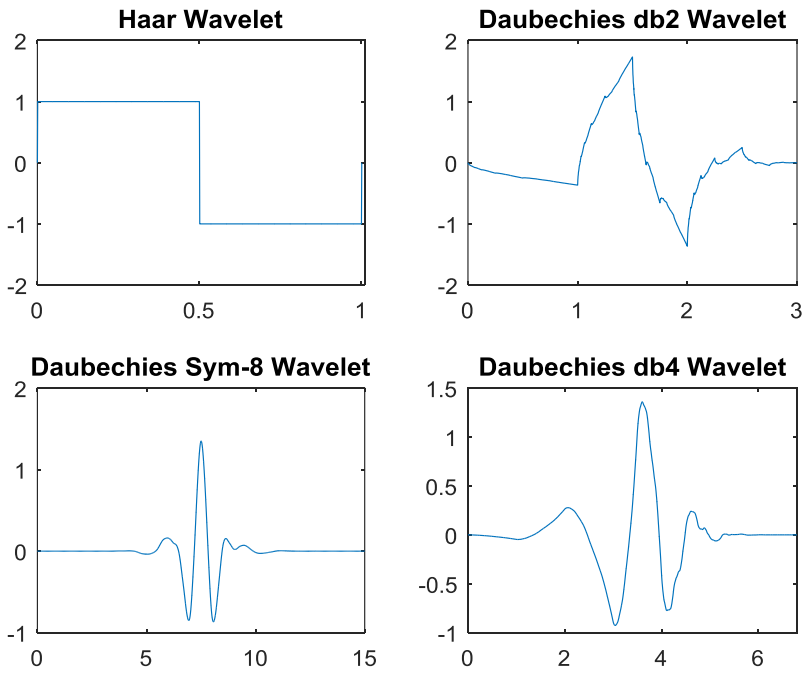

Figure 14: Examples of wavelet functions of DWT

The mathematical description of the DWT for discrete signal $x[\mathrm{n}]$ is shown in Eq. (7) and (8)

$$\psi_{\mathrm{a,b}}[\mathrm{n}] = \frac{1}{\sqrt{a}}\psi\left[\frac{n-b}{a}\right] \tag{7}$$

$$\mathrm{X}[\mathrm{a},\mathrm{b}] = \sum_{n=-\infty}^{\infty} x[\mathrm{n}]\psi_{\mathrm{a,b}}[\mathrm{n}] \tag{8}$$

where $\psi[\mathrm{n}]$ is the wavelet function that is used in the analysis and a and b are the dilation and location parameters, respectively. DWT is based on using filter banks that describe frequency content of the signal for time intervals. For this purpose low-pass filter (LPF) and high-pass filter (HPF) are employed. The coefficients of the LPF is called approximation coefficients (A) while for HPF they are called detail coefficients (D). The filtering algorithm is shown for a two level wavelet decomposition for a discrete signal $x[n]$.

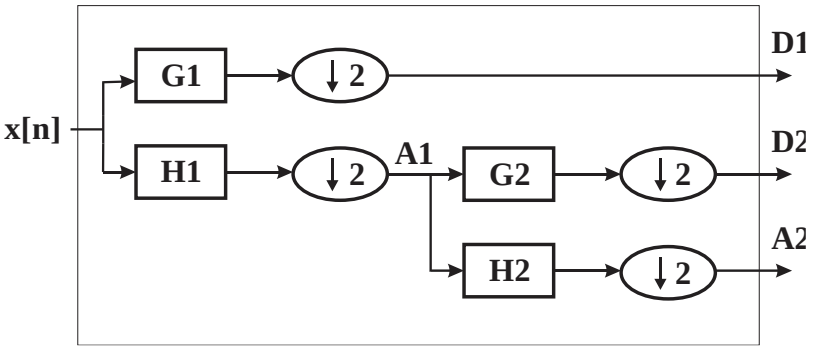

Figure 15: Two level wavelet decomposition for a discrete signal x[n]

3.1.2 Denoising with maximal overlap DWT

The maximal overlap DWT (MODWT) is a translation invariant modification of DWT [53]. Similar to DWT, linear filtering operations and scaling coefficients respect to time are to be calculated. MODWT is more convenient than DWT since it does not require the signal length (N) to be a multiple of 2^n for n level decomposition [54] preserving translational invariance.

Applying MODWT on a discrete signal needs the determination of wavelet filter and the maximum number of scale. Once these parameters adjusted, coefficients can be determined by applying MODWT on a time-series signal $x[n]$. After acquiring MODWT wavelet coefficients, one can start denoising operation for the signal by using a thresholding for the coefficients for eliminating unnecessary information on the signal.

In the proposed wavelet denoising algorithm subjected to this thesis, number of composition level is chosen empirically as 4 which preserves wheel defect faulty signal better and ‘soft thresholding” is applied on the signal as in the literature [55]. Wavelet function is chosen as Daubechies (db2) due to being efficient in bearing fault diagnosis as preferred in the research [56]. Throughout the process multi-level noise estimation is used as it is in the research [57].

Upon discarding unwanted information on the signal inverse MODWT is used to reconstruct the denoised signal.

3.2 Wavelet packet analysis

In signal processing, one common approach to extract features of non-stationary vibration signals is a Short Time Fourier Transform based method so called wavelet packet analysis is introduced. Wavelet packaging divides the Fourier spectrum of the signal into desired number of frequency bands which leads to different frequency resolution. Referring to the number of levels L_w while $n_w = 2^L$ where n represents the number of components in Wavelet Packet Transform (WPT). Afterwards, filtering is carried out on the signal to obtain low and high frequency components which is followed by downsampling to achieve next level. Referring to Figure 16, since being not time-invariant [58], energy calculation of each wavelet package is performed to rise its immunity to detection of the transients in non-stationary nature of railway vibration signals and Wavelet Packet Energy (WPE) coefficients are achieved (Figure 17).

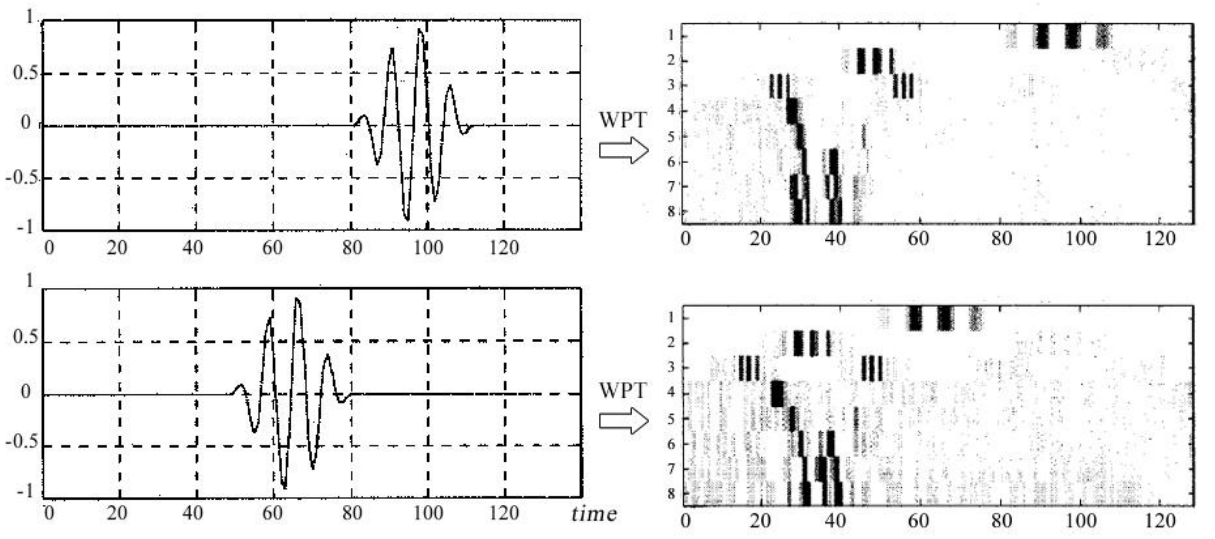

Figure 16: Transient signals shifted in time-domain (left), resultant eight level WPT (right)

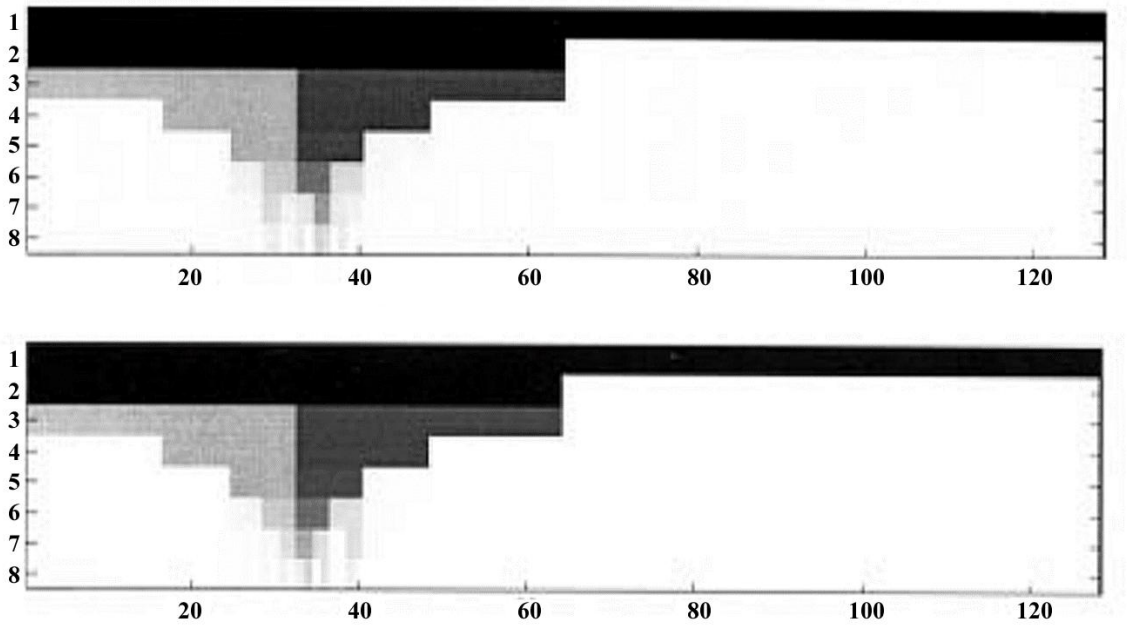

Figure 17: Eight level quantized WPE for the signals in Figure 16

In the proposed methodologies based on wavelet packet energy for the fault diagnosis, two different forms of WPE are used; three and five levels of wavelet packet energy (WPE_3, WPE_5), Weighted Wavelet Energy (W-WAV) [59]. The latter, which has proven its efficiency in motor related fault diagnosis is consistent of weighted energy of 2-step DWT coefficients; Low-High (LH), High-Low (HL) and High-High (HH) as shown in Eq. (9).

$$(\text{W-WAV}) = |LH| + |HL| + \left|\frac{HH}{2}\right| \tag{9}$$

Wavelet packet energy calculation is not time consuming since it is a direct approach and one can easily understand the frequency amount of the interested fault type with the specified frequency resolution. Thus, it may be a simple and comparable approach which can be used in faulty diagnosis of rotating machinery faults in railway vehicle diagnostic.

3.3 Kurtogram based methodologies

One of the state-of-art diagnosis techniques in condition monitoring is so called Kurtogram which is an extended method based on spectral kurtosis [60] that had been proposed long before in the literature.

Kurtogram approach provides a further and faster computation of transforming the signal into frequency-delta frequency spectrum. Even it is less time consuming than old spectral

kurtosis, another method Fast Kurtogram (FK) [61] is also introduced which divides the signal in low and high frequency bands as in the way of STFT but with different order to emphasize where spectral kurtosis is maximum on a grid view of frequency-delta frequency domain boosting its operation by a few thousand times than regular spectral kurtosis.

3.3.1 Spectral kurtosis and complex envelope

In the frequency domain, investigation of kurtosis leads to a very good indication of periodic transient determination which is connected to the faults of the rotating machinery, mostly.

Spectral kurtosis and complex envelope analysis is considered to be a proven and cutting-edge methodology for rolling element bearing fault diagnosis [62]. When the frequency of the fault for each faulty mode is known for the operating speed of the rolling element, FK approach may filter out the transients according to the level and frequency band. In Figure 18, Kurtogram calculation of 5-level for a wheel flat signal sample is shown with 51.2 kHz sample rate (more intensity on the Kurtogram refers to higher kurtosis in that decomposition level).

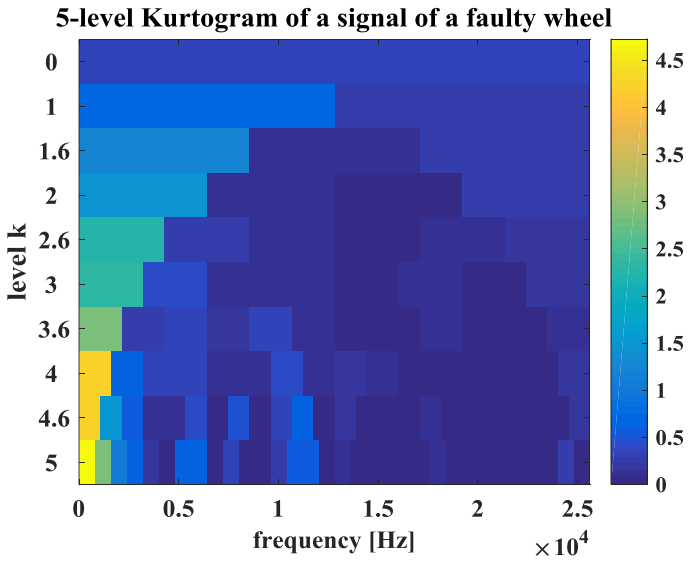

Figure 18: 5-level kurtogram of a faulty signal of a metro wheel flat.

It is obvious that highest spectral kurtosis is present on the fifth level of the FK. In the proposed algorithms subjected to this thesis, real part of fifth level of FK complex envelope (KURT-ENV) is used in the diagnosis of different faulty modes like wheel defects, rotating element bearing faults, gear tooth fault and traction motor eccentricity. Posterior features of the KURT-ENV also investigated in the diagnosis which are based on time-domain statistics or wavelet packet analysis.

3.3.2 Histogram enhanced LCP-Kurtograms

This novel method is based on Local Binary Pattern (LBP) [63] which is an efficient feature extraction tool that is used in pattern recognition especially for extracting textural features and requires the Kurtogram image of the signal to make the feature extraction.

LBP approach maximizes the mutual information by labeling the intensities of a two-dimensional (2D) signal. By using a thresholding in a window of given radius for the neighborhood of each pixel intensity regarding to center pixel, it evaluates a binary number for each segment for the whole signal which may be seen in Eq. (10) [64]

$$LBP(P,R)=\sum_{i=0}^{P-1}u(g_i-g_c)2^i \tag{10}$$

where P is the number of pixels, g_c is the center pixel and g_i belongs to i_{th} pixel intensity level. LBP approach is capable of working in conditions when color map is different in an efficient way.

Another variant of LBP is so called Local Configuration Patterns (LCP) is also presented in the contemporary literature. LCP descriptor provides local information and circularly shifted histogram of pattern occurrences which makes 2D input signal rotation invariant [65]. Combination of microscopic features and local features which represent the binary pattern occurrences constructs the feature vectors of LCP which is shown in Figure 19 [66].

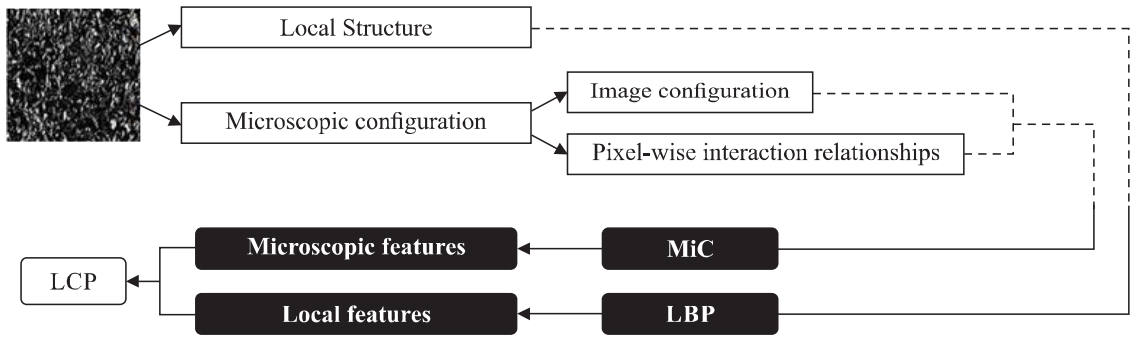

Figure 19: Schematic of the algorithm of LCP

Histogram equalization (HE) is a well-known enhancement technique that is introduced in pattern recognition literature [67]. HE normalizes pixel values according to the distribution frequencies of each intensity level and reconstruct the 2D signal in a way that reproduced pixels emphasize the differences in a much more distinctive way.

In the proposed algorithm, Kurtogram is firstly resized into 128 x 128 pixels by bi-cubic interpolation [68]. Afterwards, using three algorithms that is told in this section, the novel methodology is produced so called Histogram Enhanced LCP-Kurtogram (E-LCP-K) which is demonstrated in Figure 20 [69] and without HE it is called as LCP-K.

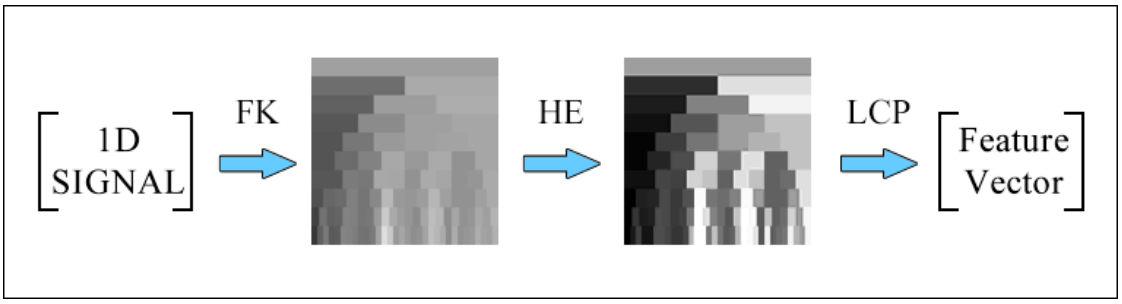

Figure 20: Procedure of Enhanced LCP-Kurtogram of five level FK

E-LCP-K method makes 2D signal processing tools and pattern recognition approaches able to use on 1D signals. Feature matrix is fixed to a feasible value of 81x1 due to the nature of LCP which may be assumed as an efficient dimension reduction independent from the input signal size.

3.4 Time-domain features

In vibration based signal processing, faulty signals show similar characteristics not only in Fourier domain but also in time domain. The simplest way is to use statistical features of related faulty signals that spans time-domain. In order to identify representative faulty patterns, statistical time-domain feature extraction methods are present in contemporary studies in mechanical fault diagnosis [70], [71].

For this purpose, statistical time-domain features; energy, mean (μ), standard deviation (σ), maximum (max), minimum (min), kurtosis, skewness and crest factor are calculated from each sample as preferred in a research [72] which especially used in bearing fault diagnosis. For a discrete signal $x(n)$ with length N, the formulation of these features can be calculated as in Eqs. (11) and (12).

$$Kurtosis: \sum_{n=1}^{N} \frac{(x_n-\mu)^4}{N\sigma^4} - 3, \qquad Skewness: \sum_{n=1}^{N} \frac{(x_n-\mu)^3}{(N-1)\sigma^3} \tag{11}$$

$$Energy: \sum_{n=1}^{N} |x_n|^2; \qquad Crest\ Factor: 20\left[\log_{10}\left(\frac{\max(x)}{\sigma(x)}\right)\right] \tag{12}$$

In addition to these time domain features, three features, which may help diagnosis of mechanical faults, are also introduced; spike energy [73], impulse factor [74] and center frequency [75].

In the proposed feature extraction methods based on time-domain data statistics, three different combination are used; STATS (Eq. (13)), TDF (Eq. (14)), TDFs (Eq. (15)).

$$STATS = [mean, standard\ deviation, mode, minimum, maximum]_{5x1} \tag{13}$$

$$TDF = \begin{bmatrix} energy, mean, standard\ deviation, max, \\ min, kurtosis, skewness, crest\ \ factor \end{bmatrix}_{8x1} \tag{14}$$

$$TDFs = \begin{bmatrix} energy, mean, std\ dev, max, min, kurtosis, skewness, \\ crest\ \ factor, impulse\ \ factor, spike\, energy, center\ \ frequency \end{bmatrix}_{11x1} \tag{15}$$

3.5 Multipoint optimal minimum entropy deconvolution adjusted

This method is an extension of an iterative algorithm so called Minimum Entropy Deconvolution (MED) [76] which is used in fault diagnosis of bearings and gearboxes.

MED is capable of deconvolving a single impulse not lack of deconvolving impulse trains. Since not being computationally efficient due to being an iterative algorithm, a non-iterative optimal solution for the deconvolution filter, optimal MED (OMED) is developed [77]. The problem of OMED is that it has a discontinuity problem due to the assumption of zero input in its initial phase. Overcoming this issue is performed by utilization of an adaptive recursive (AR) filtering which leads to OMEDA. Nevertheless, it is inefficient to determine periodic impulses of faulty modes of rotating machinery. For this reason, a cutting-edge method, Multipoint Optimal Minimum Entropy Deconvolution Adjusted (MOMEDA), is presented in the literature which provides deconvolution of infinite number of impulses without the necessity of iterative operation [78]. MOMEDA is able to solve this problem with optimized computation. In the mathematical perspective, MOMEDA introduces a non-iterative filtering window $\vec{t}$ which can be determined by period of the fault as shown in Eq. (16).

$$\vec{t} = [0\ 0\ 0\ 1\ 0\ 0\ 0\ 1\ 0\ 0]^T\ (n_f = 4) \tag{16}$$

where n_f is the example impulse period associated to the frequency of the fault mode.

$$X_0 = \begin{bmatrix} x_{L_m} & x_{L_m+1} & x_{L_m+2} \cdots & x_N \\ x_{L_m-1} & x_{L_m} & x_{L_m+1} \cdots & x_{N-1} \\ \vdots & \vdots & \vdots \ddots & \vdots \\ x_1 & x_2 & x_3 \cdots \cdots & x_{N-L_m+1} \end{bmatrix}_{L_m \; by \; [N-L_m+1]} \tag{17}$$

For the vibration measurement signal X_0, which may be assumed as the summation of dynamic system response, environmental noise and faulty transients of the related fault mode, while filter size is L_m , output response of the filter is $[N-L_m+1]$ in length as shown in Eq. (17). The filtering function for X_0, can be shown in the matrix form as in Eq. (18)

$$\vec{f} = (\mathrm{X}_0 \mathrm{X}_0{}^T)^{-1} \mathrm{X}_0 \vec{t} \tag{18}$$

and output signal $\vec{y}$ of the filtering operation can be represented as shown in Eq. (19)

$$\vec{y} = \mathrm{X}_0{}^T \vec{f} \tag{19}$$

Spectral features may also be investigated after MOMEDA is applied. Frequency spectrum of MOMEDA is an essential tool for identification of the faulty frequencies which leads to the consideration of spectral feature extraction in the area of rotating machinery. For the maximized efficiency identification of rotating machinery faults, at least five periods of the rotating element is recommended to be used as an input signal and preferred filter size may vary between 500-2000 while the signal is to be investigated is at least two times in length.

MOMEDA feature extraction methodology requires the determination of faulty frequencies and this may be achieved by the measurement of speed of the rotating machine and using a model based approach related to that model.

In the proposed methodologies for running gear fault detection associated with this thesis, for every individual investigation, filter size is chosen as quarter to one-tenth of the length of the input signals according to empirical investigation before filtering takes place.

3.6 Adaptive synthetic sampling

In wayside railway vehicle fault diagnosis most of the measurement data is healthy and that leads to having far more normal signal samples than faulty ones. Besides, acquiring faulty samples for the same type of vehicle is so much limited unless a real-time measuring is applicable. These problems affect fault diagnosis framework, which is based on classifier performances, very badly due to the fact that most classifiers require fixed sample sizes in each classes.

In the perspective of feature extraction, normally the number observations (m_o) for each class must be longer than the size of the feature vector (n_o); otherwise it is called insufficient case $(n_o \geq \mathrm{m}_o)$ [79]. Insufficient case occurs especially in voice and signature recognition applications since the number of observed samples are too much limited. Misclassification of faulty samples as normal may be irreversibly costly and data points between faulty samples are prior to avoid false negatives. Despite maintaining the optimal solution of this problem may vary in a significant level, the simplest approach to overcome this problem is to interpolate samples in a proper way.

To deal with imbalanced dataset problems synthetic minority over-sampling technique (SMOTE) is proposed in the recent literature [80] which uses linear interpolation between existing feature vectors of the minority class and create additional vectors. However, SMOTE methodology is limited to minority class and it lacks of consideration the boundaries between classes and results less realistic oversampling.

In the proposed methodology associated with this thesis, an extension of SMOTE; Adaptive Synthetic Sampling (ADASYN) [81], which generates more samples between the class boundaries adaptively, is used in order to oversample minority classes.

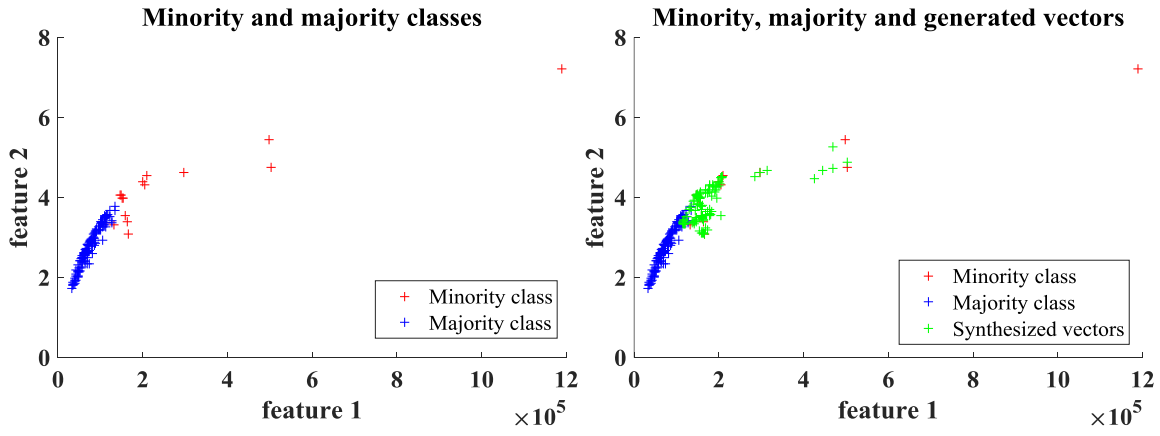

Figure 21: Synthesizing by ADASYN from minority class to balance with majority class by means of number of vectors in each class

In Figure 21 the oversampling operation of the feature vectors representing wheel defects from 16 observations ($m_0^{Faulty}=16$) to the number of observations of the normal class ($m_0^{Normal}=128$) (only adaptive sample generation of two dimensions of the given feature vectors of the minority class is shown). According to the resultant feature sets; normal and faulty classes are balanced so that $m_0^{Normal}+m_0^{Faulty}=256$.

It is important to emphasize that, ADASYN does oversampling for every separate feature in the minority class. Utilizing ADASYN for generating additional feature vectors from minority class is considered to be a realistic way since synthetic samples accumulated mostly in the boundary, which makes the dataset more challenging and also diminish the outlier effect rather than using only in-class interpolation.

3.7 Feature selection and dimensionless feature optimization

In pattern recognition, feature selection (FS) has a crucial role in the performance of the classification. The idea of feature selection is to filter out the, misleading, irrelevant or redundant features in each vector. It is a combinatorial optimization problem which tries to figure out which features minimizes the error in the classification [82]. Besides, discarding unnecessary features is more computationally efficient with high-dimensional data.

In general FS may be done in the following ways: filter approaches like, correlation-based FS [83], embedded approaches like Least Absolute Shrinkage and Selection Operator (LASSO) [84] , wrapper approaches, which uses predictive methods, like; ensemble –based wrapper FS which uses more than one classifier like random forest method [85].

To achieve a proper FS, each base classifier tries to determine the training data in the best way with the given feature set and choses the best features and combine them for resultant selected feature subset. This procedure is repeated according to either of the following methods: forward sequential selection, backwards sequential selection or hill climbing (until a criterion like number of iterations is satisfied) [86].

In the proposed method belonging to this thesis forward sequential selection using 1-knn (FSS-KNN-1) is used. In FSS-KNN-1 the training data is divided by each feature until best features are identified which is described in Eq. (20) and (21).

$$[F_{N_c}^{training}]_{N_{tv}\,x\,n_o}^{raw}=F_{N_c-1}^{training},...,F_1^{training} \tag{20}$$

$$[F_{N_c}^{training}]_{N_{tv}\,x\,n_{fs}}^{FS}=F_{N_c-1}^{training},...,F_1^{training} \tag{21}$$

where n_o is the size of the feature vectors in each class in the training set, N_C is the number of classes, N_{tv} is the number of training vectors in each class and n_{fs} is the number of features that is selected by FSS-KNN-1 according to the criterion; best two features (n_{fs}=2) or best number of features $1 \le n_{fs} \le n_o$. After feature selection of training data process is completed, same mapping can be used to testing vectors before the testing procedure is started.

Dimensionless feature normalization is a feature optimization technique that helps improving sensitivity in bearing fault diagnosis (true positive rate) by adjusting magnitudes of the features in the datasets to avoid one or more individual features to suppress the remaining ones [71]. Commonly used dimensionless approaches are shown in Table 4.

Table 4: Dimensionless methods that is commonly used for feature optimization

Dimensionless methods	**Formulation**
Extreme dimensionless method	$y_{ij} = \frac{x_{ij} - \min(x_{ij})}{\max(x_{ij}) - \min(x_{ij})}$
Dimensionless method of maximization	$y_{ij} = \frac{x_{ij}}{\min(x_{ij})}$
Dimensionless method of minimization	$y_{ij} = \frac{x_{ij}}{\max(x_{ij})}$
Average Dimensionless method	$y_{ij} = \frac{x_{ij}}{\bar{x}_{ij}}$
Dimensionless method of standardization	$y_{ij} = \frac{x_{ij} - \bar{x}_{ij}}{s_j}$
Weighting method of standardization	$y_{ij} = x_{ij} \Big/ \sqrt{\sum_{i=1}^{n} x_{ij}^2}$

where y_{ij} is the normalized data after no-dimension analysis, x_{ij} is the data belongs to the feature vectors before dimensionless analysis, $\bar{x}_{ij}$ is the average value of the observed data for each feature and s_j refers to the standard deviation of observed samples for each feature.

The average dimensionless method is capable of keeping the consistency of the raw data and correlation dimension. Thus, in the proposed framework associated with this thesis, the average dimensionless method is employed. Dimensionless feature normalization is a feature optimization. Throughout feature optimization process, combination of dimensionless analysis and feature selection is also employed to achieve better results.

3.8 Simulating running gear faults

In the investigation of wayside diagnosis of running gear faults, it is cumbersome to acquire all faulty types related to running gear components. It is vital to test the proposed approaches on different faulty conditions. For this purpose, a simulating scheme for running gear related faults with respect to model based frequencies is proposed in this section.

The method for simulating transients for vibration signals is inspired from the research [87] in the recent literature. In this method, rotating machinery defects are considered as a sequence of impulsive transients and each transients have 10 samples for sample rate of 6.4 kHz. Each transient is a composition of random number of sinusoidal functions with random frequency and random initial phase as shown in Eq. (22)

$$\mathrm{v}_f(n) = \sum_{i=1}^{U} A_i \sin(\omega_i n + \beta_i) \tag{22}$$

where A_i is a random amplitude, $1 \le U \le 10$ is a random integer, ω_i is a random frequency and β_i is the random initial phase. Figure 22 shows the generated faulty transient of frequency of 20 Hz signal for 51,2 kHz sample rate by utilizing the proposed methodology. Finally, generated faulty transient is to be multiplied by a constant to adjust the output amplitude for further use.

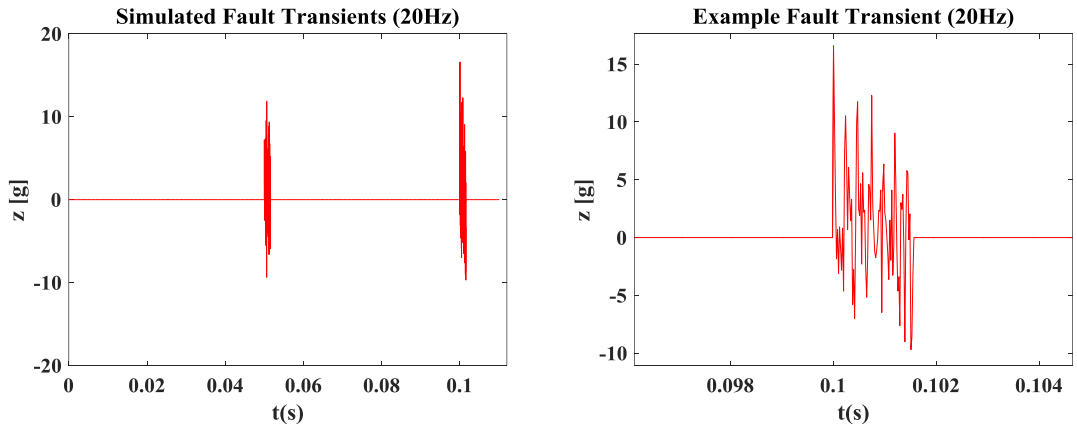

Figure 22: Simulated fault transient at 20 Hz using proposed random phase shifting technique

Simulating a fault type referring to its model based frequency is not sufficient due to measurements are not performed under constant speed. To deal with this problem, before burying the generated faults to the measurements data, each frequency for each fault type of running gear components is calculated exactly according to the wheelset speed while passing on sensors. After these adjustments, summing operation of retrieved data and faulty simulated signal are performed. In Figure 23, measurement signal which is retrieved from the test environment between Dejvická and Bořislavka, by vibration sensors while wheelset-3 of ID-108 train set with healthy condition is passing by.

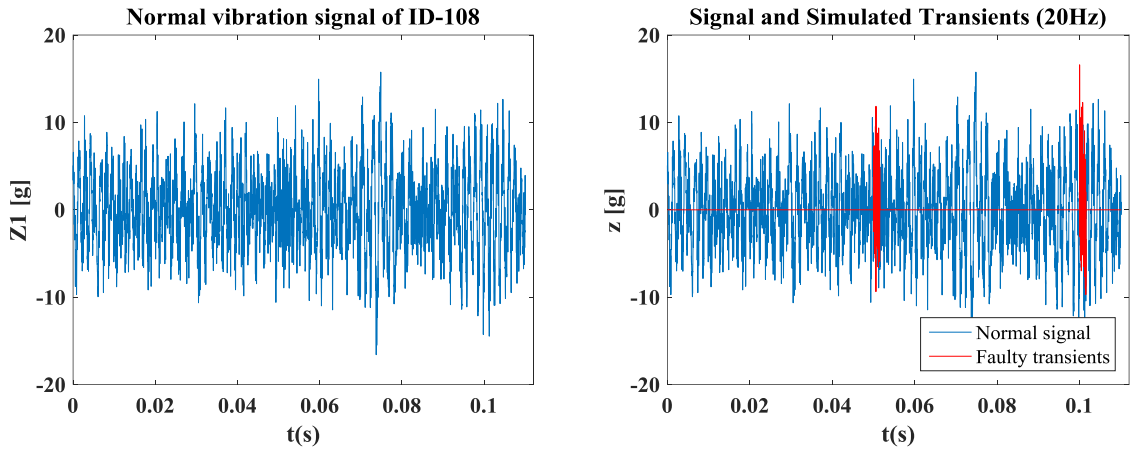

Figure 23: Vibration signal that is measured from ID-108 metro train set (left) transient locations that the simulated faults are added (right)

In the simulated fault investigations, ID-119 train set normal data which is measured from all of the sensors for each wheelset passing, according to the window length with respect to speed and wheel diameter, is used to generate faulty cases of running gear components like wheel defects, wheelset bearing faults, gear tooth fault and traction motor eccentricity.

4 RESULTS AND DISCUSSION

This section examines four main analyses subjected to the diagnosis of running gear faults. The purposes of these analysis may be categorized as follows: Discarding signals in the database that is retrieved by abnormal sensor activity (Section 4.1), validation of the proposed feature extraction methods on a ground truth database of bearing faults (Sections 4.2 and 4.6), detection of wheel defects and traction motor bearing faults of metros using validated techniques on the signals that are recorded in the wayside passages which are placed between metro stations of Prague along line A (Section 4.3), simulating model based faults and diagnose of the simulated faults of running gear components like wheel defects, wheelset bearing faults, gearbox faults and traction motor eccentricity (Section 4.5).

4.1 Detecting anomalies in sensor data

In wayside diagnostics, operation parameters differs significantly due to variations dependent to vehicles and unexpected environmental conditions. In addition, there may be some sensor related miscalibrations or uncorrelated response in comparison to other runs of the same vehicle in the environment of the measurement system.

Sensor data in many applications is degraded by environmental noise that can commonly be modelled as Gaussian additive or white noise. In wayside measurement environment of railway vehicles, the noise is heavy besides the effects of the irregularities on the rail which may be modelled as impulse noise, should also be considered. Besides, there may be some unwanted behavior in one of the components, acts as noise, which may not be easily removed or modelled because of their random characteristics. It may not be handy to utilize further processes when the obtained sensor data is more related to anomalies rather than expected signal characteristics.

In order to enhance signal characteristics while building a database for each individual train set, an experimental analysis is performed on the gathered data in the passage of Malostranská to Nemocnice Motol direction which is explained in Section 2.1. The investigation contains two sensors among eight; one accelerometer (Z2) and one microphone (M1). After having applied thresholding in optical gates G_A and G_B, sample numbers which inform about the exact location of each bogie wheelset respect to optical gates, are marked. Marked points are used to determine exact window size (W_s) in each run due to velocity variations for segmentation. For each sensor Z2 and M1, sampling is performed in the interval of before and after first (WS_1) and last wheelset (WS_{20}) according to the rule in Eq. (23)

$$W_S = \left(WS_1 - \frac{i_{\min}}{2} \right) \xleftrightarrow{interval} \left(WS_{20} + \frac{i_{\min}}{2} \right) \quad (23)$$

where $i_{\min}$ is the sample number difference of centers WS_1 and WS_2 passing on optical sensor G_A.

Since the output is not uniform, further transformations are needed to examine anomalous information in the segmented signals. Abnormal signals are determined empirically after the investigation of Kurtograms which are obtained by using FK algorithm of five-levels which is explained in Section 3.3.2 and the collected database is divided into two classes; 238 normal and 62 abnormal. It is worth to note that if any sensor data related to the same run is marked as abnormal, data from all other runs of the same train sets from all sensors are nominated as abnormal too. Finally, database is reorganized so that 60 normal signals against 60 abnormal ones.

4.1.1 Extraction of features to sense anomalies

In the feature extraction period of anomaly detection in the run, four different methods are used; time-domain features, wavelet packet energy, HE LCP-K and LCP-K without HE as a preprocessing.

Firstly, statistical time-domain features (STATS) that are selected for this duty are shown in Eq. (24) and have 5x1 length by calculating each value and concatenate in the same row. They may assumed to be the most time efficient in the process of classification.

$$STATS = [mean, standard\ deviation, mode, minimum, maximum] \quad (24)$$

Secondly, wavelet packet transform is applied on all signals and then WPE coefficients are calculated for three and five levels. These features have the length of 2^L while L is the number of levels in wavelet packet transform. Using different levels of WPE features make the results more comparable.

Thirdly, for all signals five level FK is applied and resultant Kurtograms are treated as 2D signals E-LCP-K is applied to finalize feature matrix as suggested in Figure 20. In addition to this, LCP is directly applied without histogram equalization process for comparison. Final feature vector sizes are equal and have 81x1 in length. Figure 24 shows Kurtograms of the signals of healthy and abnormal cases where MKurt is the maximum corraleted kurtosis, Bw is the bandwidth of the transients and f_c is the carrier frequency.

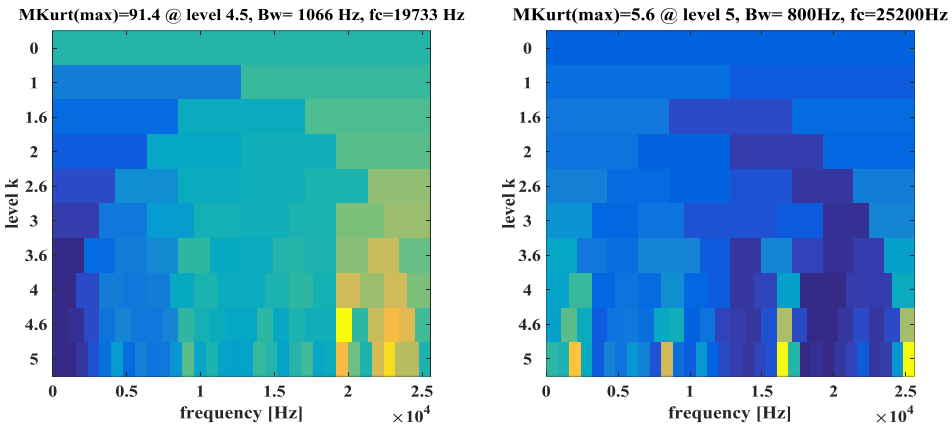

Figure 24: Resultant five level kurtograms of anomaly signal sample (left) and normal case (right)

4.1.2 Results and conclusion of anomaly classification

In the analysis, each feature that is extracted from the signals in our databases provides dimension reduction while preserving the signal characteristic components. Each feature extraction method is labeled as follows: Statistical time-domain features (STATS); mean, standard deviation, minimum, maximum, root mean square (RMS), WPE features are created both in three level (WPE_3) and five level (WPE_5), enhanced LCP of Kurtograms with (E_LCP-K) and without (LCP-K) histogram equalization [69].

Maintaining reliability in the results is vital and 6-fold cross validation is performed in the classification phase, which FLDA [88] is used, for more reliable results. Table 5 shows the classification performance of the abnormal signals.

Table 5: The average recognition accuracies of sensing anomalies with their standard deviation values obtained by 6-fold cross validation

FLDA	**Classification Success (%)**				
Test Data	**LCP-K**	**STATS**	**E_LCP-K**	**WPE_3**	**WPE_5**
1-10	70	45	65	50	70
11-20	75	50	75	50	80
21-30	75	50	70	50	85
31-40	65	80	90	85	80
41-50	65	100	80	100	55
51-60	90	95	75	90	45
Average	73.3	70.0	**75.8**	70.8	69.2
Std. Dev.	9.3	24.7	**8.6**	23.3	15.9

According to the results, highlighted LCP-K and E-LCP-K methods are clearly better than others by means of average classification performance and standard deviation.

In this analysis, a two-class classification is performed on an empirically created database in consistence of signals retrieved from both accelerometer based and acoustic sensors which are employed for condition monitoring. Despite using these two differently characterized sensor outputs, a combined feature extraction attempt is carried out by application of five different methods on the signals. The proposed novel E-LCP-K algorithm outperforms not only in average classification performance but also stability in the results, with respect to standard deviation and six-fold cross validation.

It may be considered that using higher levels of WPE does not boost the classification performance but diminishes without any preprocessing. It is also remarkable to say that Kurtogram approach may assumed to have as much information as other methods even a challenging database with combined sensor data, especially when histogram equalization is applied just before LCP phase.

Analyses in this part also indicates that there is a high correlation between an accelerometer based vibration sensor on the rail and a microphone which is aligned vertically, by means of frequencies observed thus the database is managed to be classified more than 50%.

Future study may be carried out in order to confirm the results by using more sensor data that has abnormalities. Consequently, proposed E-LCP-K approach may be used in diagnosis of other types of faults when an appropriate filtering is applied in the preprocessing according to corresponding fault mode.

4.2 One-period analysis in bearing fault diagnosis

This investigation presents several number of methods which are efficient of extracting representative features in fault diagnosis of a rotating element bearing with the contribution of one-period analysis.

Rotating element bearing (REB) faults are the most common mechanical component that is used in rotating machinery [89]. Failure modes of REB related faults may be characterized into four groups; inner ring faults, outer ring faults, rotating element bearing fault and cage fault. Among them, bearing rolling element fault is the most dominant failure mode [90]. The diagnosis of such failures are maintained by data driven and model based methods.

Plenty of methods have already been proposed for fault detection of REBs in the recent literature. Continuous Wavelet Transform, Gabor wavelets and wavelet transform [41], Hilbert Huang Transform in connection with support vector machines [72], time-domain analysis and application of fuzzy C-means [70], Kurtogram and envelope analysis [61], statistical features [71].

The analysis throughout this section proposes several methods for diagnosis of REBs multi-fault conditions in early phase and severity classification of bearing rotating element faults on a database that is highly focused by the researchers over the last decade [89].

4.2.1 Database and feature Extraction in bearing fault diagnosis

Thanks to Case Western Reserve University (CWRU) that provides a database which includes accelerometer based vibration signals that are retrieved by a test rig in laboratory environment.

The database has four main classes; healthy case (HC), ball faults (BF), inner race faults (IRF) and outer race faults (ORF) that allows up to four level of severity classification (0.18, 0.36, 0,53, 0,71 mm in diameter) and multi-fault diagnosis of rotating machinery bearings [91]. The datasets utilized in this research include faulty signals which are collected by accelerometer sensors, localized at drive end of deep groove ball bearings of the type 6205-2RSJEM, recorded at 12 kHz and healthy signals of 48 kHz, which then downsampled to 12k sampling rate, may be seen in Table 6 [92]. In the segmentation process, three different approaches taken into account; Dataset A is constructed covering five periods of rotation of the motor (5T) which is inspired by the study in [72] and includes 2000 data points in each sample. Datasets B, C and D are generated by preserving one (T) and one and a half period (1,5 T) of rotation of the motor in each sample.

Table 6: Description of classified cases and datasets; T refers to one period analysis

Dataset	Fault Type	Severity	Segment Period	Rotation Speed (RPM)	Total Samples	Label
A	HC	-	5T	1797	60	A1
	BF	0.18 mm			60	A2
	BF	0.36 mm			60	A3
	BF	0.53 mm			60	A4
	BF	0.71 mm			60	A5
B	HC	-	T	1797	300	B1
	BF	0.18 mm			300	B2
	BF	0.36 mm			300	B3
	BF	0.53 mm			300	B4
	BF	0.71 mm			300	B5
C	HC	-	1,5T	1797	200	C1
	BF	0.18 mm			200	C2
	BF	0.36 mm			200	C3
	BF	0.53 mm			200	C4
	BF	0.71 mm			200	C5
D	HC	-	T	1797	300	D1
	BF	0.18 mm			300	D2
	IRF	0.18 mm			300	D3
	ORF	0.18 mm			300	D4

In the feature extraction stage, several techniques that are subjected to fault classification of REBs are employed in the preparation of feature extraction matrices.

Firstly, wavelet packet transform is applied in order to calculate energy coefficients to detect faults in translation invariant mode. Three and five level WPE features are used which results 8x1 and 32x1 sized feature matrices, respectively.

Secondly, time domain signals are used as input vectors and eight statistical time-domain features (TDF); energy, mean, standard deviation, maximum, minimum, kurtosis, skewness and crest factor are calculated and concatenated into a 8x1 matrix as preferred in the research [72].

Thirdly, a model based MOMEDA feature extraction scheme is followed and pre-calculated model based faulty frequencies for different types of failures of REB according to rotation speed of the motor are used for extraction of MOMEDA features (Table 7). In the experiments, window size is chosen as 100 for T -1,5T period analyses and 500 for 5T analysis. An example faulty signal of ball bearings and resulting MOMEDA in the feature extraction phase for the purpose of this investigation is shown in Figure 25.

Table 7: Fault frequencies of bearing type 6205-2RS JEM at drive end

6205-2RS JEM	**Inner Ring** (f_{BFBI})	**Outer Ring** (f_{BPFO})	**Cage Train** (f_{FT})	**Rolling Element** (f_{BSF})
Defect Freq. (Hz)	5.4125	3.5848	0.3983	4.7135
Operating Freq. (Hz)	162.01	107.31	11.922	141.10

Lastly, implementation of autoregressive (AR) filtering [93] with window size of 50 for pre-whitening the signal before MOMEDA method is applied to increase its efficiency by means of fault detection of 5T segmented signals and MOMEDA-AR features created.

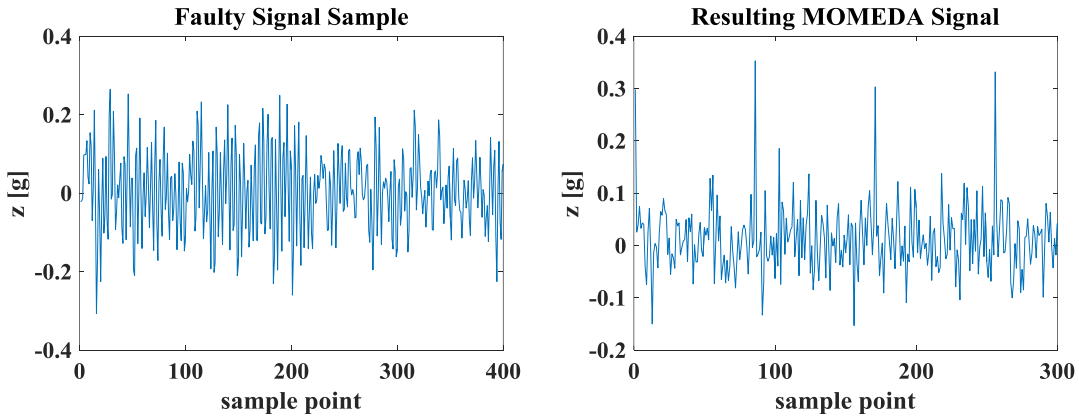

Figure 25: Faulty signal sample of medium severity level (left), resulting MOMEDA signal (right)

4.2.2 Analysis results of REB fault diagnosis

In the analyses, two main objectives are considered. Firstly, severity classification of the rotating elements of bearing faults are investigated including early faults, depending on the period of the rotation of the motor by using Dataset A, B and C. Secondly, a multi-fault diagnosis of early faults of rotating elements is performed on Dataset D using one-period analysis to show its efficiency. Feature extraction includes two different levels of wavelet packet energy (WPE_3, WPE_5), time-domain features (TDF), MOMEDA with AR (MOMEDA-AR) and without (MOMEDA) AR filtering. Two state of art classifiers; Support Vector Machine with linear (SVM-I) and second-order (SVM-II) kernel in addition to Fisher Linear Discriminant Analysis (FLDA) are employed and evaluation process is performed using five (Dataset C) and six (Dataset A,B,D) fold cross-validation which is shown in Table 8. In addition, another experiment is carried out to achieve best results. In the testing process of Dataset A, each sample is tested against remaining ones and average classification accuracy is calculated as seen in Table 9.

Table 8: Classification performance for segmented datasets A, B, C and D (* represents that using that classifier is either not applicable or dataset is already classified with 100% success rate with less computational effort)

	Average classification accuracy (%)								
	MOMEDA		**WPE_3**		**WPE_5**		**TDF**		**Labels**
FLDA	100	94.3	100	93.0	100	96.3	100	96.0	A(1,2) | A(1-5)
	100	84.5	100	90.0	100	91.8	100	75.0	B(1,2) | B(1-5)
	100	81.2	100	91.0	100	94.4	100	80.6	C(1,2) | C(1-5)
	*	**100**	*	99.8	*	99.8	*	96.8	D(1,2) | D(1-4)
SVM-I	100	98	100	93.0	100	**99.3**	100	95.0	A(1,2) | A(1-5)
	100	*	100	95.0	100	**97.3**	100	75.3	B(1,2) | B(1-5)
	100	94.0	100	97.2	100	**98.0**	100	77.8	C(1,2) | C(1-5)
	*	*	*	*	*	*	*	*	D(1,2) | D(1-4)
SVM-II	*	98.7	*	96.7	*	98.7	*	97.3	A(1,2) | A(1-5)
	100	*	100	*	100	*	100	*	B(1,2) | B(1-5)
	100	94.0	100	96.2	100	95.0	100	94.0	C(1,2) | C(1-5)
	*	*	*	*	*	*	*	*	D(1,2) | D(1-4)

Table 9: Classification performance for severity classification for Dataset A; one against rest

	Average classification accuracy (%)					
	MOMEDA AR	**MOMEDA**	**WPE_3**	**WPE_5**	**TDF**	**Labels**
FLDA	98.3	96.3	93.0	97.7	96.3	A(1-5)
SVM-I	99.3	98.3	99.0	99.0	94.7	A(1-5)
SVM-II	**99.7**	99.3	98.0	99.0	97.0	A(1-5)

Proposed methodology to obtain best results in early diagnosis; Dataset A(1,2), B(1,2), C(1,2) and multi-class classification; A(1-5), B(1-5), C(1-5), D(1-4) is illustrated in Figure 26.

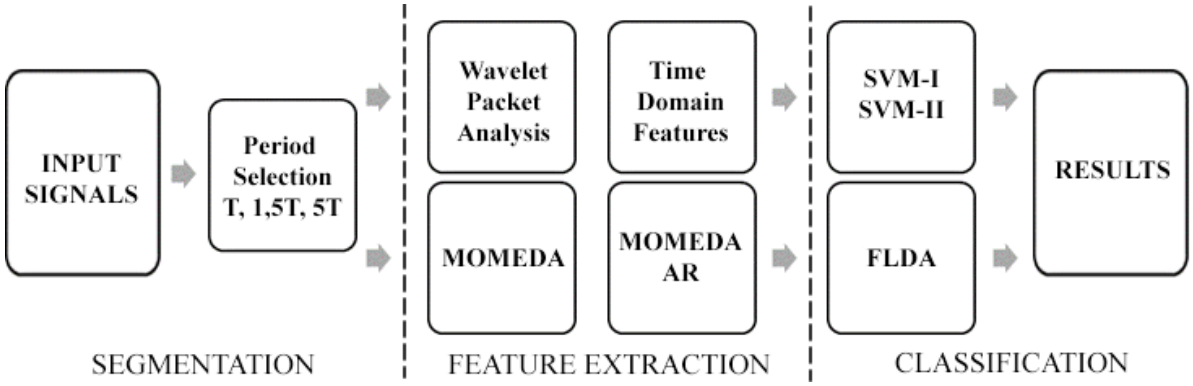

Figure 26: Proposed fault severity and early fault classification scheme of ball bearings of rotating machinery

In this section, several methods which have proven its efficiency in rotating machinery fault diagnosis by using accelerometer based vibration sensors are presented. Throughout the process, Wavelet Packet Energy (WPE), Time-domain features and Multipoint Optimal Minimum Entropy Deconvolution Adjusted (MOMEDA) feature extraction methods are used with three different sample segmentations to diagnose fault severity levels of ball bearings and early-faults.

Condition monitoring of rotating machinery is examined upon sub-segmentation of healthy and faulty signals in the database retrieved from CWRU.

According to the results, early fault detection including multi faults by the use of MOMEDA features, reaches a highest possible accuracy of 100% even in one-period analysis. However, in five level severity classification, one-period analysis is not sufficient and maximum of 97.3% classification success is observed.

Another investigation is carried out by using 1,5T analysis and detection success is increased to 98% on the same dataset with linear SVM kernel. Finally, by utilizing one test sample against all training samples using SVM-II, maximum average accuracy of 99.7% is reached in bearing fault severity detection, which may be nominated as the most challenging among all RPM levels and fault types according to Table. 6 in the recent study [72].

Proposed methodology for severity classification of ball bearings outperforms the state-of-art techniques specialized for bearing fault diagnosis by means of classification performance and simplicity.

4.3 Detecting wheel defects via one-period analysis

In vibration based wayside railway vehicle diagnosis, the interaction of wheels and vibration sensors are the most dominant which makes wheelset related faults easier to identify.

If one can gather the healthy information from a ground truth case of sufficient amount of data, an efficient diagnostic framework may be designed.

This section investigates three feature extraction methods in combination with four state-of-art classifiers; FLDA, SVM [88], decision tree (Dec. Tree) [94] and a neural-network classifier; linear perceptron (PERLC) [95] to detect a faulty conditions of a metro wheel; wavelet packet energy, time-domain features and utilization of LCP-K.

Database that is used in the investigation of wheel defects retrieved from wayside measurement system between Dejvická to Bořislavka which is told in Section 2.1. Throughout the process, one-period analysis is used in the segmentation phase on the signals which are recorded by Z1-Z2 accelerometer and M1-M2 acoustic sensors.

Known faulty data is substantial to ensure certainty in the results. Thanks to unhealthy ground truth data which is provided by ID-108 train set which has wheel defects of flat type on both left and right wheels on the seventh wheelset. The defect which was on the center of contact zone may be seen in Figure 27.

Figure 27: Wheel flat which is present on the seventh wheelset on train set ID-108

These types of defects are generally caused by blockage or partial blocking of a wheelset while the vehicle is travelling at speed; as the wheel slides along the rail, friction heats the wheel-rail contact patch in local areas [47].

Healthy data is gathered from either a newly revisioned train (two months before measurements); train set ID-119 or healthy wheelsets of ID-108. Since multiple passes of those train sets are available, it is possible to construct a database consisting of larger number of faulty cases even if only two faulty wheels are present. In Table 10, different combinations of healthy

and faulty signals are described which is used in model evaluation of classification framework special for wheel defect detection.

Table 10: Description of classes of wheel defect detection of faulty wheels of ID-108

TRAIN IDs	Measured Faulty Samples	Synth. Faulty Samples	Total Normal Samples	Faulty Wheelset Interval	Normal Wheelset Interval	Sensors	Label
108, 119	16	0	16	7	2-17 (ID-119)	Z1-Z2	A1
108	8	0	8	7	1-4, 11-14	M1-M2	A2
	16	112	128	7	1-4, 11-14	Z1-Z2	SA1
	8	56	64	7	1-4, 11-14	M1-M2	SA2

Since number of features are shorter than observation of number of faulty signals in datasets A1-A2, which is so called "insufficient case", a more reliable approach, adaptive synthesizing (ADASYN) [81] is used to generate additional faulty samples properly and SA1, SA2 are constructed to perform classification.

One-period analysis is performed on the signals to retrieve relevant data from the sensors; each wheel perimeter is calculated according to their last known exact radius (r) and sample interval is selected so that it covers all points along L which is shown in Figure 28.

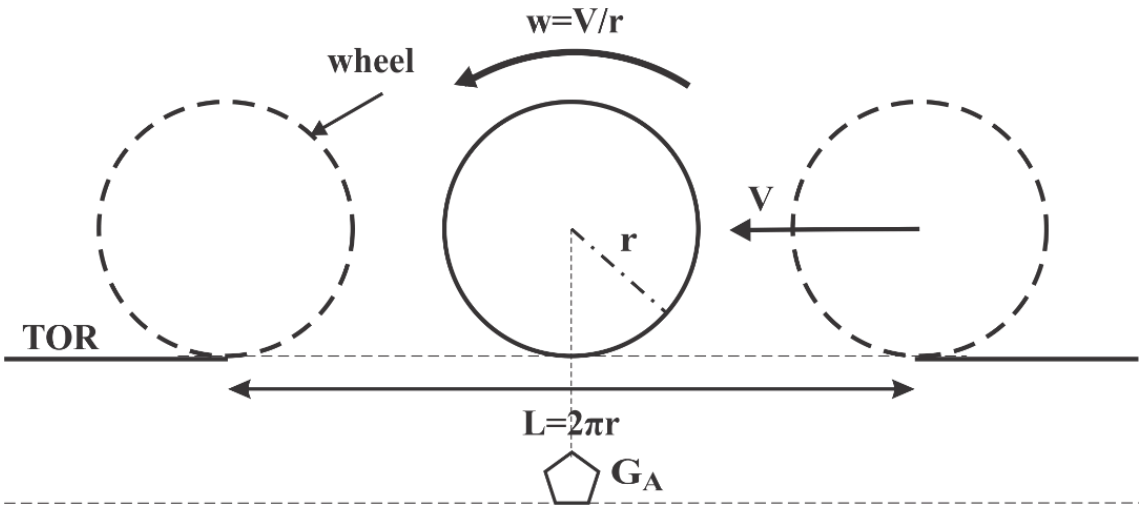

Figure 28: Segmentation using one-period analysis in the center of optical gate G_A

4.3.1 Feature extraction for wheel defects

In the process of achieving representative features of faulty cases, three different methodologies are employed on the samples in our dataset.

Firstly, fifth order wavelet packet analysis and energy calculation of each wavelet packet is performed to achieve WPE_5 features which are 32x1 in length for each sample.

Secondly, time-domain features (TDF) which are efficient in rotating machinery fault diagnosis is performed as in the way that is shown in Eq. (25) which are 8x1 in length.

$$TDF = [energy, mean, std.dev, max, min, kurtosis, skewness, crest\ \ factor]_{8x1} \quad (25)$$

Lastly, with direct calculation of LCP on five-level Kurtograms without any pre-processing like HE, LCP-K feature matrices are created for each sample which are 81x1 sized. In Figure 29, five-level Kurtograms are shown for both normal and faulty signals samples with 51,2 kHz sample rate which are segmented from faulty wheels of ID-108 and healthy wheels of ID-108, respectively (higher intensity levels refers to greater kurtosis in those frequency bands).

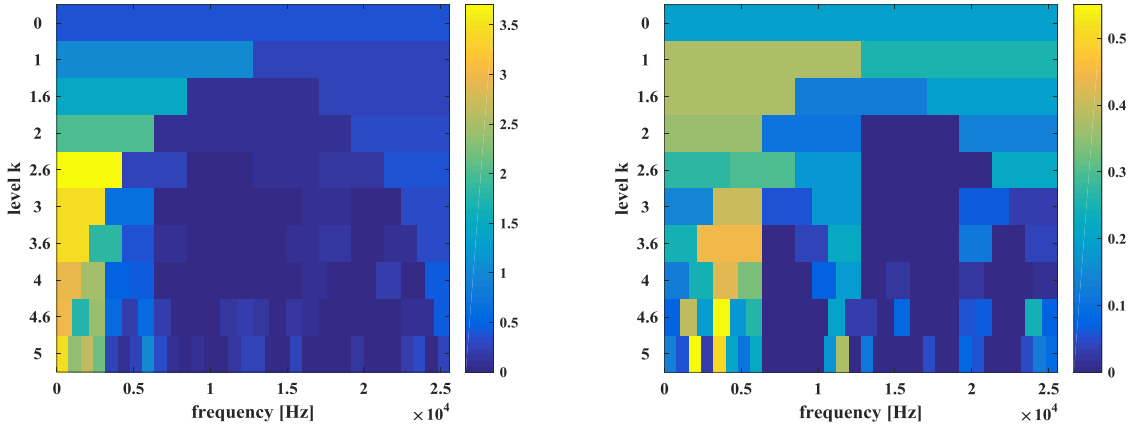

Figure 29: Resultant five level kurtograms of sample signal with wheel defect (left), health case (right)

4.3.2 Analysis results of diagnosis of wheel defects

Several different number of cross-validation are performed in diagnosis of wheel defects by proposed feature extraction and classification techniques.

Best results are obtained by 16-fold cross validation for SA1 accelerometer sensors datasets while 8-fold cross validation for SA2 microphone signals datasets and 8-fold cross validation for A1 accelerometer sensors datasets while 4-fold cross validation for A2. Recognition accuracies for microphone sensors (M1-M2) are given in Table 11 for proposed classifiers; Support Vector Machine, Linear Perceptron, Decision Tree and Fisher Linear Discriminant Analysis in combination with three proposed feature extraction techniques.

Table 11: The average recognition accuracies of wheel defects of measured and synthesized faults using M1-M2 sensors

Classifier	**Classification Accuracy (%)**			**Classifier**	**Classification Accuracy (%)**			**Class Label**
	WPE_5	**TDF**	**LCP-K**		**WPE_5**	**TDF**	**LCP-K**	
SVM-I (4-fold)				**Dec. Tree** (4-fold)				A2
Average	68.80	62.50	81.25	**Average**	87.50	68.75	**87.50**	
Std. Dev.	12.5	14.4	12.5	**Std. Dev.**	14.4	23.9	14.4	
FLDA (4-fold)				**PERLC** (4-fold)				A2
Average	62.50	56.25	62.50	**Average**	68.75	75.00	81.25	
Std. Dev.	32.3	23.9	14.4	**Std. Dev.**	12.5	37.8	12.5	
SVM-I (8-fold)				**Dec. Tree** (8-fold)				SA2
Average	82.80	85.90	**93.00**	**Average**	87.50	85.20	87.50	
Std. Dev.	14.5	5.5	**7.0**	**Std. Dev.**	9.5	8.1	6.7	
FLDA (8-fold)				**PERLC** (8-fold)				SA2
Average	82.00	**93.00**	87.50	**Average**	76.60	89.80	89.90	
Std. Dev.	10.3	**7.0**	8.2	**Std. Dev.**	16.6	4.7	6.6	

According to the results, using M1-M2 sensors have less accuracy in all classifiers in the absence of synthetically generated faulty samples (A2) and classification success reaches to 93% with both SVM-I and FLDA with LCP-K and TDF feature extraction techniques, respectively. It is also notable that LCP-K algorithm works the best for both insufficient case (A2) and adaptively generated minority (faulty) samples case (SA2).

In Table 12, recognition rates for accelerometer sensors are given. Referring to the results, using Z1-Z2, it may clearly be seen that TDF feature extraction is the leading one with best possible classification accuracy of 100% in classifying wheel flats on A1 dataset. WPE_5 and LCP-K are also promising despite using no preprocessing or filtering before feature extraction is carried out.

Upon generating faulty samples, the model is investigated in a more reliable way and classification of SA1 dataset shows that TDF feature extraction is still the best among all proposed feature extraction techniques when using SVM-I and Decision Tree classifier.

Further model evaluation may be carried out to increase the results with different ground truth data whenever it is available.

Table 12: The average recognition accuracies of wheel defects of measured and synthesized faults using Z1-Z2 sensors

Classifier	Classification Accuracy (%)			Dataset Label
	WPE_5	**TDF**	**LCP-K**	
SVM-I (16-fold)				SA1
Average	99.60	**100**	97.30	
Std. Dev.	2.2	0.0	5.2	
FLDA (16-fold)				SA1
Average	95.70	99.20	97.30	
Std. Dev.	6.8	3.0	6.0	
Dec. Tree (16-fold)				SA1
Average	98.10	**100**	89.10	
Std. Dev.	5.6	0.0	11.2	
PERLC (16-fold)				SA1
Average	98.40	99.20	97.30	
Std. Dev.	5.3	3.0	5.2	
SVM-I (8-fold)	90.6	**100**	90.6	A1
FLDA (8-fold)	68.6	**100**	96.9	A1

As a result, it may be considered that wayside diagnosis of wheel flats is possible by utilizing proposed feature extraction and pattern recognition techniques without pre-processing or additional filtering.

4.4 Efficiency of one-period analysis in comparison to fixed sampling

In previous sections, signal segmentation is done according to the rule of one-period analysis to construct datasets of healthy and faulty cases of metro wheelsets. This investigation is carried out to understand the advantages and disadvantages of wheel defect detection with one-period analysis against the implementation of fixed diameter when retrieving signals.

In this investigation, instead of using k-fold cross validation, randomly chosen faulty and healthy samples are used in order to diagnose wheelset faults. In addition, a feature optimizing technique; forward sequential feature selection according to FSS-KNN-I [86] and an additional classifier combining method; Product Combiner [96] is used to increase accuracy. Throughout the classifier combining approach, five state-of-art classifiers are employed; SVM-I, FLDA, Dec. Tree, Naive Bayes (N-Bayes), PERLC and product combining of them (Prod. comb).

Signals that are used in this analysis are retrieved from ID-108 train set and the database segmentation is shown in Table 13.

Table 13: Description of classes of faults and datasets; T refers to one period analysis and AVG refers to average diameter sampling

Dataset	Fault Type	Sensors	Segment Period	Num. Training	Num. Testing	Class Label
A3	HC	Z1-Z2	AVG	8	8	A31
	WF			8	8	A32
A4	HC	M1-M2	AVG	8	8	A41
	WF			8	8	A42
A5	HC	Z1-Z2	T	8	8	A51
	WF			8	8	A52
A6	HC	M1-M2	T	8	8	A61
	WF			8	8	A62

In the preparation of A3-A4 datasets, each test sample is retrieved according to velocity of individual wheelset as it is in one-period analysis. However, instead of using individual wheel diameters in the operation, which may vary in 730 – 790 mm range, average value of minimum and maximum of wheel diameters; 760 mm is used. Figure 30 shows the difference between utilization of average diameter sampling in comparison to one-period approach nearby optical gate G_A. When the diameter of the measured wheel is greater than the average value, $L+2\pi\Delta r$ samples are acquired whereas on condition that the measured wheel has smaller diameter, $L-2\pi\Delta r$ samples are employed where Δr refers to the difference of the radius in the measured wheel and fixed average diameter. Similar to one-period analysis, operation speed of each wheel (V) is considered to diminish the adverse effects of fluctuating speed conditions.

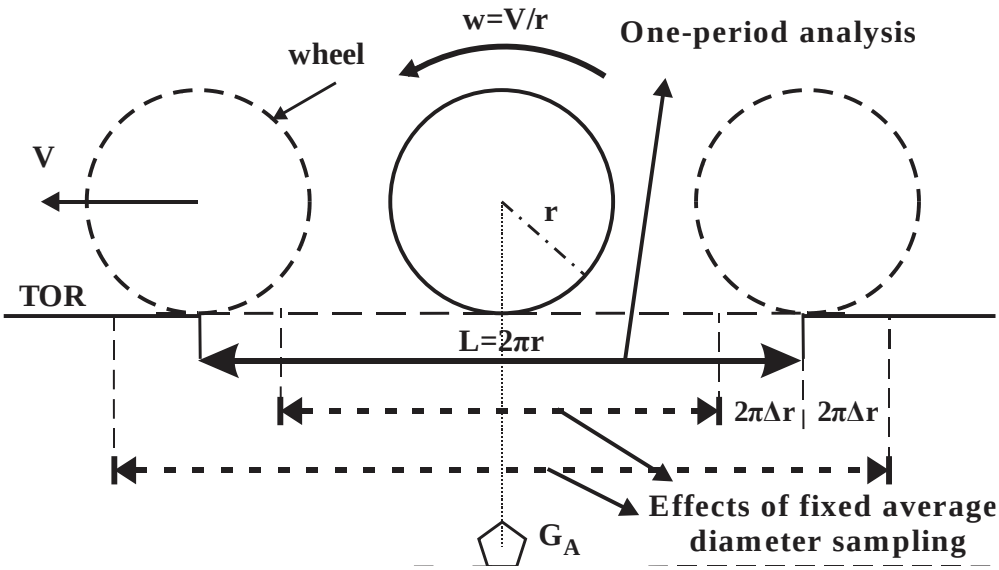

Figure 30: Difference between one-period analysis and fixed diameter sampling

4.4.1 Feature extraction for comparative sampling

In the diagnosis of wheel defects with different sampling techniques, time-domain features are extracted from the retrieved health and faulty signals and concatenated in a matrix as in Eq. (26).

$$TDFs = \begin{bmatrix} \text{energy, mean, std dev, max, min, kurtosis, skewness,} \\ \text{crest factor, impulse factor, spike energy, center frequency} \end{bmatrix}_{11x1} \quad (26)$$

Despite of the fact that one may not sense which element in TDFs matrix is more beneficial to classification result, sequential k-nn feature selection [86] is performed to get more relevant features and two features that distinguish the classes of training data best, are chosen.

4.4.2 Analysis results of comparative sampling

Detection of faults may strongly depends on the relevancy of the features and classifier capabilities. In this investigation, five different classifiers and the combined version of them; Product combiner is used to observe classification accuracy of randomly chosen data from the wheelsets ID-108 train set. Classification results for Product Combiner for A3-A5 and A4-A6 may be seen in Table 14.

Table 14: Classification performance for fixed average diameter sampling in comparison to one-period analysis with insufficient dataset

(%) Average classification accuracy					
Feature Selection	**TDFs**		**Number of Training Vectors**	**Number of Test Vectors**	**Dataset Labels**
NO	93.8	93.8	8	8	A3-A5
	50.0	37.5	8	8	A4-A6
YES	**100**	93.8	8	8	A3-A5
	37.5	81.3	8	8	A4-A6

It is urgent to determine the best classifier to ensure the best fault detection performance. The resulting graphs include Receiver Operator Characteristics (ROC), which is the indication of false positive ratio respect to true positive detection, Area under ROC Curve (AUC) and classification accuracy (ACC). Classification results for A3-A5 datasets, which belongs to vibration sensors are shown in Figure 31 and Figure 32.

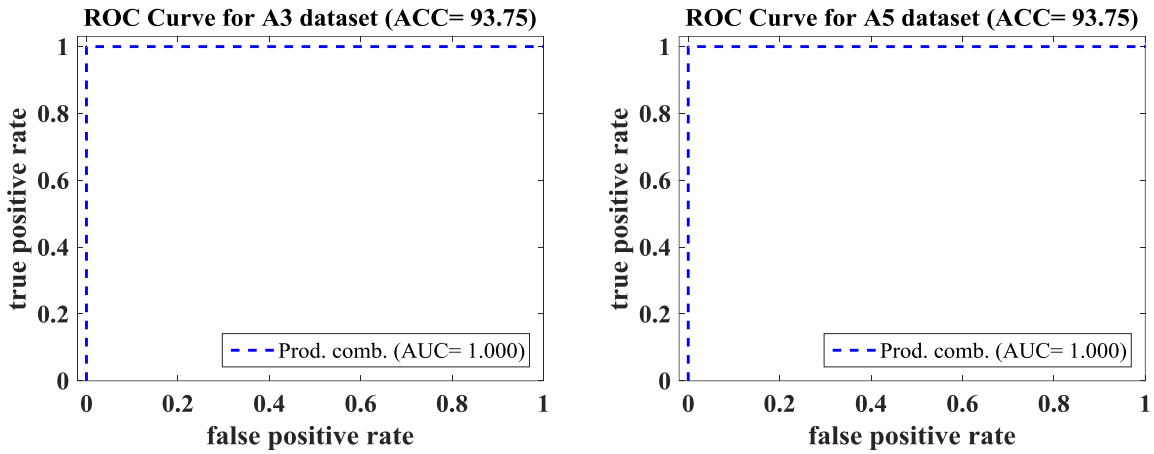

Figure 31: Classification results of A3-A5 datasets using Product Combiner classifier

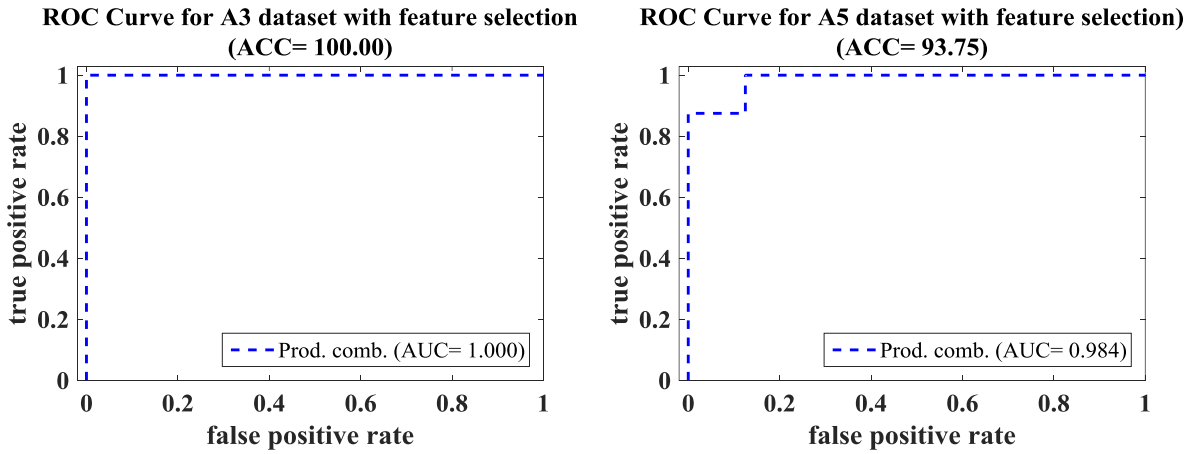

Figure 32: Classification results of A3-A5 datasets using Product Combiner classifier with feature selection

Referring to the results, without feature selection, both one-period and fixed average sampling has exactly the same classification performance. However, when feature selection is performed, using average diameter approach is managed to classify all test data properly.

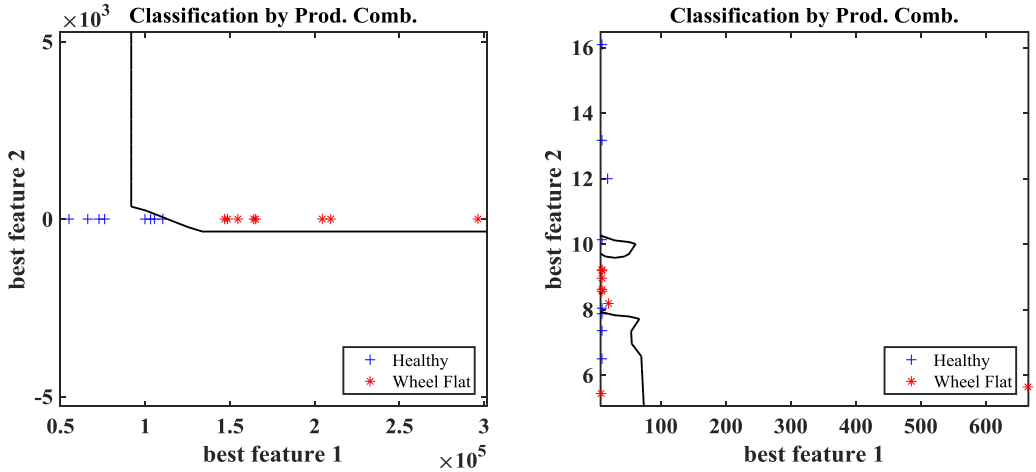

Figure 33: Scatter of the test data in A3 (left), A6 (right) datasets and Product Combiner curve

Figure 33 shows the distribution of healthy and faulty test data with splitting curve of Product Combiner classifier for A3 and A6 datasets with feature selection.

Classification of A4-A6, which belongs to microphone sensors data, is not promising when no feature selection is performed according to Figure 34 and Figure 35.

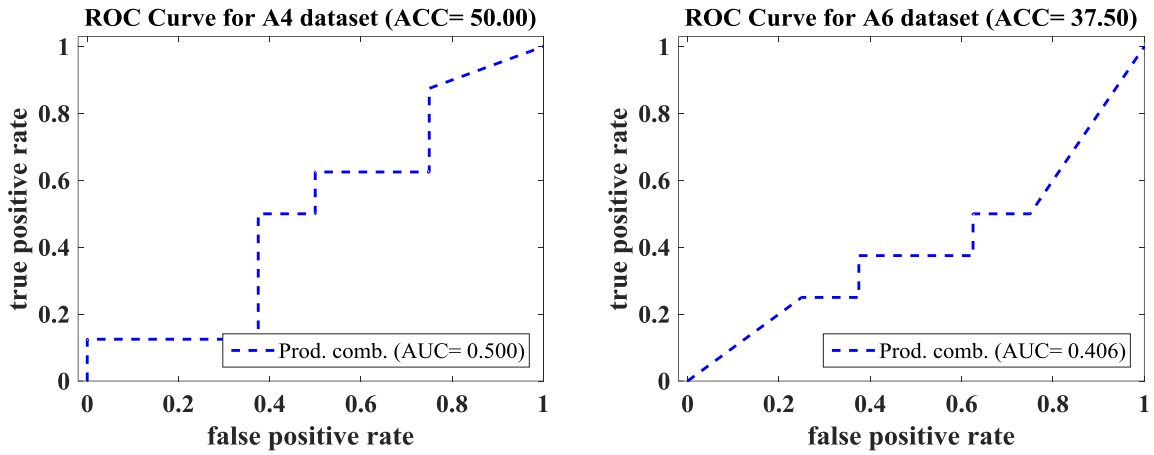

Figure 34: Classification results of A4-A6 datasets using Product Combiner classifier

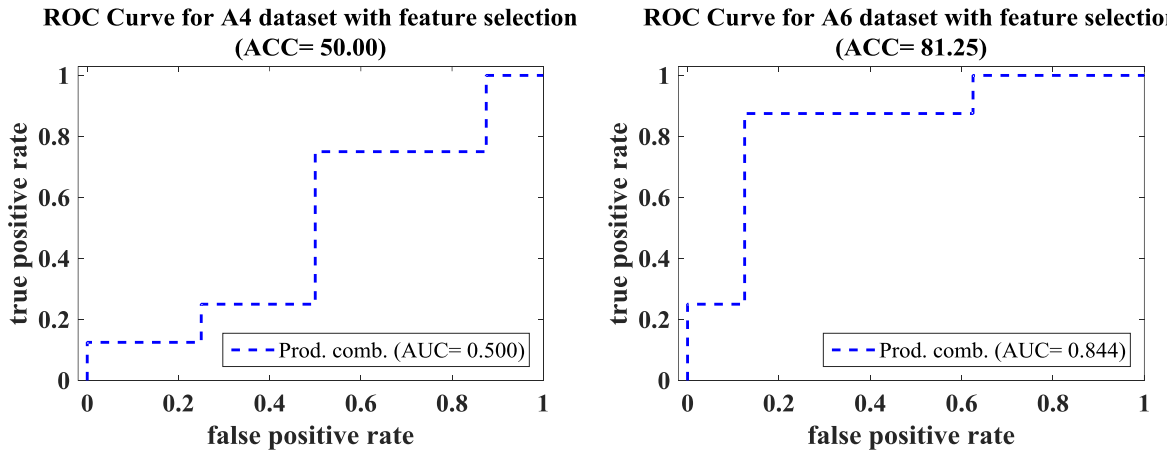

Figure 35: Classification results of A4-A6 datasets using Product Combiner classifier with feature selection

Although being not very promising, after feature selection, classification rate of A6 dataset, which is retrieved by one-period approach, is risen fairly to 81,25%. Distribution of the test data in A6 dataset classification is shown in Figure 33.

4.5 Diagnosis of simulated faulty cases of running gear components

Wayside diagnosis of running gear components requires faulty ground truth data for each component. Although there are some available problematic components like wheel flat and traction motor bearing faults, acquiring these samples is challenging while continuous real-

time measurement is not present. In order to validate the proposed methods in detection of different fault types, a model based fault simulation is performed.

Simulated faults include wheel and rail faults, wheelset bearing faults and gearbox faults. It is known that those faults have impulsive characteristics and in the process of simulating fault types of vibration signals are generated according to random sinus wave amplitude and phase shifting which the frequency is determined according to fault mode and operational speed of the passing bogie as told in Section 3.8.

To clarify how fault simulation and detection are performed, schematic of the algorithm is given in Figure 36.

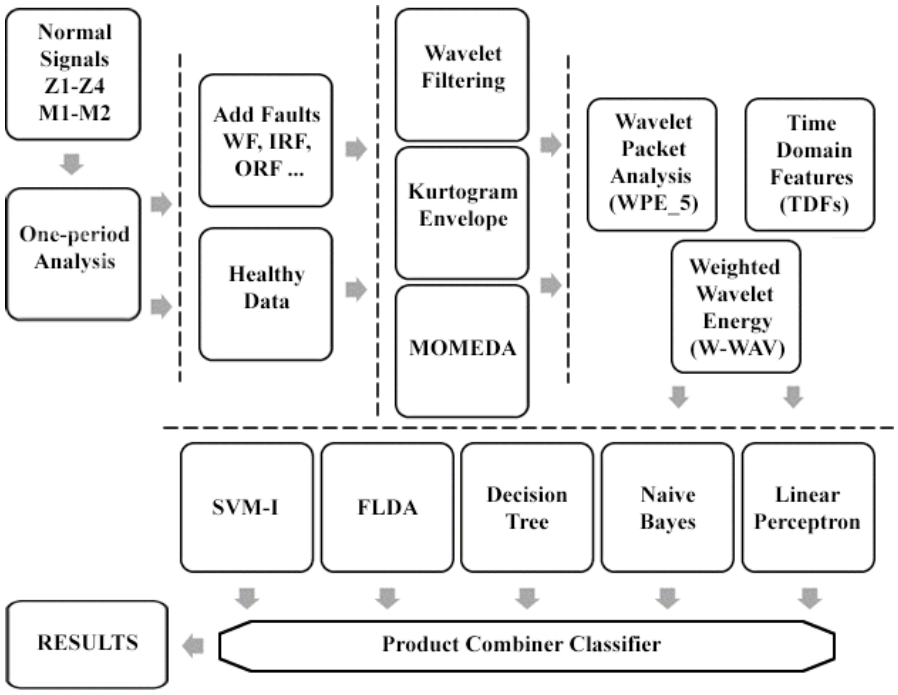

Figure 36: Proposed algorithm for simulating faults diagnosis for running gear components

4.5.1 Feature extraction for diagnosis of simulated faulty cases of running gear compononets

Three different feature extraction techniques are used to achieve representative features for simulated fault diagnosis; five-level Wavelet Packet Energy (WPE_5) which has a size of 32x1, W-WAV that is 3x1 in length and finally Time-domain features (TDFs) which includes eleven features as shown in Eq. (27).

$$TDFs = \begin{bmatrix} energy, mean, std\ dev, max, min, kurtosis, skewness, \\ crest\ \ factor, impulse\ \ factor, spike\ energy, center\ \ frequency \end{bmatrix}_{11\,x\,1} \quad (27)$$

4.5.2 Preparation of the datasets of simulated faults of running gear components

In the diagnosis of simulated faults, measurement data of all three passes of a ground truth healthy train set, ID-119, is used to construct healthy and faulty classes. Table 15 describes the classes of different conditions of the components; healthy case (HC), wheel and rail profile faults (WRF), wheelset bearing outer race fault (ORF), wheelset bearing inner race fault (IRF), traction motor eccentricity (F-TM), gear tooth fault (F-z).

Table 15: Description of classified faults and datasets including simulated faults of running gear components of metro type 81-71M

Datasets	Fault Type	Segment Period	Num. Training	Num. Testing	Sensors	Class Labels
A1	HC	T	120	120	Z1-Z4	A11
	WRF		120	120		A12
A2	HC	T	60	60	M1-M2	A21
	WRF		60	60		A22
B1	HC	T	120	120	Z1-Z4	B11
	ORF		120	120		B12
B2	HC	T	120	120	Z1-Z4	B21
	IRF		120	120		B22
B3	HC	T	60	60	M1-M2	B31
	IRF		60	60		B32
C1	HC	T	120	120	Z1-Z4	C11
	F-TM		120	120		C12
C2	HC	T	120	120	Z1-Z4	C21
	F-z		120	120		C22
C3	HC	T	60	60	M1-M2	C31
	F-z		60	60		C32

Throughout the process, one-period approach is used to retrieve samples from the sensors M1-M2 and Z1-Z4 and same number of wheelset samples are used in the same way for each method to observe classification results. In addition, Kurtogram Envelope (KURT-ENV) and MOMEDA are employed. Moreover, dimensionless approach, feature selection and classifier combining of SVM-I, FLDA, Decision tree, Naive Bayes and Linear Perceptron; Product Combiner, are also carried out if the result may increase into higher levels.

Example simulated faulty signals for wheel defects, wheelset bearings and traction motor are shown in Figure 37, Figure 38 and Figure 39 with respect to normal signal that is retrieved by measurement.

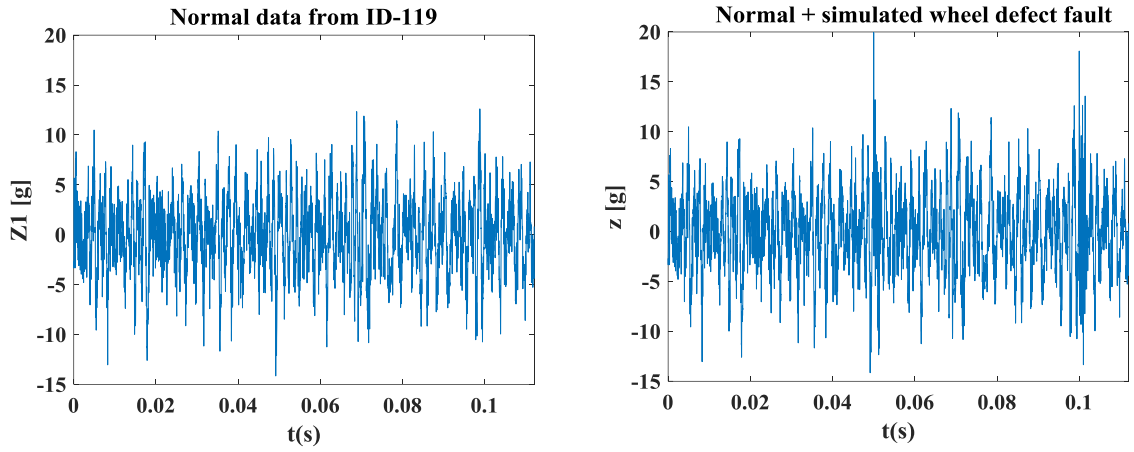

Figure 37: Measured normal vibration signal from ID-119 (left), simulated faulty signal of wheel defects that is buried into normal measurement data from ID-119 (right)

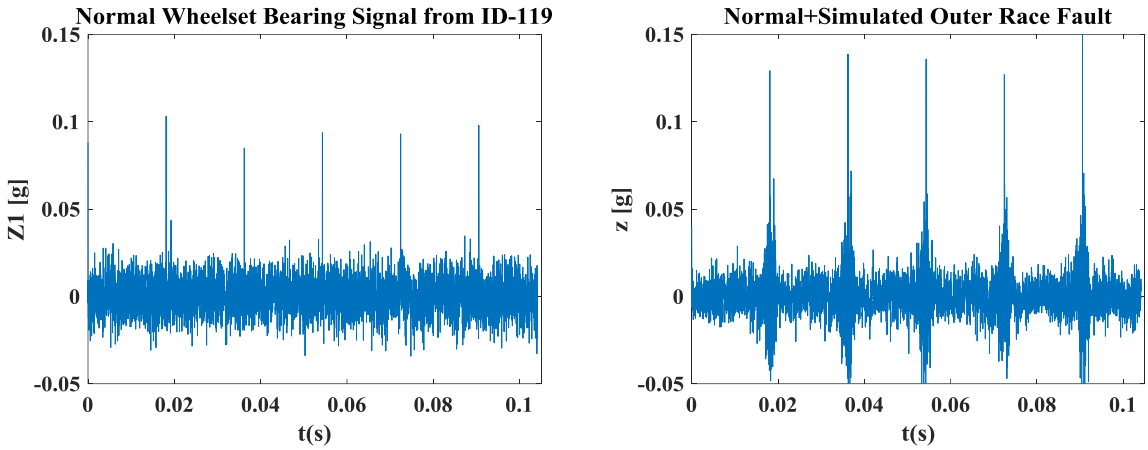

Figure 38: Measured normal vibration signal from ID-119 after MOMEDA filtering (left), simulated outer race fault signal that is buried into normal measurement data from ID-119 after MOMEDA filtering (right)

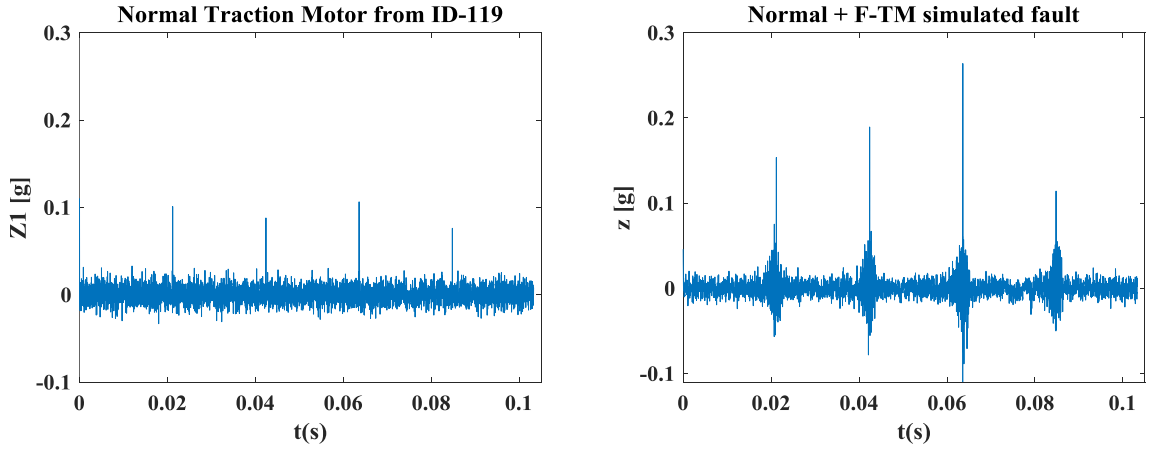

Figure 39: Measured normal vibration signal from ID-119 after MOMEDA filtering (left), simulated traction motor eccentricity fault buried into normal measurement data from ID-119 after MOMEDA (right)

4.5.3 Classification results for simulated faults of running gear components

Classification results of datasets in Table 15 are shown in Table 16 and Table 17 without and with feature selection, respectively.

Table 16: Classification performance for normal and simulated faults using three runs of ID-119 healthy trainset without feature selection with Product Combiner classifier (*: dimensionless approach is used due to achiving better classification accuracy)

	Average classification accuracy (%)						
	WPE_5		**TDFs**		**W-WAV**		**Dataset Labels**
No-filter	*88.8	*98.3	99.2	90.8	*69.6	**100**	A1-A2
	x	x	x	x	x	x	B1 | B2
	x		x		x		B3
	x	x	x	x	x	x	C1 | C2
	x		x		x		C3
Wavelet	*95.0	**100**	*70.0	*70.9	96.3	**100**	A1-A2
	x	x	x	x	x	x	B1 | B2
	x		x		x		B3
	x	x	x	x	x	x	C1 | C2
	x		x		x		C3
KURT-ENV	96.3	95.0	*94.5	96.7	*82.5	83.3	A1-A2
	93.8	96.3	94.2	97.1	*75.0	*87.0	B1 | B2
	100		**100**		**100**		B3
	*87.9	96.7	78.3	**100**	78.3	**100**	C1 | C2
	*97.5		**100**		**100**		C3
MOMEDA	92.1	*93.3	**100**	**100**	88.3	98.3	A1-A2
	79.2	74.5	**100**	**98.3**	80.0	86.7	B1 | B2
	*71.7		**100**		**100**		B3
	*86.7	*88.75	**99.2**	**100**	78.3	**100**	C1 | C2
	*85.0		**100**		**100**		C3

Table 17: Classification performance for normal and simulated faults using three runs of ID-119 healthy trainset with feature selection and Product Combiner classifier (*: dimensionless approach is used due to achiving better classification accuracy)

	Average classification accuracy (%)						
	WPE_5		**TDFs**		**W-WAV**		**Dataset Labels**
No-filter	*86.3	*96.7	**99.6**	89.2	69.6	*85.0	A1-A2
	x	x	x	x	x	x	B1 | B2
	x		x		x		B3
	x	x	x	x	x	x	C1 | C2
	x		x		x		C3
Wavelet	*93.8	**100**	82.9	*71.7	*96.3	**100**	A1-A2
	x	x	x	x	x	x	B1 | B2
	x		x		x		B3
	x	x	x	x	x	x	C1 | C2
	x		x		x		C3
KURT-ENV	*94.1	94.2	94.2	96.7	*83.3	85.8	A1-A2
	*93.3	*98.8	94.2	97.1	*76.7	85.0	B1 | B2
	x		97.5		x		B3
	86.7	*97.1	76.7	**100**	76.7	**100**	C1 | C2
	95.8		**100**		**100**		C3
MOMEDA	66.3	77.5	98.8	**100**	*88.75	98.3	A1-A2
	68.8	67.9	*99.2	97.1	72.9	*85	B1 | B2
	57.5		99.2		**100**		B3
	*72.5	76.7	**99.2**	**100**	73.8	**100**	C1 | C2
	74.2		**100**		**100**		C3

Without utilization of any filters, best possible method is considered to be TDFs for dataset A1 (99.6% with feature selection) and W-WAV (100%) for dataset A2 with respect to the results. WPE_5 method is also managed to classify all test samples in A2 correctly after wavelet filtering is performed. Best results for classification of A1-A2 datasets without filtering, are shown in Figure 40 and Figure 41 with distribution of test data when feature selection has higher results.

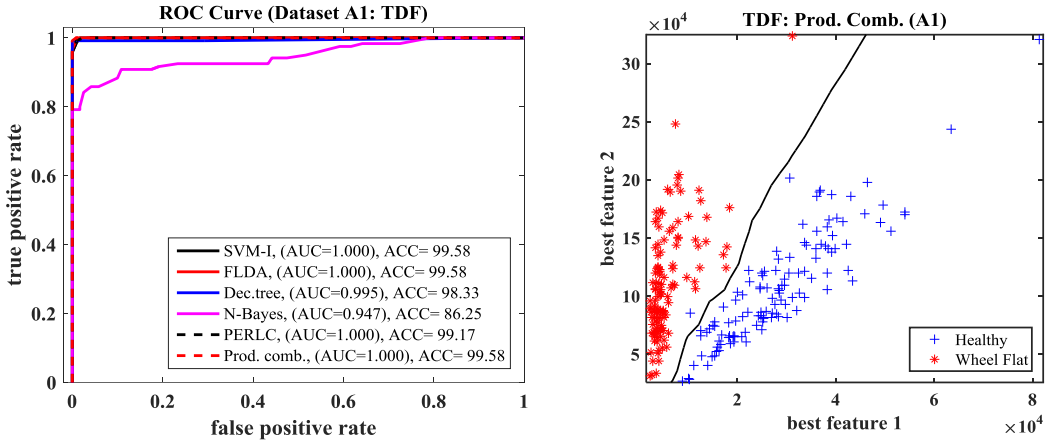

Figure 40: Classification results and ROC curve for A1 dataset with feature selection without filtering (left) for TDFs, scattering of test data (right)

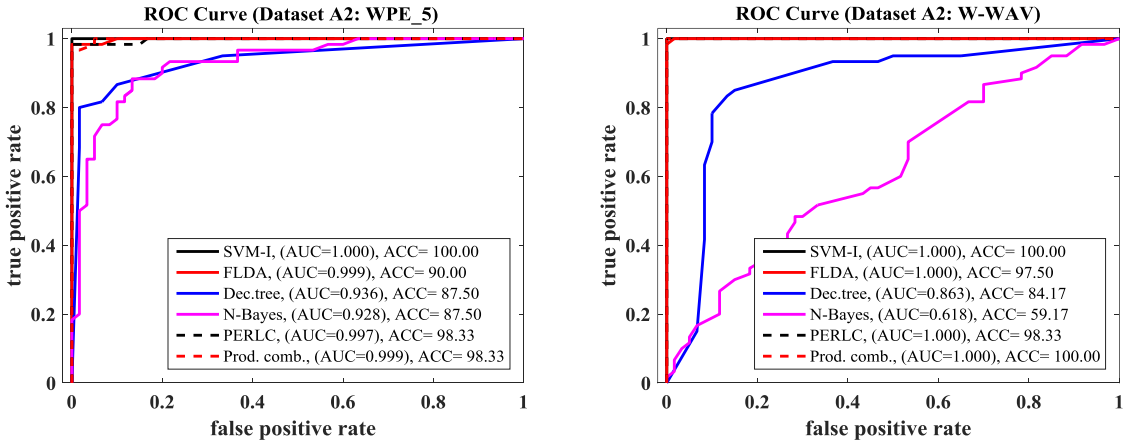

Figure 41: Classification results and ROC curve for A2 dataset without filtering; WPE_5 (left), W-WAV (right)

When wavelet denoising is performed before feature extraction phase, the efficiency of TDFs decreases dramatically whereas performance of WPE_5 and W-WAV increases significantly on dataset A1.

Upon using model based filtering, classification of A1-A2 datasets are increased to 100% with MOMEDA-TDFs without any feature selection or dimensionless feature normalization which (Figure 42).

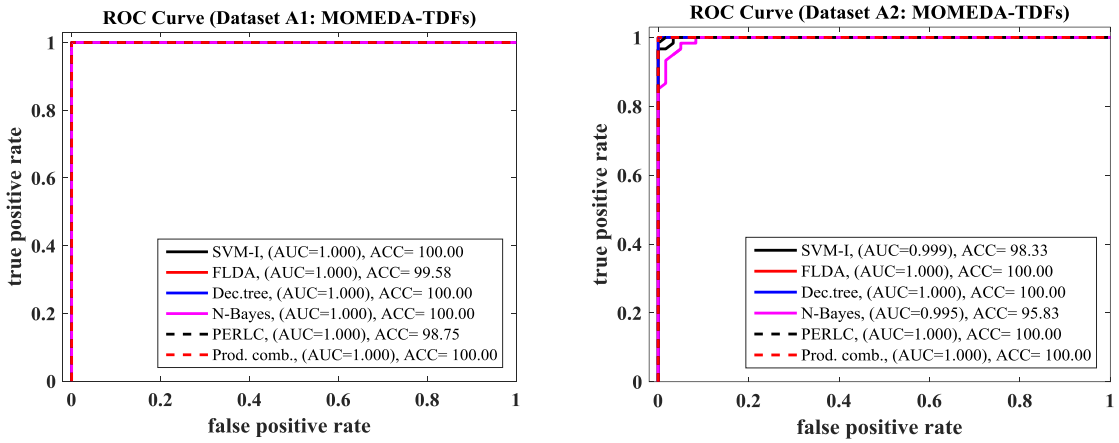

Figure 42: Classification results and ROC curves for A1 and A2 datasets by MOMEDA-TDFs

In bearing fault diagnosis, MOMEDA-TDFs still leads with 100% and 98.8% success in classification of B1 (ORF) and B2 (IRF), respectively (Figure 43). B3 (IRF) is classified by 100% rate with both KURT-ENV and MOMEDA features (Figure 44 and Figure 45).

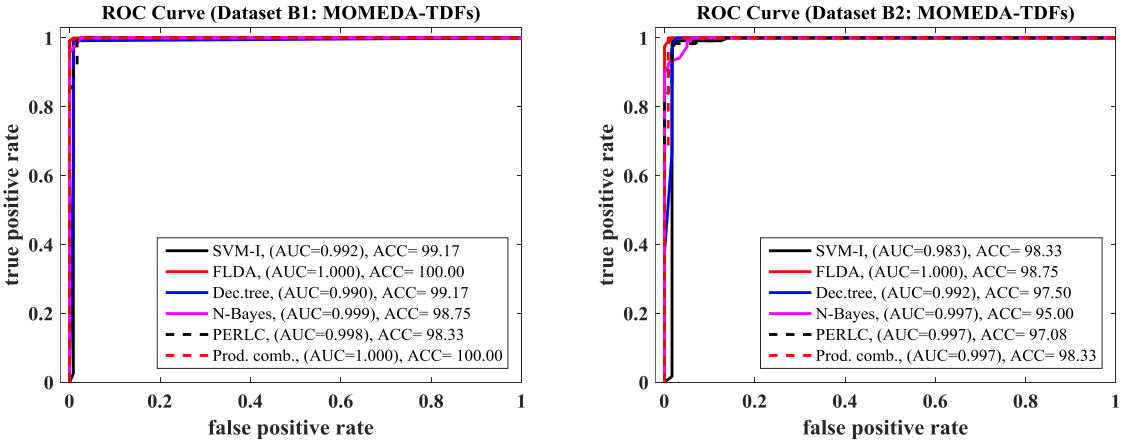

Figure 43: Classification results and ROC curves for B1 and B2 datasets by MOMEDA-TDFs

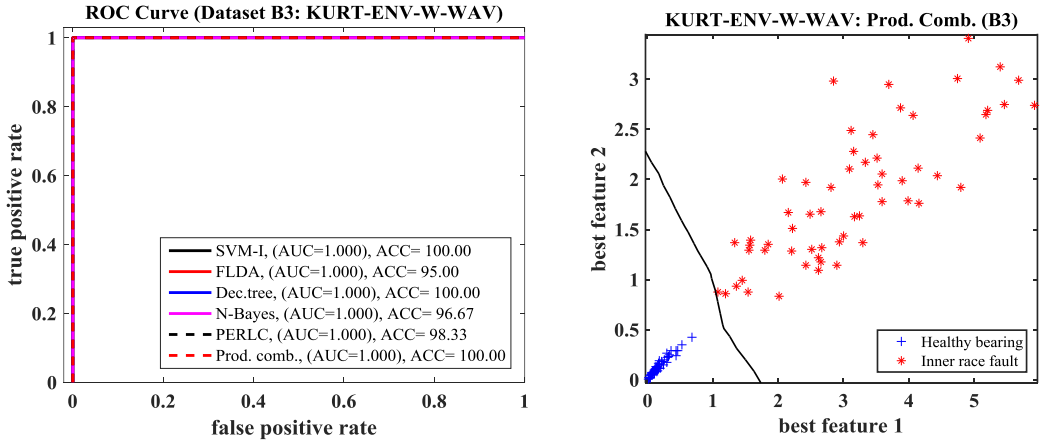

Figure 44: Classification results for B3 dataset using KURT-ENV-W-WAV (left), scattiring of test data (right)

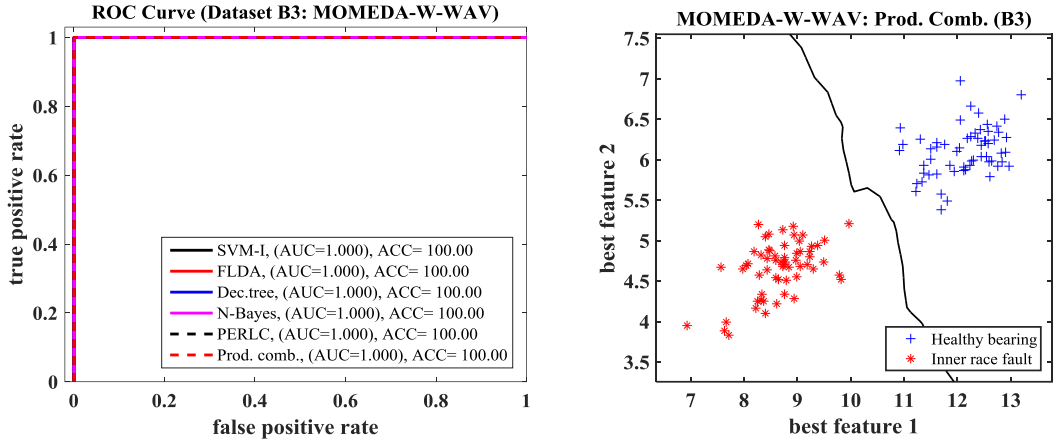

Figure 45: Classification results for B3 dataset using MOMEDA-W-WAV (left), scattiring of test data (right)

In the classification of C2-C3 (gear tooth faults), both MOMEDA and KURT-ENV works well by succeeding in classifying all test samples properly (Figure 47 and Figure 48). However, classification of C1 (traction motor eccentricity) can only be done to its highest rate by MOMEDA-TDFs up to 99.2% with and without feature selection (Figure 46).

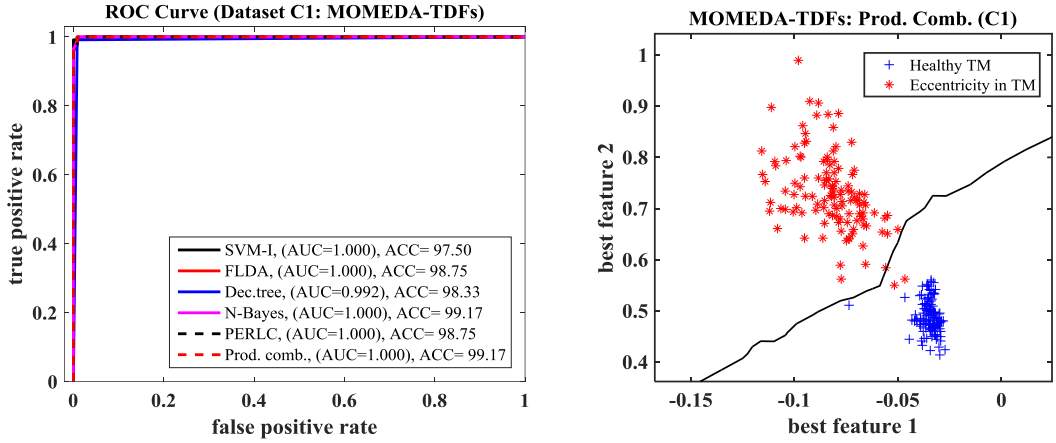

Figure 46: Classification results for C1 dataset using MOMEDA-TDFs (left), scattiring of test data (right)

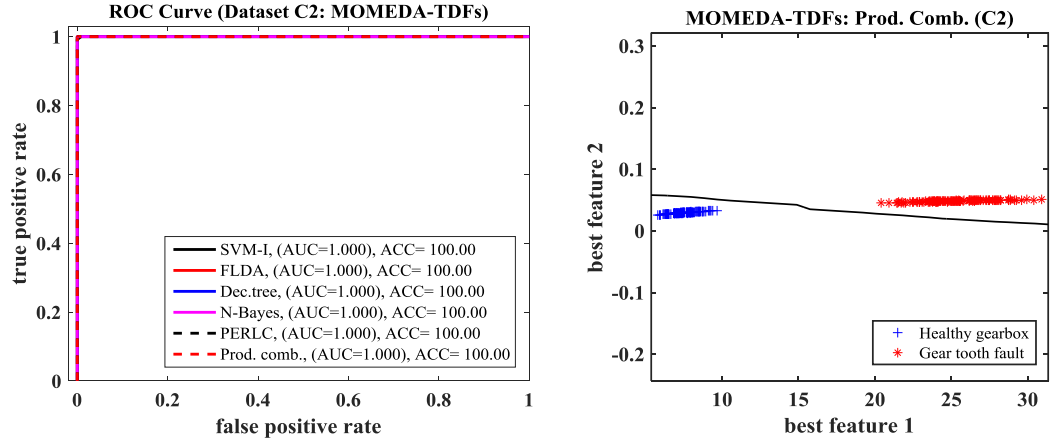

Figure 47: Classification results for C2 dataset using MOMEDA-TDFs (left), scattiring of test data (right)

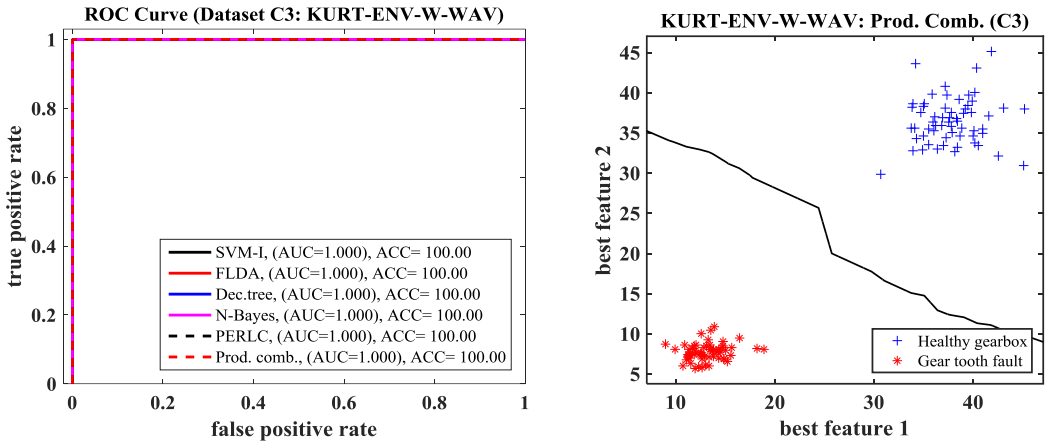

Figure 48: Classification results for C3 dataset using KURT-ENV-W-WAV (left), scattiring of test data (right)

It is concluded that using Product Combiner classifier in most cases share the best performance with the most successful classifier for the related faulty mode and simulated faulty cases on both microphone and vibration signals may successfully classified without any false positive (AUC=1.000), according to ROC curves with the proposed algorithms in this section.

4.6 Detection of traction motor bearing faults using acoustic sensors

Final investigation is focused on traction motor bearing fault detection using acoustic sensors. For this purpose, prior knowledge of a faulty traction motor bearing from ID-131 metro train set is used. In the investigation, two validated methods from simulated fault detection; KURT-ENV-TDFs and MOMEDA-TDFs are employed in combination with one-period analysis as in Section 4.5.

In the classification phase, five classifiers; SVM-I, FLDA, Decision Tree, Naive Bayes, Linear Perceptron and combined classifier method (Product Combiner) are used in training and testing phases.

The database used in this analysis include normal samples of ID-119 healthy train set and faulty samples of train set ID-131 which has inner race faults (TM-IRF) and outer race faults (TM-ORF) on two separate traction motors. Dataset descriptions are shown in Table 18.

Table 18: Description of database that is used for traction motor bearing fault diagnosis

TRAIN IDs	Condition	Nearby Wheelset Numbers	Number of Training Vectors	Number of Test Vectors	Sensors	Class Labels
119	Healthy IR	1-20	7	8	M1-M2	D1(1,1)
	Healthy OR		7	8		D2(1,1)
131	TM-IRF	12, 19, 20	7	8	M1-M2	D1(1,2)
	TM-ORF		7	8		D2(1,2)

The process of bearing fault diagnosis for traction motors is described in Figure 49.

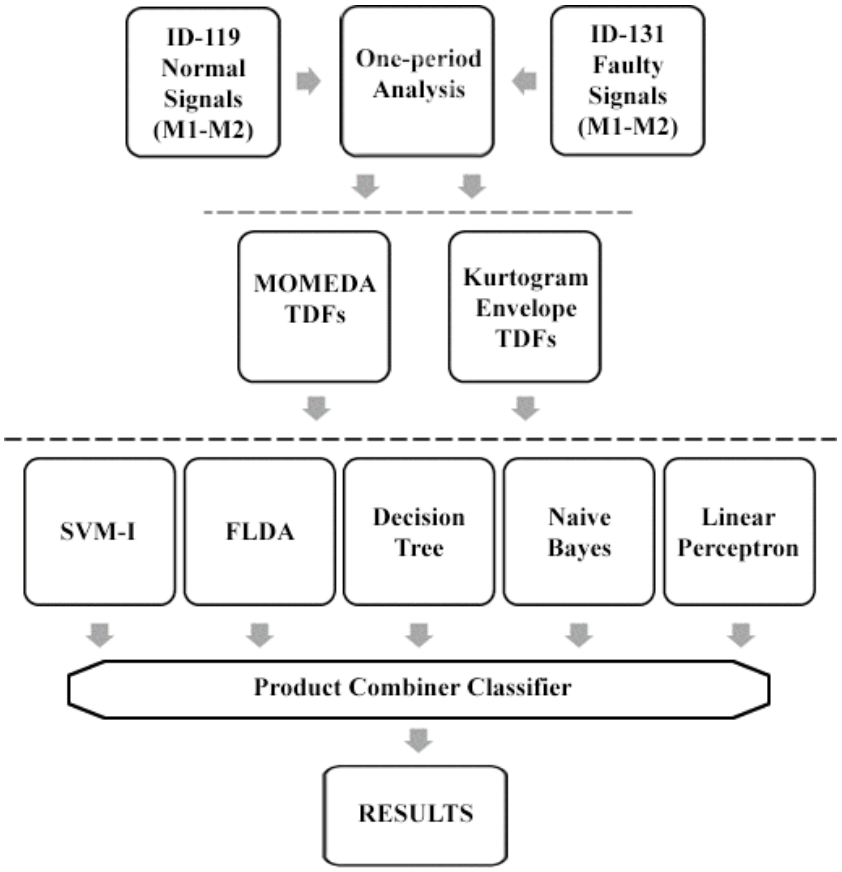

Figure 49: Proposed algorithms for detection of traction motor bearing faults

Examples of measured faulty signals and normal traction motor bearing acoustic signal after MOMEDA filtering are shown in Figure 50.

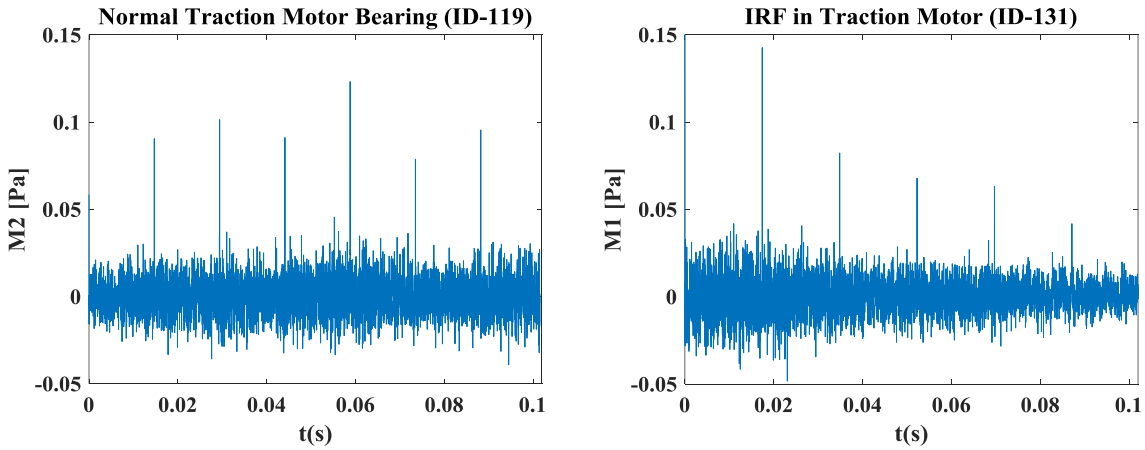

Figure 50: Normal traction motor bearing signal from ID-119 after MOMEDA filtering on acoustic sensor (left), measured signal nearby wheelset-19 from ID-131 after MOMEDA on an acoustic sensor filtering (right)

The results of traction motor bearing fault detection both for inner and outer race faults are shown in Table 19 using Product Combiner classifier. Best results, are shown in a more detailed way in Figure 51 and Figure 52 for KURT-ENV-TDFs and Figure 53 and Figure 54.

Table 19: Classification performance proposed methods in TM bearing fault diagnosis using Product Combiner (*: dimensionless process carried out due to better success)

Classifier	Average classification accuracy (%)				
	Feature Selection	MOMEDA TDFs	KURT-ENV-TDFs	Dataset Labels	Fault Mode
Prod. Comb.	NO	99,18	75	D1	IRF
	YES	**100**	87,5	D1	IRF
	NO	**100**	62,5	D2	ORF
	YES	*93,8	***100**	D2	ORF

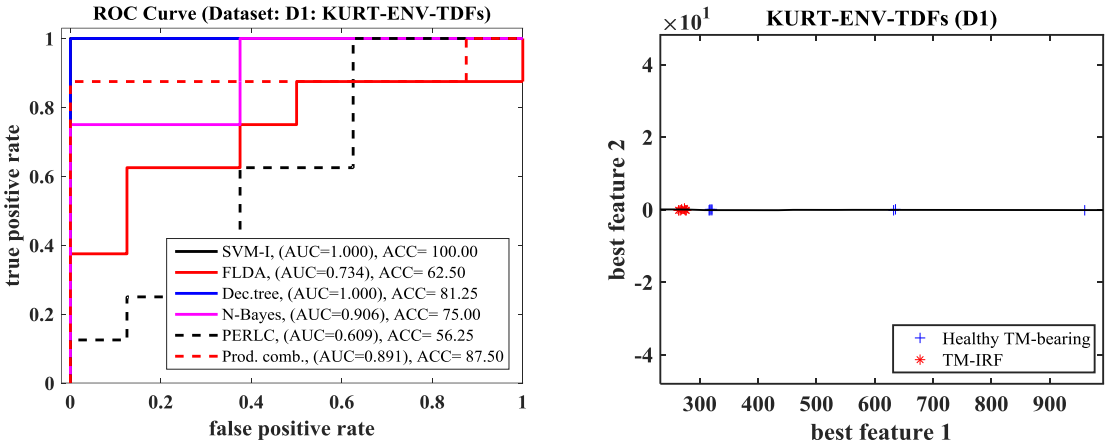

Figure 51: Detailed results of traction motor IRF (dataset D1) with KURT-ENV-TDFs method after feature selection (left), scattering of test data and division by Product Combiner classifer (right)

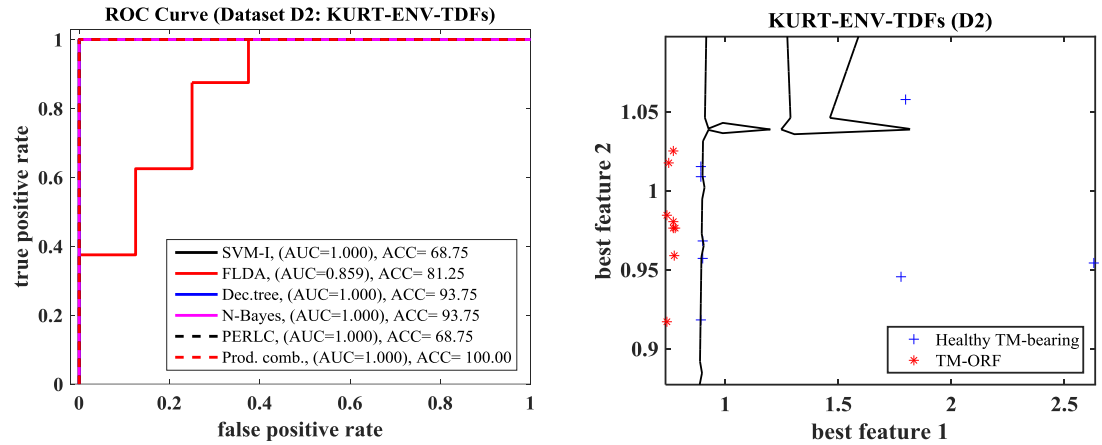

Figure 52: Detailed results of traction motor ORF (dataset D2) with KURT-ENV-TDFs method after feature selection and dimensionless normalization (left), scattering of test data and division by Product Combiner classifer (right)

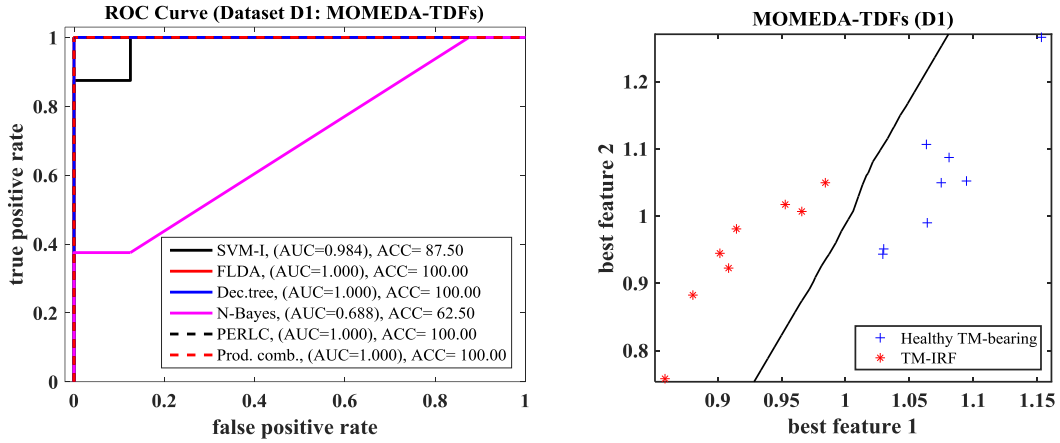

Figure 53: Detailed results of traction motor IRF (dataset D1) with MOMEDA-TDFs method after feature selection and dimensionless normalization (left), scattering of test data and division by Product Combiner classifer (right)

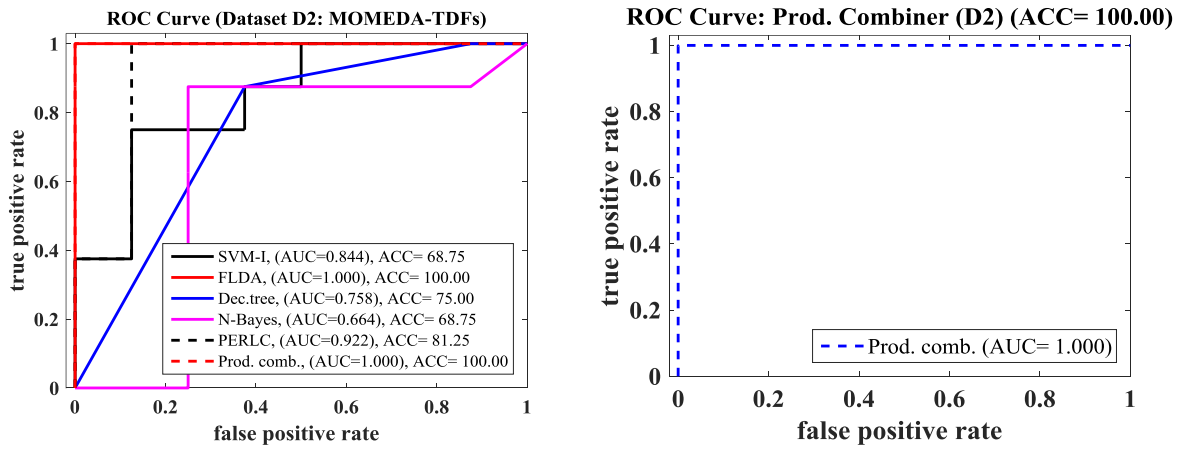

Figure 54: Detailed results of traction motor ORF (dataset D2) with MOMEDA-TDFs method (left); ROC curve for Product Combiner classifer (right)

Referring to the results, both KURT-ENV-TDFs and MOMEDA-TDFs feature extraction approaches are managed to classify all cases properly when a convenient feature selection method and the proper classifier is used. Furthermore, using classifier combination has superior results than any of individual classifier in KURT-ENV-TDFs method such as in Figure 52.

In this investigation, prepared set of data include both IRF and ORF faulty conditions of traction motor bearings and by using acoustic sensors data M1-M2, diagnosis of those may efficiently be performed by proposed algorithms in this section in a very efficient way up to 100%.

5 OWN CONTRIBUTION OF THE PHD. STUDENT

Automatic identification of the faults and real time condition monitoring are the key points of this thesis which the proper consistency of statistical methods throughout wavelet based methods and other cutting-edge techniques are to be employed as well as filtering in the preprocessing on vibration and acoustic signals.

The main objective of this thesis is to design an adaptive fault diagnosis framework that can diagnose running gear faults like wheel defects, wheelset bearing faults and gearbox faults. In order to do so, a multi-functional MATLAB software is created with a user-friendly graphical user interface (GUI) that can read meta data of each measurement and segment signals referring to their train set ID, make a filtration and feature extraction automatically for the given intervals, from wayside diagnosis measurements.

Thanks to the contribution of a ground truth database which is provided by CWRU. With it, efficiency of the algorithms like WPE, TDF and MOMEDA with the proposed novel one-period analysis in bearing fault detection is validated.

In the case of wheel defect detection of metro train sets, with the contribution of one-period analysis, which requires wheel diameters and individual speed calculation, diagnosis of wheel flats is performed by 100% accuracy with different methods. Further validation is done by synthetically oversampling of the faulty class with ADASYN and with different bogie wheelset samples from different train IDs, by utilizing one period analysis and average fixed sampling. Best results obtained by TDFs method up to 100% and proposed novel E-LCP-K has also promising results up to 96.9% in insufficient case.

In simulated faulty modes section, faulty signal frequencies are calculated according to the model based approaches given in Section 2.2 by a speed adaptive way both for normal and faulty samples for bearings and gearboxes. Kurtogram envelope is used to filter out the transients in the fifth scale which is based on speed adaptive determination of rotating machinery components. Noise removal is applied by using wavelet denoising and detection accuracy of the faults improve significantly in W-WAV and WPE_5 wavelet energy methods. In all classification results both dimensionless feature normalization and best feature selection are investigated to achieve better results which in some cases aid improving overall classification accuracy of several feature extraction techniques. It is observed the novel combined methodologies; MOMEDA-TDFs and KURT-ENV-W-WAV techniques have outstanding classification accuracies; wheel defects by 100%, wheelset bearing IRF by 100%,

ORF by 98.8%, TM-eccentricity by 99.2% with the vibration sensor data and both wheelset bearing IRF and gear tooth faults by 100% by the acoustic sensor data.

In the classification stage, the novel classifier combination is done by the involvement of five different classifiers; SVM-I, FLDA, Dec. tree [97], N-Bayes and PERLC [95] and Product Combiner classifier is constructed. Product combiner, which is considered to be the most convenient way since classification accuracy for different classifiers vary significantly in different faulty modes, helps improving the performance in distinguishing classes.

Final investigation is subjected to classifying real faulty cases of traction motor bearings; TM-IRF and TM-ORF. Faulty data is provided by maintenance information from Prague metro that ID-131 metro has faulty bearings in two of its bogies. The analysis results show that validated techniques of simulated faulty cases; KURT-ENV-TDFs and MOMEDA-TDFs are appropriate way of diagnosing TM-IRF and TM-ORF in the real environment by acoustic sensor data with the contribution of one period analysis up to 100% when proper classifiers are used.

6 CONCLUSION

Wayside diagnosis of running gear of railway vehicles has a crucial role by means of cost efficiency in comparison to scheduled or on-condition maintenance. The investigation subjected to this problematic in the area of this thesis includes the evaluation of the data obtained from two passages of Prague metros that runs on metro line-A via instrumentation device that can handle meta-data information and raw signal recording that are measured by acoustic, accelerometer and optical sensors. Processing all data that are measured in these two passages is done according to the wheelset positions of each wheelset during all passes of the metro train sets.

After checking the validation of the signals, two main database are constructed from the passages of Malostranská and Dejvická. In the former one, since the speed of the run varies significantly and the existence of a transition curve along the measurement, some signal samples are out of the range of the accelerometers and abnormal activity is observed in both accelerometer and acoustic sensors due to the presence of random heavy flange noise.

Firstly, to discard the unwanted signal outputs, an empirical approach is proposed in combination with the novel LCP-K variants as well as WPE and TDFs. According to the results, E-LCP-K may nominated to be the best way of solving the problem when both acoustic and vibration based signals are used.

Secondly, an attempt to validate the efficiency of the proposed algorithms WPE, TDF MOMEDA and MOMEDA-AR, is made by utilizing FLDA and SVM for classifying the signal classes of up to five different levels of severity and early fault diagnosis of three different fault types; IRF, ORF, BF, belong to ball bearings on a trusted database which is retrieved from CWRU. Early-fault diagnosis of three types of faults is succeeded by MOMEDA with FLDA as 100%. Furthermore, even other WPE-3, WPE-5 and TDF feature extraction techniques have promising results. MOMEDA-AR with SVM-II outperforms in classifying 5-class severity levels of the rolling element faults of ball bearings by a rate of 99.7%.

Thirdly, the vibration signals retrieved from Dejvická passage are used to identify the wheel defects and outstanding results are observed up to 100% by TDF with both FLDA and SVM classifiers. Further investigations are carried out with the measured data from Dejvická metro station. Two more classifiers; Dec. tree and PERLC are added in the classifying stage. Both acoustic and vibration sensor information are evaluated with the proposed techniques in non-stationary signal processing. Further, measured raw data in comparison to synthetically oversampled data using ADASYN is also examined to see real detection rates in a more reliable

way. According to the results, 100% detection of wheel flats is possible by using vibration sensor data with TDF and 93% with LCP-K and acoustic sensors.

Fourthly, one-period analysis and fixed average sampling are examined in comparison. In the investigation, feature selection is also performed and referring to the results one-period analysis outperforms the average diameter sampling in acoustic sensor diagnosis whereas fixed sampling approach has higher results in vibration sensor data up to 100%. This is because the examined flat wheel have smaller diameter than the average metro wheel diameter. However, if the investigated wheel had a bigger diameter than average diameter, the diagnosis success of fixed diameter sampling could have far worse. Besides, it may highly likely that false positive rates would have improved in other wheelset samples.

Fifthly, since some of the faults are far less frequent, model based fault simulation approach is also carried out to see the performance of the proposed techniques in recognition of several fault types like; wheel and rail faults, wheelset bearing faults, gear tooth fault and traction motor eccentricity. For this purpose, simulated faults are buried into the measurement signals of ID-119, which is marked as healthy, using one-period analysis. In the classification, half of the sensor information is used in training and remaining vectors are used in testing and five different classifiers and classifier combining approach are also employed.

Upon using wavelet denoising, efficiency of wavelet energy features like WPE_5 and W-WAV has significantly improved in detecting wheel and rail faults. However, results with TDFs dropped dramatically. Using TDFs with feature selection slightly improved the recognition rates to 99.6% from 99.2% with vibration sensors data. Nevertheless, a model based filtering scheme MOMEDA-TDFs outperforms by recognizing all simulated wheel and rail type faults as 100% with vibration sensors data.

When it comes to bearing fault diagnosis, both KURT-ENV (with all feature extraction techniques; WPE_5, TDFs and W-WAV) and MOMEDA-TDFs have outstanding results in detecting wheelset IRF by acoustic sensors as 100%. Wheelset IRF can also be detected by MOMEDA-TDFs and vibration sensors flawlessly and recognition of wheelset ORF reaches at 98.8% with feature selection.

Furthermore, traction motor eccentricity and gear tooth fault can be detected respectively, up to 99.2% and 100% by utilizing MOMEDA-TDFs in the simulated faulty cases.

Lastly, final investigation is performed to diagnose real faulty cases of TM-IRFs and TM-ORFs using acoustic sensors. According to the results, both MOMEDA-TDFs and KURT-ENV-TDFs have outstanding performances in detecting both TM-ORFs and TM-IRFs as 100% when the appropriate classifier is used.

The study belonging to this thesis includes both real and simulated validations of proposed methodologies and in most cases the results are considered to be outstanding. The proposed schemes are efficient in wayside fault diagnosis of running gear related faults of railway vehicles by using vibration and acoustic sensors and accompanying optical gates for wheelset position detection.

As a result, the research that is subjected to this thesis may aid specialist who are focused on the condition monitoring systems or maintenance. Further adjustments and improvements may be done when more faulty data information is available and the framework may work in a better performance.

7 REFERENCES

[1] O. Kilinc and A. Onat, “Simple test procedure of strain gage measurement: an introductory implementation towards railway vehicle testing,” *1st International Workshop on Construction and Electricity Applications on Vocational Education*, vol. 2, no. Special Issue (December), pp. 393–405, 2015.

[2] S. M. Zakharov and I. A. Zharov, “Criteria of bogie performance and wheel/rail wear prediction based on wayside measurements,” *Wear*, vol. 258, no. 7–8, pp. 1135–1141, Mar. 2005.

[3] D. Barke and W. K. Chiu, “Structural health monitoring in the railway industry: a review,” *Structural Health Monitoring*, vol. 4, no. 1, pp. 81–93, 2005.

[4] C. P. Ward, R. M. Goodall, R. Dixon, and G. Charles, “Condition monitoring of rail vehicle bogies,” in *UKACC International Conference*, 2010, pp. 1–6.

[5] František Netušil, “Diagnostika závad jedoucích drážních vozidel systémem ASDEK,” Bachalor thesis, University of Pardubice, Digital Library of University of Pardubice, 2014.

[6] M. Vaško, M. Sága, and M. Handrik, “Comparison study of the computational methods for eigenvalues IFE analysis,” *Applied and Computational Mechanics*, vol. 2, pp. 157–166, 2008.

[7] Saga M. and Medvecký S., “Analysis of vehicle vibration with uncertain system parameters,” *Scientific Letters of University of Zlina*, vol. 7, pp. 16–21, 2005.

[8] S. Iwnicki, “Handbook of Railway Vehicle Dynamics,” vol. 1, Boca Raton : CRC / Taylor & Francis, 2006, p. 201.

[9] Z. Kulpa, A. Pownuk, and I. Skalna, “Analysis of linear mechanical structures with uncertainties by means of interval methods,” *Computer Assisted Mechanics and Engineering Sciences*, vol. 5, no. 4, pp. 443–477, 1998.

[10] R. Tipireddy, H. A. Nasrellah, and C. S. Manohar, “A Kalman filter based strategy for linear structural system identification based on multiple static and dynamic test data,” *Probabilistic Engineering Mechanics*, vol. 24, no. 1, pp. 60–74, Jan. 2009.

[11] W. Ding, J. Wang, C. Rizos, and D. Kinlyside, “Improving adaptive Kalman estimation in GPS/INS integration,” *Journal of Navigation*, vol. 60, no. 03, pp. 517–529, Sep. 2007.

[12] Altan Onat, Onur Kılınç, and Michael Lata, “A linear Kalman filtering scheme for estimation of secondary vertical suspension of railway vehicles,” presented at the The 21st VIBROENGINEERING Conference, 2016, vol. 7, pp. 124–128.

[13] Ş. Yildirim and İ. Uzmay, “Neural network applications to vehicle’s vibration analysis,” *Mechanism and Machine Theory*, vol. 38, no. 1, pp. 27–41, 2003.

[14] C. Mao, Y. Jiang, D. Wang, X. Chen, and J. Tao, “Modeling and simulation of non-stationary vehicle vibration signals based on Hilbert spectrum,” *Mechanical Systems and Signal Processing*, vol. 50–51, pp. 56–69, 2015.

[15] P. Hloušek, “Phase analysis of interference currents of railway vehicles,” *Electroscope, Applied Electronics*, vol. 2008, no. 3, pp. 241–244, 2008.

[16] A. Aherwar, “An investigation on gearbox fault detection using vibration analysis techniques: A review,” *Australian Journal of Mechanical Engineering*, vol. 10, no. 2, pp. 169–183, 2012.

[17] B. KAMEL and A. MILOUDI, “Detection of gear defects by resonance demodulation detected by wavelet transform and comparison with the kurtogram,” *21st French Mechanical Congress, Bordeaux, France*, 2013.

[18] P. Li, F. Kong, Q. He, and Y. Liu, “Multiscale slope feature extraction for rotating machinery fault diagnosis using wavelet analysis,” *Measurement*, vol. 46, no. 1, pp. 497–505, 2013.

[19] G. L. McDonald, Q. Zhao, and M. J. Zuo, “Maximum correlated kurtosis deconvolution and application on gear tooth chip fault detection,” *Mechanical Systems and Signal Processing*, vol. 33, pp. 237–255, Nov. 2012.

[20] A. Alemi, F. Corman, and G. Lodewijks, “Condition monitoring approaches for the detection of railway wheel defects,” *Proceedings of the Institution of Mechanical Engineers, Part F: Journal of Rail and Rapid Transit*, Jun. 2016.

[21] B. Stratman, Y. Liu, and S. Mahadevan, “Structural health monitoring of railroad wheels using wheel impact load detectors,” *Journal of Failure Analysis and Prevention*, vol. 7, no. 3, pp. 218–225, Jul. 2007.

[22] M. Palo, H. Schunnesson, U. Kumar, P.-O. Larsson-Kråik, and D. Galar, “Rolling stock condition monitoring using wheel/rail forces,” *Insight - Non-Destructive Testing and Condition Monitoring*, vol. 54, no. 8, pp. 451–455, Aug. 2012.

[23] M. Palo, D. Galar, T. Nordmark, M. Asplund, and D. Larsson, “Condition monitoring at the wheel/rail interface for decision-making support,” *Proceedings of the Institution of Mechanical Engineers, Part F: Journal of Rail and Rapid Transit*, vol. 228, no. 6, pp. 705–715, Aug. 2014.

[24] S. J. Buggy *et al.*, “Railway track component condition monitoring using optical fibre Bragg grating sensors,” *Measurement Science and Technology*, vol. 27, no. 5, p. 055201, May 2016.

[25] K. Y. Lee, K. K. Lee, and S. L. Ho, “Exploration of using FBG sensor for derailment detector,” *WSEAS Transactions Topics Systems*, vol. 3, pp. 2433–2439, 2004.

[26] M. L. Filograno *et al.*, “Real-time monitoring of railway traffic using fiber Bragg grating sensors,” *IEEE Sensors Journal*, vol. 12, no. 1, pp. 85–92, Jan. 2012.

[27] H. J. Salzburger, M. Schuppmann, W. Li, and G. Xiaorong, “In-motion ultrasonic testing of the tread of high-speed railway wheels using the inspection system AUROPA III,” *Insight - Non-Destructive Testing and Condition Monitoring*, vol. 51, no. 7, pp. 370–372, Jul. 2009.

[28] J. Brizuela, A. Ibañez, P. Nevado, and C. Fritsch, “Railway wheels flat detector using Doppler effect,” *Physics Procedia*, vol. 3, no. 1, pp. 811–817, Jan. 2010.

[29] J. Brizuela, C. Fritsch, and A. Ibáñez, "Railway wheel-flat detection and measurement by ultrasound," *Transportation Research Part C: Emerging Technologies*, vol. 19, no. 6, pp. 975–984, Dec. 2011.

[30] S. Kenderian, B. B. Djordjevic, D. Cerniglia, and G. Garcia, "Dynamic railroad inspection using the laser-air hybrid ultrasonic technique," *Insight-Non-Destructive Testing and Condition Monitoring*, vol. 48, no. 6, pp. 336–341, 2006.

[31] K. Bollas, D. Papasalouros, D. Kourousis, and A. Anastasopoulos, "Acoustic emission monitoring of wheel sets on moving trains," *Construction and Building Materials*, vol. 48, pp. 1266–1272, Nov. 2013.

[32] A. Bracciali and G. Cascini, "Detection of corrugation and wheel flats of railway wheels using energy and cepstrum analysis of rail acceleration," *Proceedings of the Institution of Mechanical Engineers, Part F: Journal of Rail and Rapid Transit*, vol. 211, no. 2, pp. 109–116, Mar. 1997.

[33] D. Skarlatos, K. Karakasis, and A. Trochidis, "Railway wheel fault diagnosis using a fuzzy-logic method," *Applied Acoustics*, vol. 65, no. 10, pp. 951–966, Oct. 2004.

[34] V. Belotti, F. Crenna, R. C. Michelini, and G. B. Rossi, "Wheel-flat diagnostic tool via wavelet transform," *Mechanical Systems and Signal Processing*, vol. 20, no. 8, pp. 1953–1966, Nov. 2006.

[35] M. L. Lee and W. K. Chiu, "Determination of railway vertical wheel impact magnitudes: Field trials," *Structural Health Monitoring*, vol. 6, no. 1, pp. 49–65, Mar. 2007.

[36] R. W. Ngigi, C. Pislaru, A. Ball, and F. Gu, "Modern techniques for condition monitoring of railway vehicle dynamics," *Journal of Physics: Conference Series*, vol. 364, p. 012016, May 2012.

[37] K. Yang, L. Ma, X. Gao, and L. Wang, "Profile parameters of wheelset detection for high speed freight train," 2012, p. 83341W–83341W–6.

[38] F. Liu, C. Shen, Q. He, A. Zhang, Y. Liu, and F. Kong, "Wayside bearing fault diagnosis based on a data-driven doppler effect eliminator and transient model analysis," *Sensors*, vol. 14, no. 5, pp. 8096–8125, May 2014.

[39] M. Zhao, J. Lin, X. Xu, and Y. Lei, "Tacholess envelope order analysis and its application to fault detection of rolling element bearings with varying speeds," *Sensors*, vol. 13, no. 8, pp. 10856–10875, Aug. 2013.

[40] M. R. A. A. Abad, A. Moosavian, and M. Khazaee, "Wavelet transform and least square support vector machine for mechanical fault detection of an alternator using vibration signal," *Journal of Low Frequency Noise, Vibration and Active Control*, vol. 35, no. 1, pp. 52–63, Mar. 2016.

[41] R. Yan, R. X. Gao, and X. Chen, "Wavelets for fault diagnosis of rotary machines: A review with applications," *Signal Processing*, vol. 96, pp. 1–15, Mar. 2014.

[42] R. B. Randall and J. Antoni, "Rolling element bearing diagnostics—A tutorial," *Mechanical Systems and Signal Processing*, vol. 25, no. 2, pp. 485–520, Feb. 2011.

[43] K. Jakimovska, V. Vasilev, N. Stoimenov, S. Gyoshev, and D. Karastoyanov, "Train control system for railway vehicles running at operational speed," *Manufacturing Engineering*, vol. 69, no. 2, pp. 86–92, 2015.

[44] B. Brickle, R. Morgan, E. Smith, J. Brosseau, and C. Pinney, "Identification of existing and new technologies for wheelset condition monitoring," TTCI Ltd, TTCI(UK), RSSB Report T607 UK P-07-005, 2008.

[45] Zelenka J., Vágner J., Kohout M., Hába A., Musil K., and Havlíček P., "Senzorické systémy pro indikaci poruch jedoucích vozidel v podmínkách metra," University of Pardubice, Česká Třebová, 2015.

[46] Zelenka J., Vágner J., Kohout M., Havlíček P., and DiMet P., "Systém pro indikaci poruch jedoucích vozidel v podmínkách metra," Pardubice, TA ČR, 2016.20s.

[47] R. Müller, P. Gratacos, P. Mora, J. C. O. Nielsen, J. Feng, and S. Cervello, "Definition of wheel maintenance measures for reducing ground vibration," *RIVAS (SCP0-GA-2010-265754), Deliverable*, vol. 2, 2013.

[48] A. Oulmane, A. A. Lakis, and N. Mureithi, "Automatic fault diagnosis of rotating machinery," *European Journal of Mechanical Engineering Research*, vol. 3, no. 2, pp. 19–41, 2016.

[49] Zelenka J., Vágner J., Hába, A., Kohout, M., and Musil K., "Analýzy poruchových stavů v provozu kolejových vozidel indikovaných na jedoucím vlaku," University of Pardubice, Česká Třebová, 2015.

[50] "SKF CAD models." [Online]. Available: http://skf.partcommunity.com/3d-cad-models/. [Accessed: 21-Mar-2017].

[51] S. Chabchoub, S. Mansouri, and R. B. Salah, "Impedance cardiography signal denoising using discrete wavelet transform," *Australasian Physical & Engineering Sciences in Medicine*, vol. 39, no. 3, pp. 655–663, Sep. 2016.

[52] P. S. Addison, "Wavelet transforms and the ECG: a review," *Physiological Measurement*, vol. 26, no. 5, pp. R155–R199, Oct. 2005.

[53] C. Varadharajan and H. F. Hemond, "Time-series analysis of high-resolution ebullition fluxes from a stratified, freshwater lake: Analyzing high-resoultion bubbling data," *Journal of Geophysical Research: Biogeosciences*, vol. 117, no. G02004, pp. 1–15, Jun. 2012.

[54] C. R. Cornish, C. S. Bretherton, and D. B. Percival, "Maximal overlap wavelet statistical analysis with application to atmospheric turbulence," *Boundary-Layer Meteorology*, vol. 119, no. 2, pp. 339–374, 2006.

[55] J. Joy, S. Peter, and N. John, "Denoising using soft thresholding," *International Journal of Advanced Research in Electrical, Electronics and Instrumentation Engineering*, vol. 2, no. 3, pp. 1027–1032, 2013.

[56] J. Xu, Z. Wang, C. Tan, L. Si, and X. Liu, “A novel denoising method for an acoustic-based system through empirical mode decomposition and an improved fruit fly optimization algorithm,” *Applied Sciences*, vol. 7, no. 3, p. 215, Feb. 2017.

[57] D. L. Donoho and I. M. Johnstone, “Adapting to unknown smoothness via wavelet shrinkage,” *Journal of the American Statistical Association*, vol. 90, no. 432, p. 1200, Dec. 1995.

[58] G. G. Yen and K.-C. Lin, “Wavelet packet feature extraction for vibration monitoring,” *IEEE transactions on industrial electronics*, vol. 47, no. 3, pp. 650–667, 2000.

[59] S. Ergin, A. Uzuntas, and M. B. Gulmezoglu, “Detection of stator, bearing and rotor faults in induction motors,” *Procedia Engineering*, vol. 30, pp. 1103–1109, 2012.

[60] R. F. Dwyer, “Detection of non-Gaussian signals by frequency domain kurtosis estimation,” in *Acoustics, Speech, and Signal Processing, IEEE International Conference*, 1983, vol. 8, pp. 607–610.

[61] J. Antoni, “Fast computation of the kurtogram for the detection of transient faults,” *Mechanical Systems and Signal Processing*, vol. 21, no. 1, pp. 108–124, Jan. 2007.

[62] F. Gu, X. Tian, Z. Chen, T. Wang, I. Rehab, and A. Ball, “Fault severity diagnosis of rolling element bearings based on kurtogram and envelope analysis,” Institute of Research Engineers and Doctors, 2014.

[63] S.-R. Zhou, J.-P. Yin, and J.-M. Zhang, “Local binary pattern (LBP) and local phase quantization (LBQ) based on Gabor filter for face representation,” *Neurocomputing*, vol. 116, pp. 260–264, Sep. 2013.

[64] S. Ergin and O. Kilinç, “Using DSIFT and LCP features for detecting breast lesions,” in *International Symposium on Computing in Science & Engineering. Proceedings*, 2013, pp. 216–220.

[65] Y. Guo, G. Zhao, and M. Pietikäinen, “Texture classification using a linear configuration model based descriptor,” 2011, pp. 119.1–119.10.

[66] S. Ergin and O. Kilinc, “A new feature extraction framework based on wavelets for breast cancer diagnosis,” *Computers in Biology and Medicine*, vol. 51, pp. 171–182, Aug. 2014.

[67] M. F. Khan, E. Khan, and Z. A. Abbasi, “Image contrast enhancement using normalized histogram equalization,” *Optik - International Journal for Light and Electron Optics*, vol. 126, no. 24, pp. 4868–4875, Dec. 2015.

[68] L. Zeng, X. Li, and J. Xu, “An improved joint dictionary training method for single image super resolution,” *COMPEL - The international journal for computation and mathematics in electrical and electronic engineering*, vol. 32, no. 2, pp. 721–727, Mar. 2013.

[69] Onur Kilinc and Jakub Vágner, “Sensing anomalous sensor data in wayside diagnostic using enhanced LBP-Kurtograms,” *Scientific papers of the University of Pardubice. Series B, The Jan Perner Transport Faculty*, vol. 21, no. Series B, In press.

[70] S. Fu, K. Liu, Y. Xu, and Y. Liu, “Rolling bearing diagnosing method based on time domain analysis and adaptive fuzzy C -Means clustering,” *Shock and Vibration*, vol. 2016, pp. 1–8, 2016.

[71] M. Wang, N.-Q. Hu, L. Hu, and M. Gao, “Feature optimization for bearing fault diagnosis,” in *Quality, Reliability, Risk, Maintenance, and Safety Engineering (QR2MSE), 2013 International Conference on*, 2013, pp. 1738–1741.

[72] X. Yu, E. Ding, C. Chen, X. Liu, and L. Li, “A novel characteristic frequency bands extraction method for automatic bearing fault diagnosis based on Hilbert Huang transform,” *Sensors*, vol. 15, no. 11, pp. 27869–27893, Nov. 2015.

[73] M. Martín Torrego and others, “Dynamic model of a ball bearing, vibration analysis,” 2015.

[74] B. Sreejith, A. K. Verma, and A. Srividya, “Fault diagnosis of rolling element bearing using time-domain features and neural networks,” in *Industrial and Information Systems, 2008. ICIIS 2008. IEEE Region 10 and the Third international Conference on*, 2008, pp. 1–6.

[75] A. Naji and M. H. Soliman, “Center frequency stabilization in planar dual-mode resonators during mode-splitting control,” *Scientific Reports*, vol. 7, p. 43855, Mar. 2017.

[76] R. A. Wiggins, “Minimum entropy deconvolution,” *Geoexploration*, vol. 16, no. 1–2, pp. 21–35, Apr. 1978.

[77] C. A. Cabrelli, “Minimum entropy deconvolution and simplicity: A noniterative algorithm,” *Geophysics*, vol. 50, no. 3, pp. 394–413, 1985.

[78] G. L. McDonald and Q. Zhao, “Multipoint optimal minimum entropy deconvolution and convolution fix: application to vibration fault detection,” *Mechanical Systems and Signal Processing*, Jun. 2016.

[79] M. Koç, A. Barkana, and Ö. N. Gerek, “A fast method for the implementation of common vector approach,” *Information Sciences*, vol. 180, no. 20, pp. 4084–4098, Oct. 2010.

[80] N. V. Chawla, K. W. Bowyer, L. O. Hall, and W. P. Kegelmeyer, “SMOTE: synthetic minority over-sampling technique,” *Journal of artificial intelligence research*, vol. 16, pp. 321–357, 2002.

[81] H. He, Y. Bai, E. A. Garcia, and S. Li, “ADASYN: Adaptive synthetic sampling approach for imbalanced learning,” presented at the International Joint Conference on Neural Networks (IJCNN 2008), 2008, pp. 1322–1328.

[82] T. Rückstie\s s, C. Osendorfer, and P. van der Smagt, “Sequential feature selection for classification,” in *Australasian Joint Conference on Artificial Intelligence*, 2011, pp. 132–141.

[83] L. Yu and H. Liu, “Feature selection for high-dimensional data: A fast correlation-based filter solution,” in *ICML*, Washington DC, 2003, vol. 3, pp. 856–863.

[84] R. Tibshirani, “Regression shrinkage and selection via the lasso: a retrospective,” *Journal of the Royal Statistical Society: Series B (Statistical Methodology)*, vol. 73, no. 3, pp. 273–282, 2011.

[85] L. Breiman, “Random forests,” *Machine learning*, vol. 45, no. 1, pp. 5–32, 2001.

[86] C. H. Park and S. B. Kim, “Sequential random k-nearest neighbor feature selection for high-dimensional data,” *Expert Systems with Applications*, vol. 42, no. 5, pp. 2336–2342, Apr. 2015.

[87] W. He, Y. Ding, Y. Zi, and I. W. Selesnick, “Sparsity-based algorithm for detecting faults in rotating machines,” *Mechanical Systems and Signal Processing*, vol. 72–73, pp. 46–64, May 2016.

[88] J. KIM, B.-S. Kim, and S. Savarese, “Comparing image classification methods: K-nearest-neighbor and support-vector-machines,” presented at the 6th WSEAS international conference on Computer Engineering and Applications, Harvard, 2012, pp. 133–138.

[89] W. A. Smith and R. B. Randall, “Rolling element bearing diagnostics using the Case Western Reserve University data: A benchmark study,” *Mechanical Systems and Signal Processing*, vol. 64–65, pp. 100–131, Dec. 2015.

[90] M. Žvokelj, S. Zupan, and I. Prebil, “EEMD-based multiscale ICA method for slewing bearing fault detection and diagnosis,” *Journal of Sound and Vibration*, vol. 370, pp. 394–423, May 2016.

[91] X. Lou and K. A. Loparo, “Bearing fault diagnosis based on wavelet transform and fuzzy inference,” *Mechanical Systems and Signal Processing*, vol. 18, no. 5, pp. 1077–1095, Sep. 2004.

[92] Onur Kılınç and Jakub Vágner, “Fault severity detection of ball bearings and efficiency of one-period analysis in early fault diagnosis of rotating machinery,” presented at the 21st VIBROENGINEERING Conference, Brno, Czech Republic, 2016, vol. 7, pp. 76–81.

[93] V. C. M. N. Leite *et al.*, “Detection of localized bearing faults in induction machines by spectral kurtosis and envelope analysis of stator current,” *IEEE Transactions on Industrial Electronics*, vol. 62, no. 3, pp. 1855–1865, Mar. 2015.

[94] S. R. Safavian and D. Landgrebe, “A survey of decision tree classifier methodology,” *IEEE transactions on systems, man, and cybernetics*, vol. 21, no. 3, pp. 660–674, 1991.

[95] A. Sholahuddin, A. P. Ramadhan, and A. K. Supriatna, “The application of ANN-linear perceptron in the development of DSS for a fishery industry,” *Procedia Computer Science*, vol. 72, pp. 67–77, 2015.

[96] I. N. DIMOU, “Design and implementation of support vector machines and information fusion methods for bio-medical decision support systems,” Technical University of Crete, 2011.

[97] C. E. Brodley and P. E. Utgoff, “Multivariate decision trees,” *Machine learning*, vol. 19, no. 1, pp. 45–77, 1995.

8 PUBLICATIONS OF THE PHD STUDENT RELATED TO THE THEME OF THE DISSERTATION

[I] *Kilinc O., 2015, Freight wagons in Turkey: a comparative study, 32nd International Colloquium on Advanced Manufacturing and Repair Technologies in Vehicle Industry, ISBN: 978-80-7395-902-6, 17-24.*

[II] *Kilinc O., Onat A., 2015, Simple test procedure of strain gauge measurement: An introductory implementation towards railway vehicle testing, Electronic Journal of Occupational Improvement and Research, ISSN: 2147-8503, December Special Issue, 2, 151-164.*

[III] *Kilinc O., 2016, Multi-fault detection of ball bearings in rotating machinery using Fisher linear discriminant analysis, International Congress on Fundamental and Applied Sciences, p. 71.*

[IV] *Kilinc O., Vágner J., In press, Sensing anomalous sensor data in wayside diagnostics using enhanced LBP-kurtograms, Scientific papers of the University of Pardubice. Series B, Jan Perner Transport Faculty, 21.*

[V] *Onat A., Kilinc O., Lata M., 2016. A linear Kalman filtering scheme for estimation of secondary vertical suspension of railway vehicles, 21st VIBROENGINEERING Conference, ISSN: 2345-0533, Brno, Czech Republic, pp. 124–128.*

[VI] *Kilinc O., Vágner J., 2016. Fault severity detection of ball bearings and efficiency of one-period analysis in early fault diagnosis of rotating machinery, 21st VIBROENGINEERING Conference, ISSN: 2345-0533, Brno, Czech Republic, pp. 76–81.*

[VII] *Kilinc O., Vágner J., In press. Wayside diagnosis of metro wheelsets using acoustic sensor data and one-period analysis, Engineering Mechanics 2017, Svratka, Czech Republic.*

[VIII] *Kilinc O., Vágner J., In press. Vibration based diagnosis of wheel defects of metro train sets using one period analysis on the wayside, 25st VIBROENGINEERING Conference, Liberec, Czech Republic.*